



# MASTERARBEIT | MASTER'S THESIS

Titel | Title

Investigating the predictive power of in vitro drug testing in multicellular spheroids  
for in vivo activity.

verfasst von | submitted by

Ramona Velasco-Pelaez BSc

angestrebter akademischer Grad | in partial fulfilment of the requirements for the degree of  
Master of Science (MSc)

Wien | Vienna, 2024

Studienkennzahl lt. Studienblatt |  
Degree programme code as it appears on the  
student record sheet:

UA 066 863

Studienrichtung lt. Studienblatt | Degree  
programme as it appears on the student record  
sheet:

Masterstudium Biologische Chemie

Betreut von | Supervisor:

o. Univ.-Prof. Dr. Dr. Bernhard Keppler

Mitbetreut von | Co-Supervisor:

Mag. Dr. Michael Jakupec

## Acknowledgements

I would like to thank o. Univ.-Prof. Dr. Dr. Bernhard Keppler for the opportunity to carry out my master thesis in the department of inorganic chemistry.

I would like to thank Mag. Dr. Michael Jakupc for all his support throughout the different stages of this thesis, his input, criticism, ideas and creating a working environment that was truly inspiring.

I would like to thank the chemists that provided the compounds for my experiments and Univ.-Prof.in Mag.a Dr.in Petra Heffeter for providing the *in vivo* data of the tested compounds.

I thank my colleagues that made the lab a wonderful place to be. Thank you for the opportunity to learn from you and your help: Anton, Dominik, Debora, Klaudia, Mate, Michaela.

I would like to thank all my colleagues and professors that provided food for thoughts in seminars, and those, who provided snacks after work.

I would like to thank my friends and family that supported me by getting excited with me over results, proofreading, constant moral support and just being there for me when I needed them.









# Zusammenfassung

Bei der Entwicklung neuer Medikamente zur Behandlung von Krebs gibt es eine Diskrepanz zwischen der Anzahl an Substanzen, welche vielversprechende Ergebnisse *in vitro* zeigen, und jenen, welche auch im Tiermodell Wirksamkeit aufweisen. Um die Anzahl der Tierversuche zu reduzieren und eine höhere Treffsicherheit in der Vorauswahl von Substanzen zu erreichen, wurden die *In-vitro*-Testbedingungen optimiert. Entwicklungen der letzten Jahre ermöglichen die Verwendung von multizellulären Tumor-Sphäroiden (3D Zellkultur) im Hochdurchsatz-Screening. Diese weisen gewisse Charakteristika von Tumoren auf (Hypoxie, Nekrose) und ähneln stärker dem ursprünglichen Tumorgewebe hinsichtlich Morphologie und Genexpression. Daher wird ihnen eine höhere Prädiktivität für *In-vivo-Aktivität* zugeschrieben, wofür jedoch kaum Evidenz vorliegt.

Von den zahlreichen am Institut für Anorganische Chemie der Universität Wien synthetisierten Verbindungen wurden bereits mehr als 30 an einem Kolonkarzinommodell (CT26) *in vivo* getestet. Dabei handelt es sich um Pt(II)-, Pt(IV)-, La(III)-, Ru(II)-, Ru(III)-, Ga(III)-, Os(II)-, Rh(III)- und Mo(IV)-Verbindungen, sowie Thiosemicarbazone. Die daraus gewonnenen Daten dienen nun als Grundlage, die Vorhersagekraft verschiedener *In-vitro*-Testmethoden zu untersuchen. Hierzu wurden im Laufe dieser Masterarbeit 29 Substanzen parallel in zwei Darmkrebs-Zelllinien, CT26 (murin) sowie HCT116 (human), in 2D Zellkulturen sowie an multizellulären Sphäroiden derselben Zelllinie getestet, um die Prädiktivität dieser zwei *In-vitro*-Modelle zu vergleichen.

Zunächst wurden die Test-Bedingungen an CT26-Sphäroiden optimiert, um die Hypoxie und die Zone ruhender Zellen im Inneren von Tumorgewebe widerzuspiegeln. Diese Bedingungen wurden mittels Konfokalmikroskopie nachgewiesen. Weiters wurde die Wirksamkeit der Substanzen mittels eines luminiszenz-basierten ATP-Assays ermittelt, welcher eine vergleichbare Bestimmung der Lebensfähigkeit von Zellen in 2D und 3D Kulturen erlaubt. Die erhaltenen  $IC_{50}$ -Werte sowie deren 3D/2D-Quotienten wurden mittels Korrelationsanalyse mit den Ergebnissen der *In-vivo*-Testungen verglichen. Die Analyse ergab eine höhere Korrelation der  $IC_{50}$  Werte in HCT116- und CT26-Sphäroiden mit der Wachstumshemmung in murinen CT26 Tumormodellen, als die entsprechenden Werte in Monolayer-Kulturen. Um eine höhere Prädiktivität von Hochdurchsatz-Screenings zu erreichen wird der Einsatz von multizellulären Tumor-Sphäroiden empfohlen.

# Abstract

There is a high divergence in anti-cancer drug development between the number of substances that show promising activity *in vitro* and those for which activity can be confirmed *in vivo* in animal models. Optimized conditions for *in vitro* compound testing could lead to a reduction of necessary animal experiments by increasing the accuracy in substance preselection. Advances in compound testing include the implemented use of multicellular tumor spheroids (3D cell culture) in high-throughput screenings. They exhibit characteristics of tumor tissue such as hypoxia and quiescence and resemble their tissue of origin more closely in terms of morphology and gene expression than monolayer cell culture. This is why a higher predictivity for *in vivo* activity has generally been attributed to them despite a lack of clear evidence.

From the variety of compounds synthesized at the Institute of Inorganic Chemistry of the University of Vienna more than 30 were already tested in a murine colon carcinoma model (CT26) *in vivo*. These substances comprise Pt(II), Pt(IV), La(III), Ru(II), Ru(III), Ga(III), Os(II), Rh(III) and Mo(IV) complexes as well as thiosemicarbazones. The data obtained from these experiments were the basis for analyzing the predictivity of different *in vitro* tests for *in vivo* activity. For this purpose, cytotoxicity testing in two colon cancer cell lines was carried out in this master thesis, using CT26 (murine) and HCT116 (human) cells in monolayer and spheroid cultures in parallel.

In a first step, test conditions in CT26 spheroids were optimized to mimic hypoxia and quiescence in inner layers of tumor tissue. These conditions were confirmed via confocal microscopy. This was followed by cytotoxicity tests, using a luminescence-based ATP assay which facilitates sensitive and analogous testing of cell viability in both 2D and 3D cell culture. The received  $IC_{50}$  values and 3D/2D quotients thereof were compared with *in vivo* results using correlation analysis. Higher correlation between  $IC_{50}$  values in HCT116 and CT26 spheroid culture with *in vivo* results in the murine colon carcinoma CT26 tumor model compared to corresponding values in monolayer culture was proven. The use of multicellular spheroids for high-throughput testing is recommended to achieve a higher predictivity for *in vivo* results.

## Table of Contents

Acknowledgement.....	i
Zusammenfassung.....	i
Abstract.....	ii
1 Introduction.....	1
1.1 Cancer and Cancer Therapy.....	1
1.2 Drug Development.....	4
1.3 Cell Culture.....	7
1.3.1 Monolayer Cell Culture.....	7
1.3.2 Three-dimensional Cell Culture.....	8
1.4 Metal Complexes.....	12
1.4.1 Platinum(II).....	13
1.4.2 Platinum(IV).....	14
1.4.3 Ruthenium Complexes.....	16
1.4.4 Thiosemicarbazones.....	21
1.4.5 Osmium.....	23
1.4.6 Rhodium.....	24
1.4.7 Molybdenum.....	25
1.4.8 Lanthanum.....	26
2 Aims.....	27
3 Material and Methods.....	28
3.1 Substances.....	28
3.2 Cell lines.....	33
3.3 Media.....	33
3.4 Other Chemicals and Solutions.....	34
3.5 Instruments and Labware.....	34
3.6 Culture Conditions.....	35
3.7 MTT Testing.....	36
3.7.1 Principle.....	36
3.7.2 Procedure.....	36
3.8 Optimization of CT26 Cell Number for Cytotoxicity Test in Monolayer Cultures.....	38

3.9	Microscopy and Spheroid Measuring .....	39
3.10	Cytotoxicity Testing Using the CellTiter-Glo® 2.0 Assay in Monolayer Cultures and CellTiter-Glo® 3D in Spheroids.....	40
3.10.1	Principle.....	40
3.10.2	Procedure for Monolayer Cell Culture .....	40
3.10.3	Procedure for Spheroids .....	41
3.11	In-vivo data.....	43
3.12	Statistical Analysis of the Data .....	45
3.13	Spheroid Characterization Using Immuno-fluorescence .....	45
4	Results & Discussion .....	47
4.1	Optimization of CT26 Cell Number .....	47
4.2	Spheroid Growth Curve .....	50
4.2.1	Optimization of Cell Number for CT26 Spheroids .....	50
4.2.2	Choice of Medium .....	52
4.3	Spheroid Characterization via Immunofluorescence .....	54
4.3.1	Cell Proliferation.....	54
4.3.2	Hypoxic Core Regions.....	56
4.3.3	Apoptosis .....	57
4.3.4	Necrosis .....	59
4.4	Cytotoxicity tests .....	60
4.4.1	MTT assay in SW480 Monolayer Cultures .....	60
4.4.2	Cytotoxicity tests in HCT116 and CT26 Monolayer and Spheroid Cultures .....	61
4.5	Statistical Analysis of the Data .....	70
4.5.1	Analysis of CT26 <i>in vivo</i> vs SW480 <i>in vitro</i> Data .....	71
4.5.2	Analysis of CT26 <i>in vivo</i> vs HCT116 Monolayer <i>in vitro</i> Data.....	77
4.5.3	Analysis of CT26 <i>in vivo</i> vs CT26 Monolayer <i>in vitro</i> Data .....	82
4.5.4	Analysis of CT26 <i>in vivo</i> vs HCT116 Spheroid <i>in vitro</i> Data .....	87
4.5.5	Analysis of CT26 <i>in vivo</i> vs CT26 Spheroid <i>in vitro</i> Data.....	92
4.5.6	Analysis of CT26 <i>in vivo</i> vs HCT116 <i>in vitro</i> IC50 Quotients .....	97
4.5.7	Analysis of CT26 <i>in vivo</i> vs CT26 <i>in vitro</i> IC50 Quotients.....	97
4.6	Discussion of <i>in vitro</i> Model Predictivity .....	104
5	Conclusion.....	108
	References.....	109



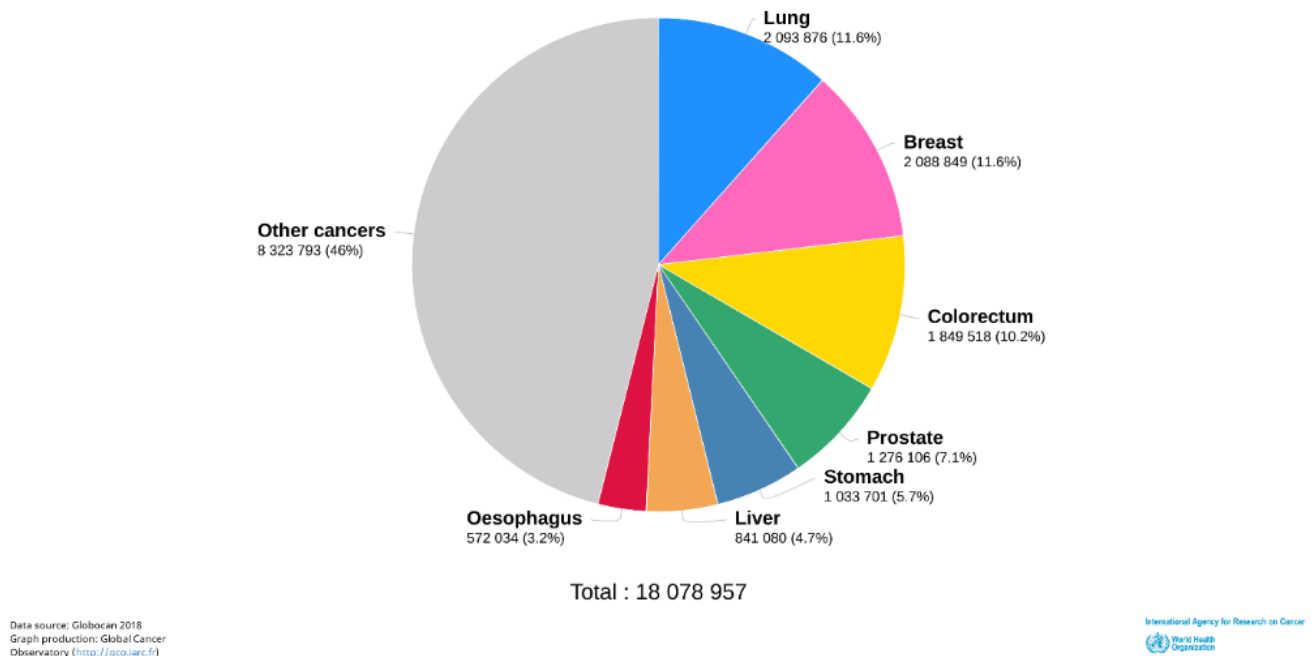


# 1 Introduction

## 1.1 Cancer and Cancer Therapy

According to Statistik Austria, cancer is the second most common cause of death in Austria. About 40,000 people are diagnosed with cancer every year in Austria alone, with breast, colorectal, prostatic and lung cancer among the most common types. As of 2018, the most common type of cancer among men is prostate cancer (23%), whilst it is breast cancer for women (29%). Pancreatic cancer (5% in women; 4% in men) is the type of cancer with the highest mortality rate with only 9% survival in a 5-year interval. There is a 25% chance to be diagnosed with cancer before the age of 75 years. An increase in the percentage of people diagnosed with cancer cannot only be attributed to a rise in demographic age and increased lifespans, but also to improved life expectancy of affected people. It is being predicted that by 2030 there will be an increase in cancer prevalence to 4.9% of the Austrian population, which is about twice as much as in the year of 2000.<sup>1</sup> It is estimated that worldwide there are about 18 million new cases of cancer per year and 9.6 million people die from cancer. Figure 1 shows that worldwide lung, breast, colorectal and prostate cancer are the most common types of cancer, with lung cancer having a higher prevalence compared to Austria.<sup>2</sup>

Estimated number of new cases in 2018, worldwide, all cancers, both sexes, all ages

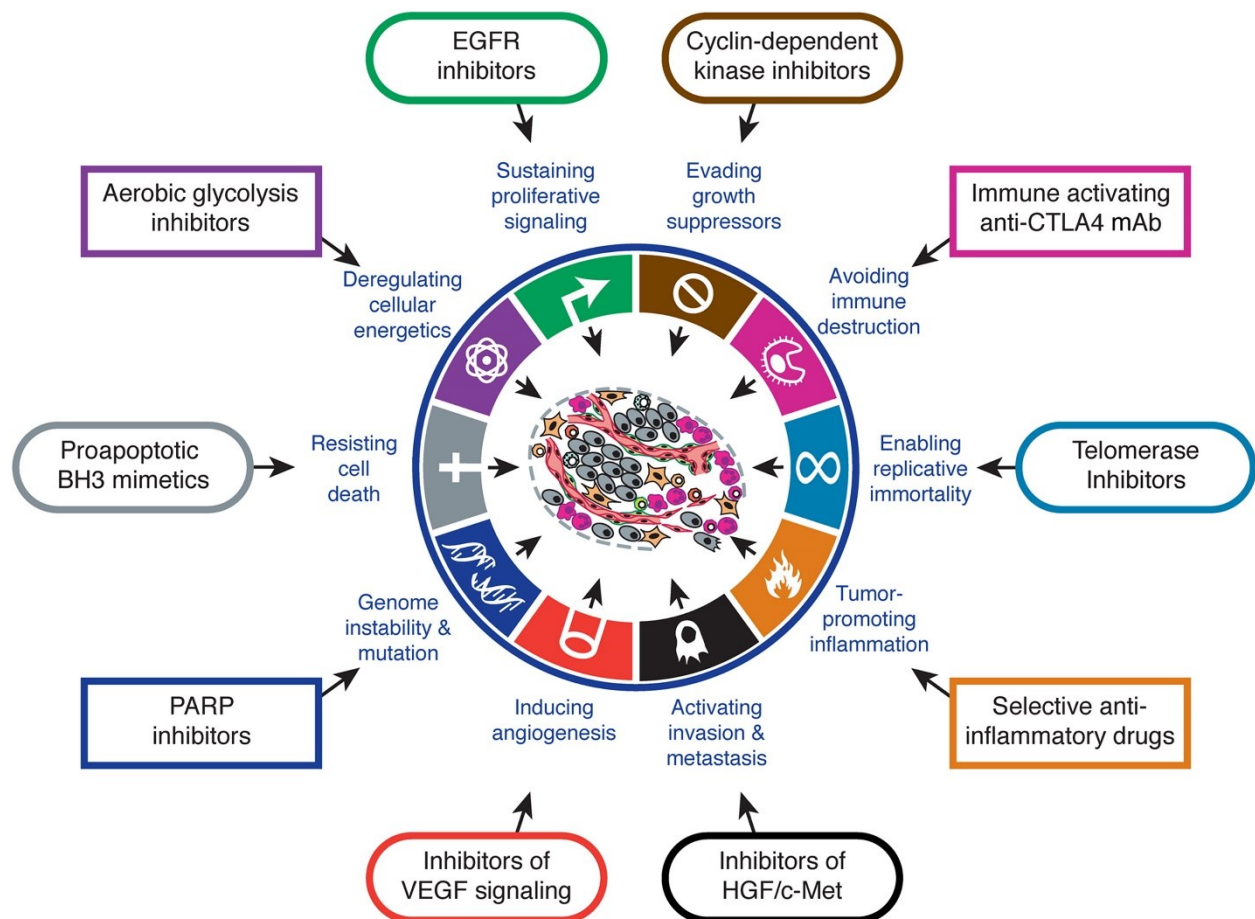


**Figure 1:** Pie chart of estimated number of cancer incidents divided by site, worldwide.<sup>2</sup>

The transformation of normal cells into cancer cells is caused by a variety of factors. A World Health Organization (WHO) report from 2008 states that tobacco contributes to 22% of all cancer deaths and in particular to 71% of lung cancer deaths. 16.4% of all new cancer cases are caused by infections, especially in less developed countries. Most prominent among these cancer-causing infections are those with *Helicobacter pylori*, hepatitis B and C virus and the human papilloma virus. Reproductive behavior, hormones as well as factors such as weight, physical exercise and diet influence breast cancer risk. Colorectal cancer risk is mostly influenced by diet, body weight and physical activity. Sunlight exposure increases the risk of developing melanoma.<sup>2</sup>

Each cell in the human body is normally closely regulated in the way it behaves. Proliferation, differentiation and cell death are dictated by their environment. The transformation into cancer cells occurs when healthy cells acquire mutations that give them proliferation advantages over their neighboring cells. Mutations occur frequently, but one mutation is not enough to cause cancer. Only if these mutations accumulate in one cell, this cell eventually generates a clone of cells with invasive, malignant behavior. A growing number of aberrant cells will increase the chance of further mutations and natural selection will favor cells that are better adapted to the tumor

environment.<sup>3</sup> Hanahan and Weinberg defined the hallmarks of cancer, key features that normal cells acquire along the progression into a malignant state. The six originally published hallmarks included sustained proliferative signaling, evasion of growth suppressors, resistance to cell death, activation of invasion and metastasis, enabling of replicative immortality and induced angiogenesis. In addition two emerging characteristics (deregulating cellular energetics, avoiding immune destruction) have been described as well as enabling characteristics (genome instability and mutation, tumor-promoting inflammation). Figure 2 provides an overview of these hallmarks as well as possible targeted therapy approaches<sup>4</sup>. These hallmarks emerge as the result of various mutations in tumor-suppressor genes (e.g. RB) and oncogenes (e.g. RAS).



**Figure 2:** The eight hallmarks of cancer and the two enabling characteristics with examples of possible targeted therapy strategies directed at them.<sup>4</sup>

There are different ways to treat cancer, which can also be combined with each other to increase the chance of survival:

- Surgery
- Radiation
- Chemotherapy
- Hormone therapy
- Targeted therapy

While surgical excision of solid tumors may be sufficient for curing cancer at an early stage, it is often combined with radiation or chemotherapy at later stages to reduce the tumor volume in advance (neoadjuvant therapy) or to reduce the risk of developing metastases from disseminated cancer cells within the whole body (adjuvant therapy). There is also a great variety in treatment options with regard to drugs. Cytotoxic drugs are aimed at eliminating fast proliferating cells from the body, therefore primarily affecting cancer cells due to their high mitotic activity. Hormonal therapy is being applied to treat hormone dependent tumors, such as estrogen-receptor-positive breast cancer or androgen-dependent prostate cancer. Targeted therapy acts on molecular targets specifically (over-)expressed in cancer cells, such as inhibition of growth factor receptors. Further examples of targeting approaches are given in Figure 2. Drugs may be either small molecules, able to penetrate into the cells and act on regulatory pathways, or monoclonal antibodies, binding to specific sites on cancer cells.<sup>5</sup>

A new approach for cytotoxic drugs is to increase their specific effect on cancer cells. This can be achieved by creating metal-based drugs that are activated by reduction, developing their full potential only in the hypoxic environment of a solid tumor. Another approach is to use macromolecules as carriers, which will accumulate at the tumor site due to the enhanced permeability and retention (EPR) effect.<sup>6</sup>

## 1.2 Drug Development

Drugs are closely regulated by governments worldwide. In the United States of America (USA) the Federal Food and Drug Administration (FDA) oversees the approval of new drugs. Over the last decades the process for drug approval has evolved, especially influenced by tragedies in the

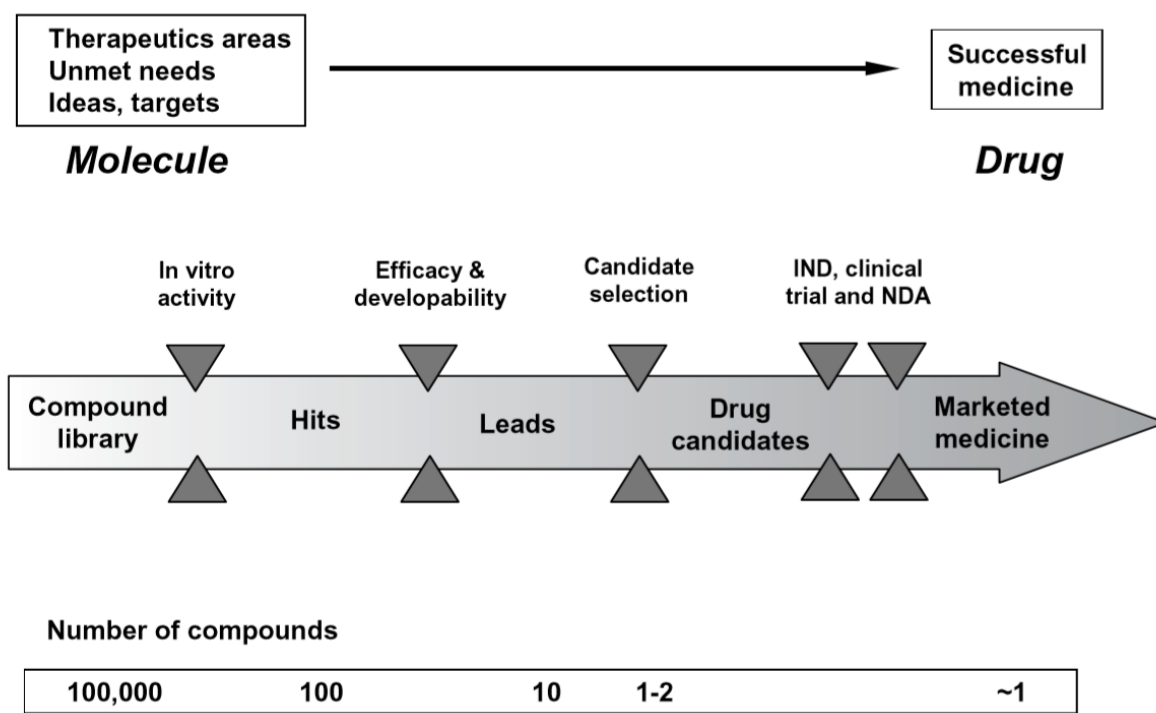
twentieth century. Since over 100 people were killed in the sulfanilamide incident in the 30s, producers have to prove the safety of their drugs. In the wake of the thalidomide crisis, where use of this drug in pregnant women in the 1950s resulted in birth defects, voices for stricter testing grew louder.<sup>7</sup> Drugs now have to be assessed thoroughly for their properties, including toxicity, efficacy and pharmacokinetic properties. The goal is to prevent unforeseen side effects and to insure that benefits of a new drug outweigh its negative impacts on the patient. Optimal dosage is sought, at which a drug shows maximal therapeutic benefits and minimal side effects or tolerable adverse effects in the case of anticancer drugs. For example, most anticancer drugs are teratogenic but patients are strongly advised not to get pregnant while in chemotherapy.<sup>8</sup> Later, thalidomide got approval in myeloma treatment, under strict guidelines and monitoring of the therapy to prevent its teratogenic effects.<sup>9</sup> This is a difficult process and, even with modern standards, drugs occasionally have to be withdrawn from the market after their licensing due to unexpected side effects.<sup>5</sup>

In the European Union (EU) different routes are available for the authorization of medicine. For new compounds that treat cancer the centralized procedure is compulsory. Applications must be directed at the European Medicines Agency (EMA) to receive an EU-wide approval for a new drug. The Committee for Medicinal Products for Human Use assess the drugs and a final decision is made by the European Commission.<sup>10</sup>

In history, chemical compounds have first shown their anti-cancer properties in various ways. The observation of anti-neoplastic effects of sulfur mustard on humans during World War I led to the discovery of nitrogen mustard as the first cytotoxic agent. A few years later, the unfavorable effects of folic acid and favorable effects of folic acid-reduced diet on childhood leukemia led to the development of the antifolate methotrexate, the first drug to cure cases of metastasized cancers. Screening for anti-proliferative agents in the 1950s in murine tumor models resulted in the discovery of daunorubicin, and in 1965 Rosenberg discovered the anticancer activity of cisplatin due to its effect on cell division of *Escherichia coli*.<sup>11</sup>

Nowadays many steps are involved in finding and developing suitable drug candidates. Figure 3 illustrates how compounds that show *in vitro* activity ("hits") are optimized for activity ("leads") and for their biopharmaceutical properties, resulting in a drug candidate that will progress through

clinical trials. Only one of 100,000 investigated compounds is released for the application in patients. Clinical trials alone have drug attrition rates of about 90% but contribute most to the immense costs of drug development (\$400–650 million per drug in total). Most of these drugs fail in clinical trial because of their pharmacokinetic properties, their toxicity and lack of efficacy. Methods to test for factors other than *in vitro* activity are sought to minimize the costs in development.<sup>12</sup>



**Figure 3:** Illustration of steps in drug development and drug attrition rates.<sup>12</sup>

Safety, effectiveness and toxicity are critical properties of drugs that had to be tested before they can proceed into clinical trials. In the USA, the National Cancer Institute (NCI) conducts and finances research into cancer treatment. The Development Therapeutics Program (DTP) of the NCI initially used three different *in vivo* models in rodents to assess the anti-tumor activity of compounds. In 1975 an *in vitro* prescreen in the P388 leukemia model was introduced to reduce the number of animal experiments. The *in vivo* rodent tumor models were complemented with human xenografts with the purpose of a higher predictivity for the activity of the tested drugs in human solid tumors. The P388 prescreen was replaced in 1990 by the NCI 60-cell line panel.<sup>13</sup>

Initially the panel comprised 60 different human tumor cell lines of different origin (lung, colon, melanoma, renal, ovarian, brain and leukemia) suitable for high-throughput cytotoxicity testing. Up to this date, 88,000 pure compounds and 34,000 crude extracts have been tested and are the basis for the COMPARE analysis of new compounds tested. Currently 1,000 new drugs and natural products are tested each month against 59 cell lines.<sup>14</sup>

After preclinical evaluation, clinical trials will consist of phases I-IV. Phase I serves the purpose of evaluating drug safety and dosage in a small number of patients. In Phase II a larger group of patients is used to study the efficacy of the drug and safety in selected tumor entities. Efficacy of the investigational drug is compared to current standard therapy in Phase III. Phase IV clinical trials are conducted after drug approval for marketing to monitor risks and benefits. These phases of clinical trials have been initiated by the FDA.<sup>15</sup>

## 1.3 Cell Culture

The first *ex vivo* experiments in the beginning of the 20<sup>th</sup> century used organ explants to study cell development and behavior. Tumor explants of mice were used to develop the first continuous cell line in 1943. The HeLa cell line, derived from a human cervical tumor, is the oldest human cell line and still in use. Facilitated by the use of trypsin, it was possible to grow these cells as adherent monolayer cultures and use them for a variety of experiments. Although the cells will retain some of the features of their tissue of origin, many of them are lost. It was shown that cell signaling, gene expression, cell morphology and proliferation are altered by culturing cells as monolayers. The term cell culture usually refers to the use of such monolayer cultures or single cell suspensions, whilst organ culture describes the use of tissue that is not disrupted or damaged and is thereby an organ model *in vitro*. Histotypical culture tries to simulate tissue-like conditions by three-dimensional cell culturing. Organotypical culture does the same and tries to resemble the *in vivo* conditions more closely by using different cell types.<sup>16</sup>

### 1.3.1 Monolayer Cell Culture

Working with cell lines has several advantages over experiments *in vivo*. Conditions such as pH value, temperature, osmotic pressure and availability of nutrients can be kept constant throughout the experiments in addition to the intrinsic feature of the cell lines being homogenous populations.

The second major advantage of cell culture experiments is their cost efficiency. There is no substance loss due to drug delivery and high-throughput screens (use of multiwell plates, automatic plate readers) further reduce material and personnel costs.<sup>16</sup> Many of these advantages also contribute to the biggest shortcomings of this system - the inability to properly mimic the conditions in tumors.<sup>17</sup> In the NCI 60 cell line screen at least six cell lines represent one tumor type and correlations between the *in vitro* results in 2D cell culture and *in vivo* testing can only be found if the compound is active in at least four of these cell lines. No correlation could be found between *in-vitro* cytotoxic potency in the NCI colon carcinoma cell lines and activity in hollow-fiber assays using the same cell lines *in vivo*.<sup>13</sup>

### 1.3.2 Three-dimensional Cell Culture

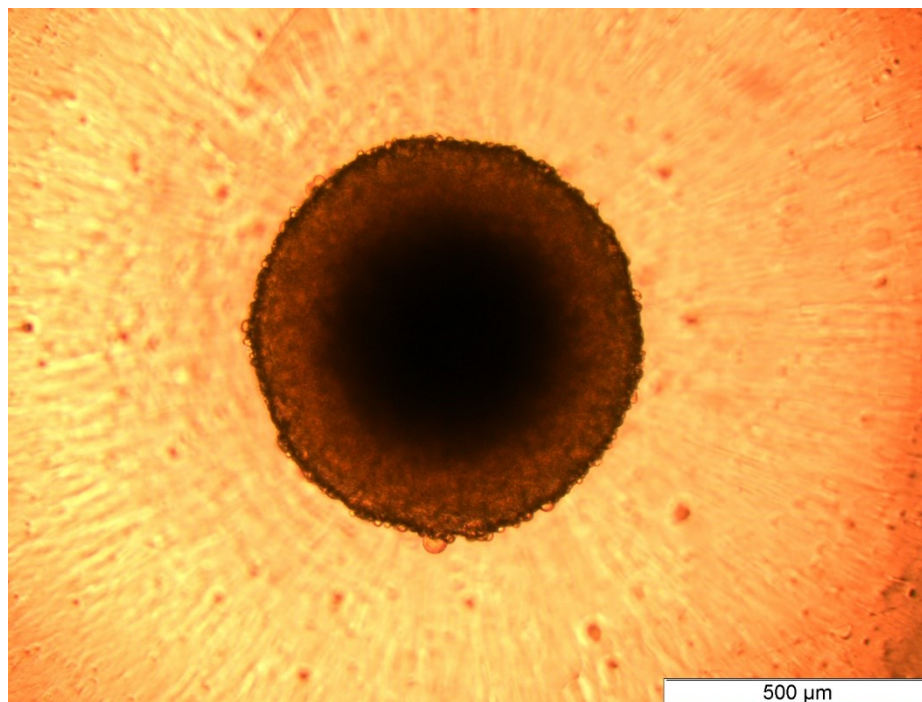
Cells that are cultured on a flat surface will have a flatter morphology and a forced apical-basal polarity. In their tissue of origin, they depend on interactions with the extracellular matrix (ECM) and their neighboring cells to retain their natural organization and shape. One option to grow cells *in vitro* in three dimensions is to provide them with an environment to not only grow horizontally but also vertically.<sup>18</sup> Collagen gel can be penetrated by cells, enabling them to form tissue-like structures, depending on the kind of cells. Matrigel, a product derived from extracellular matrix, also provides a scaffold for cells and consists of laminin, collagen, fibronectin and polyglycans in a complex, not completely defined composition. While gels are limited in their size by oxygen exchange, hollow fibers provide a way to grow cells in high density and provide them with sufficient amounts of oxygen and nutrients.

Another option is to force cells to form cell-cell contacts by inhibiting surface attachment. Cells that are transferred to a vessel where their attachment to any surface is inhibited by constant stirring will form aggregates - multicellular spheroids that resemble avascular micrometastases.<sup>16</sup> By transferring established cell lines into three-dimensional cell culture, some of the original features of the tissue can be regained. However, these effects might be caused by factors associated with their changed microenvironment, rather than the dimension itself, such as levels of adhesion or ECM composition.<sup>18</sup> Signaling via cell-cell or cell-ECM interaction is crucial for cell differentiation, proliferation and many cellular functions. Drug penetration into prevascular micrometastases can be modelled *in vitro* using spheroids, enabling closer predictions for *in vivo*

penetration depths.<sup>19</sup> Hypoxia is also an important factor in tumors and essential for modern drug targeting of cytotoxic agents. Activation by reduction is facilitated by the hypoxic environment and can be mimicked by using multicellular spheroids with a hypoxic core region.<sup>20</sup>

### 1.3.2.1 Generating Multicellular Spheroids

Multicellular spheroids can, for example, be generated by putting a single cell suspension onto a plate coated with agar. Cells will not adhere to the substrate and start to form loose cell aggregates after a few hours. Within 2-4 days, compact round-shaped spheroids will form, in which cells cannot be distinguished from each other with simple optical means. Other methods include the spinner flask method or the use of a gyratory rotation system.<sup>21</sup> Depending on the cell line the spheroids can adopt different shapes. They either form highly condensed spheroids or spheroidal shapes with a rougher, more uneven perimeter. Some cell lines will only form aggregates with individual cells still distinguishable or loose aggregates of entirely irregular shape.<sup>22</sup> An example of a compact spheroid is depicted in Figure 4. In an attempt for generating spheroids suitable for high-throughput screening, the hanging drop method and the use of ultra-low attachment (ULA) plates were examined, with the latter generating spheroids in a highly reproducible size and form.<sup>23</sup>



**Figure 4:** A compact spheroid consisting of CT26 cells, seeded in ULA plates, 8 days after seeding.

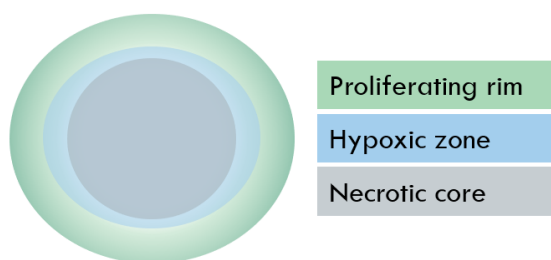
### 1.3.2.2 Properties of Multicellular Spheroids

While some cells fail to form compact spheroids and will only take the shape of loose aggregates, others will assemble into compact structures over time. Suitable cells hindered from attaching to any surface in hanging drops will form ECM fibers resulting in rapid aggregation. A delay period is then followed by E-cadherin homophilic attachment, resulting in the formation of compact spheroids. Shapes of these spheroids resemble those of multicellular aggregates of breast, ovarian or prostate cancer cells found in body fluids of patients.<sup>24</sup>

Cells grown as spheroids show different protein expression levels than cells grown as monolayers. These variations in protein expression have been ascribed to the close cell-cell contacts.<sup>25</sup> It has been argued that these changes in protein expression, consisting of cell-cell junctions and formation of ECM can also be found in confluent monolayers. These results suggest that resistance mechanisms based on altered gene expression are more similar between confluent monolayers and spheroids grown on poly-HEMA than they are between spheroids and *in vivo* tumors.<sup>26</sup> However, this study was carried out using only one spheroid generating process, using only four test drugs (adriamycin, depsipeptide, daunorubicin and cisplatin) and focusing only on gene expression.

The three-dimensional arrangement of multiple cell layers with their ECM and cell-cell junctions also serves as a diffusion barrier to drugs, enabling simulations of the *in vivo* pharmacokinetic behavior of drugs penetrating into tumor tissue.<sup>27</sup>

Another important characteristic of spheroids is the distinct cell proliferation profile depending on the cell layer. While the outer cell layers largely consist of highly proliferating cells, proliferation decreases with depth, resulting in a quiescent zone. Spheroids with a diameter > 400  $\mu\text{m}$  also develop a necrotic core.<sup>27</sup> A schematic drawing of these layers, which are more pronounced in bigger spheroids (diameter > 550  $\mu\text{m}$ ) and less distinctive in smaller spheroids (diameter < 500  $\mu\text{m}$ ), is shown in Figure 5. To characterize the layers of spheroids, cryosections can be prepared and analyzed via immunohistochemistry.<sup>28</sup>



**Figure 5:** Schematic drawing of different cell layers in spheroids as shown in the literature<sup>28</sup> for larger spheroids and confirmed in previous experiments in HCT116 spheroids

### 1.3.2.3 Spheroids in Drug Screenings

A reaction specific to the kind of three-dimensional organization was received upon treatment of malignant HMT-3522 cells grown in Matrigel and treated with antibodies against  $\beta 1$ -integrin. While the normal breast cells HMT-3522 formed acini structures, similar to their *in vivo* organization and went into apoptosis upon antibody treatment, the malignant cells only formed loose aggregates that changed to the normal phenotype upon treatment.<sup>17</sup>

As mentioned above, spheroids also contain hypoxic regions, which are important for drugs that are activated by reduction such as Pt(IV) compounds or tirapazamine (TPZ). A three-dimensional model was used to investigate metabolic consumption vs. tissue penetration of TPZ, after loss of activity was initially observed in hypoxic multicellular spheroids.<sup>20</sup> Pt(IV) complexes, known for their activation by reduction, have been investigated for their activity in monolayer, hypoxic monolayer and spheroid culture. It was found that hypoxia is not the only criterion for the activity of the investigated drugs. These were rather small-scale studies with only five investigated compounds, using Alamar Blue to test for cytotoxicity, since MTT reagent cannot penetrate into spheroids.<sup>29,30</sup> Another reagent for testing cytotoxicity is CellTiter-Glo<sup>®</sup>, further described on page 40.<sup>31</sup>

A different study using spheroid-generating cell lines from the NCI 60 cell line screen also did only take a few compounds into account for cytotoxicity testing, leaving unclear whether spheroids are indeed a more predictive model.<sup>22</sup> Nevertheless spheroids have been claimed to bridge the gap between 2D cell culture and animal models, giving more conclusive insight into whether or not drugs should be further developed and cutting costs thereby.<sup>17,23</sup>

## 1.4 Metal Complexes

In 1969 Rosenberg published observations on the first metal complex to show antitumor activity in animal models, *cis*-diamminedichloridoplatinum(II), also known as cisplatin.<sup>32</sup> The compound had been known for over 100 years<sup>33</sup> when Rosenberg discovered in one of his experiments on *E. coli* that the formation of cisplatin led to an inhibition of cell division in the bacteria. Further studies in mice showed the antineoplastic properties of cisplatin<sup>32</sup> and first trials in human patients with testicular cancer in 1974 led to its approval for cancer chemotherapy in 1979.

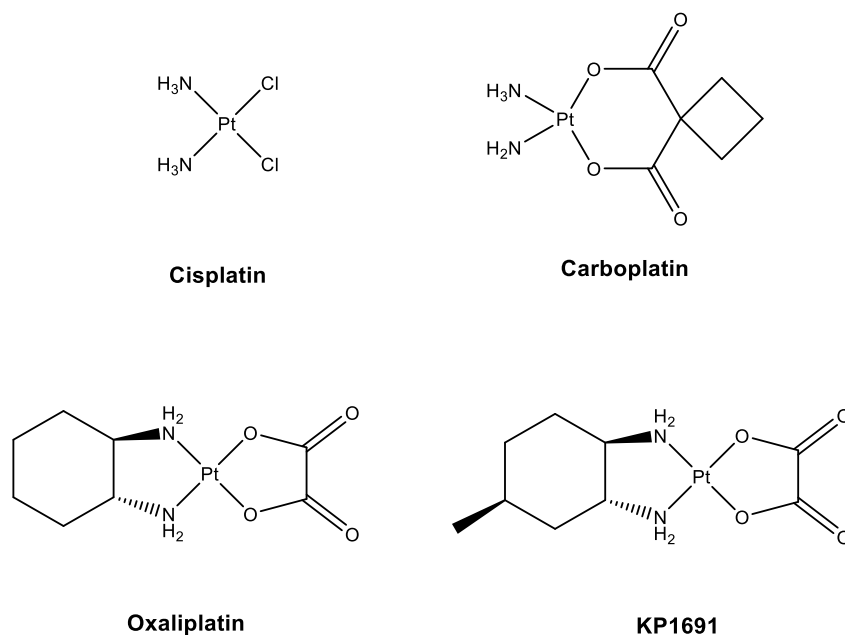
Further studies showed that its mechanism of action is similar to that of alkylating agents, cross-linking DNA. The chlorido ligands can be replaced by aqua ligands, and the monoaqua complex  $\text{cis-}[\text{PtCl}(\text{NH}_3)_2(\text{H}_2\text{O})]^+$  can exchange its aqua ligand for coordination to DNA bases, with guanine being the preferred one. If the remaining chlorido ligand is replaced by another nucleobase, the resulting DNA cross-link leads to cell cycle arrest prior to replication or mitosis. Intrastrand cross-linking between two neighboring guanines is the most common type of adduct. When the cellular DNA repair mechanisms fail, intrastrand cross-linking is the major contribution to apoptosis induction by cisplatin. Side effects of cisplatin include nephro-, neuro-, and ototoxicity as well as nausea and emesis.<sup>33</sup>

Structural derivatives were tested, and second-generation platinum complexes emerged, leading to the approval of carboplatin for medical use in 1989. This drug is used in several cancer types such as ovarian and lung cancer and has the same mechanism of action as cisplatin. Myelosuppression is one of the side effects, but overall carboplatin is much safer to use than cisplatin due to the avoidance of nephrotoxicity. This was followed by the approval of oxaliplatin in 2004, which is especially active against colorectal cancer in contrast to its predecessors. The replacement of the ammine ligands with the *trans*-1,2-diamminocyclohexane (DACH) ligand leads to an increased inhibition of DNA synthesis.<sup>34</sup>

The established structure-activity relationships demanded neutral platinum complexes with planar or octahedral geometry, with two monodentate leaving groups in *cis* position (chloride ions in cisplatin) or one bidentate leaving group (oxalate in oxaliplatin, cyclobutane dicarboxylate in carboplatin)<sup>35</sup> as shown in Figure 6. While early research followed this idea, the failure of the resulting compounds in clinical trials and the need for drugs overcoming both intrinsic and

acquired cisplatin resistance of many tumors led to a great variation in the design of newly developed metal-based drugs. Amongst them are ruthenium-based drugs such as KP1019 and NAMI-A, which showed new mechanisms of action involving targeting cytoplasmic organelles or cell–ECM interactions, respectively. Different metal centers and ligands (including biologically active ones) have been used to synthesize countless potential new drugs, leading to a great variety of metal-based substances hitherto investigated, but from thousands of compounds screened in preclinical trials only a small number proceed to clinical trials.<sup>6</sup> Substances investigated in this master thesis are listed in the following chapters.

### 1.4.1 Platinum(II)



**Figure 6:** Structures of used Pt(II) compounds.

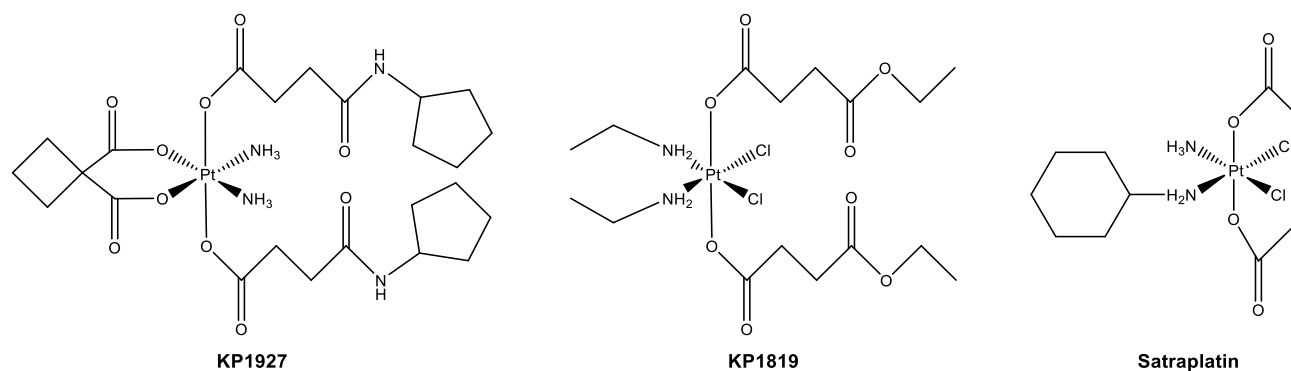
The first class of metal-based drugs that has been investigated for their antitumor activity and still the only of these substances to have been approved for use in cancer chemotherapy worldwide are Pt(II) drugs.<sup>6</sup> Their mechanisms of action, side effects and mechanisms of resistance have been extensively studied. Replacement of the leaving group(s) by aqua ligands precedes the formation of various DNA adducts. These adducts are recognized by damage-response proteins, which leads to cell-cycle arrest. Failure to repair the damaged DNA leads to cell death via apoptosis. While

**carboplatin** (here also called **KP1342**) shows cross-resistance to **cisplatin** (**KP1**), activity for **oxaliplatin** (**KP1343**) in various cisplatin-resistant models has been shown, consistent with a different set of clinical indications. Mechanisms of resistance can be tied to altered uptake and efflux of the drug, increased cellular thiol levels, which react with these platinum drugs, higher tolerance for DNA damage and failure of apoptotic pathways.<sup>36</sup> It has been claimed that more than 50% of all treated cancer patients receive either cisplatin, carboplatin or oxaliplatin as part of their treatment.<sup>6,37</sup>

### Pt1537 & Pt1691

The rationale behind the design of these drugs was to increase the steric bulk and lipophilicity of oxaliplatin, whilst adhering to its mechanism of action, therefore not altering the oxalato ligand. The substitution in the 4' position with a methyl group resulted in increased cytotoxicity for the axially substituted isomer (KP1691) and similar cytotoxicity for the (enantiomerically pure) equatorially substituted isomer (KP1537) compared to oxaliplatin. These *in vitro* results, received from standard 2D assays, could not be entirely confirmed by the *in vivo* results. KP1691 did not show any advantage over oxaliplatin in the leukemia model L1210 in mice, whilst KP1537 exhibited the highest efficacy of the analogues, due to its higher therapeutic index.<sup>34</sup>

## 1.4.2 Platinum(IV)



**Figure 7:** Structures of used Pt(IV) compounds.

The rationale behind the design of Pt(IV) compounds is to overcome the side effects of Pt(II) drugs. Compared to Pt(II) compounds these molecules are more inert, can therefore be administered orally and cause fewer reactions with other proteins. They offer more sites that allow modification

of pharmacological properties. Activation is facilitated by various mechanisms, depending on the ligand (e.g. activation by reduction, enzymatic activation). Therefore, these octahedral complexes are often referred to as prodrugs. They are eventually transformed into Pt(II) species that may then exert a mode of action similar to that of known platinum(II) drugs, depending on the equatorial ligands.

**Satraplatin** is one of the first Pt(IV) drugs that completed phase III clinical trials and shows several benefits over cisplatin. It can be administered orally, leads to increases in progression-free survival, has a similar activity as carboplatin but a more favorable toxicity profile.<sup>37</sup> However, it was not approved by the FDA due to the lack of benefit in overall survival.<sup>38</sup>

Modification of the axial ligands can lead to a great variation in the reduction potential, which correlates with efficacy as a prodrug. An ideal Pt(IV) drug would have a redox potential low enough to prevent extracellular reduction and would therefore show lower toxicity, but high enough for the reductive milieu of the tumor cells and tissue to form the active species. The redox potential of carboxylato ligands, such as in satraplatin, was deemed suitable for that purpose and therefore led to the design of **KP1819**, a bis(carboxylato)dichloridobis(ethylamine)platinum(IV) complex. *In vitro*, MTT results showed slightly higher cytotoxicity in the cisplatin-sensitive CH1 (PA-1) cell line and a 10-fold increase in cytotoxicity in the intrinsically cisplatin-resistant SW480 cell line.<sup>39</sup> In an *in vivo* study, this compound was compared to satraplatin. Whereas satraplatin seems to be quite ineffective against CT26 tumors in mice, KP1819 showed clearly higher efficacy.<sup>38</sup>

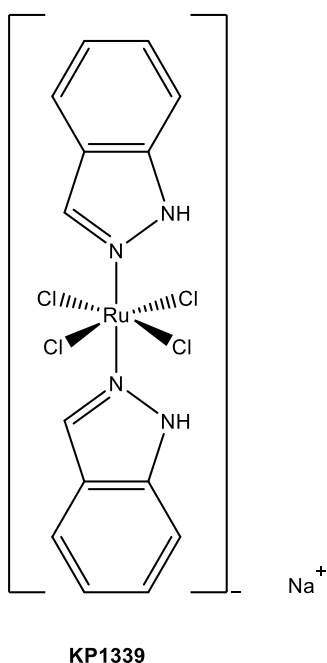
**KP1927** was designed to get an analogue of carboplatin that might have a higher cytotoxicity due to the increased lipophilicity provided by the axial ligands. Despite the compound's higher lipophilicity, the cytotoxicity in the CH1 (PA-1) cell line is 10 times decreased compared to carboplatin and negligible in SW480.<sup>40</sup> Despite its higher IC<sub>50</sub> (see page 28) values *in vitro* compared to KP1819, it did show comparable antitumor activity in the CT26 tumor model in mice when administered orally. In contrast to KP1819 it did not show any significant effects when given intraperitoneally. Therefore MTT testing seems to be inconclusive for oral administration for these substances.<sup>38</sup>

### 1.4.3 Ruthenium Complexes

Ruthenium complexes have an octahedral geometry and therefore differ from the square-planar geometry of the approved Pt(II) drugs, which can be an advantage at overcoming resistance mechanisms. Various oxidation states of the metal are achievable (II, III, IV) and ligand exchange rates similar to platinum complexes can be obtained. Its similarity to iron facilitates the binding to serum transferrin and, together with binding to serum albumin, is likely to contribute to its lower toxicity.<sup>6</sup>

NAMI-A (a ruthenium-DMSO compound) and KP1019 (a Ru(III) compound) were evaluated in clinical trials, whereas KP1339 (a close analog of KP1019, see below) still is and might be the first ruthenium compound with a high chance of being approved for application. A completely different class of ruthenium complexes are Ru(II)-arene compounds in a half-sandwich conformation.

#### 1.4.3.1 Ru(III): KP1339



**Figure 8:** Structural formula of KP1339, the only Ru(III) compound used here.

KP1019 (indazolium *trans*-[tetrachloridobis(1*H*-indazole)ruthenate(III)] ) is a Ru(III) complex that has been under investigation for over three decades. It showed promising results in clinical phase

I trials, leading to disease stabilization in 5 out of 6 patients with advanced solid tumors. **KP1339**

– sodium *trans*-[tetrachloridobis(1*H*-indazole)ruthenate(III)], the sodium salt analogue, was designed to improve the solubility and to facilitate intravenous administration of the drug. Figure 8 shows the structure of the sodium analog.

For Ru(III) complexes such as KP1339 activation by reduction is proposed as part of its mechanisms of action. The reductive environment in solid tumors, caused by hypoxic conditions as discussed in sections 3.1 and 3.3.2, can facilitate the transition from Ru(III) to Ru(II), therefore generating a more reactive species formed in tumor tissue.

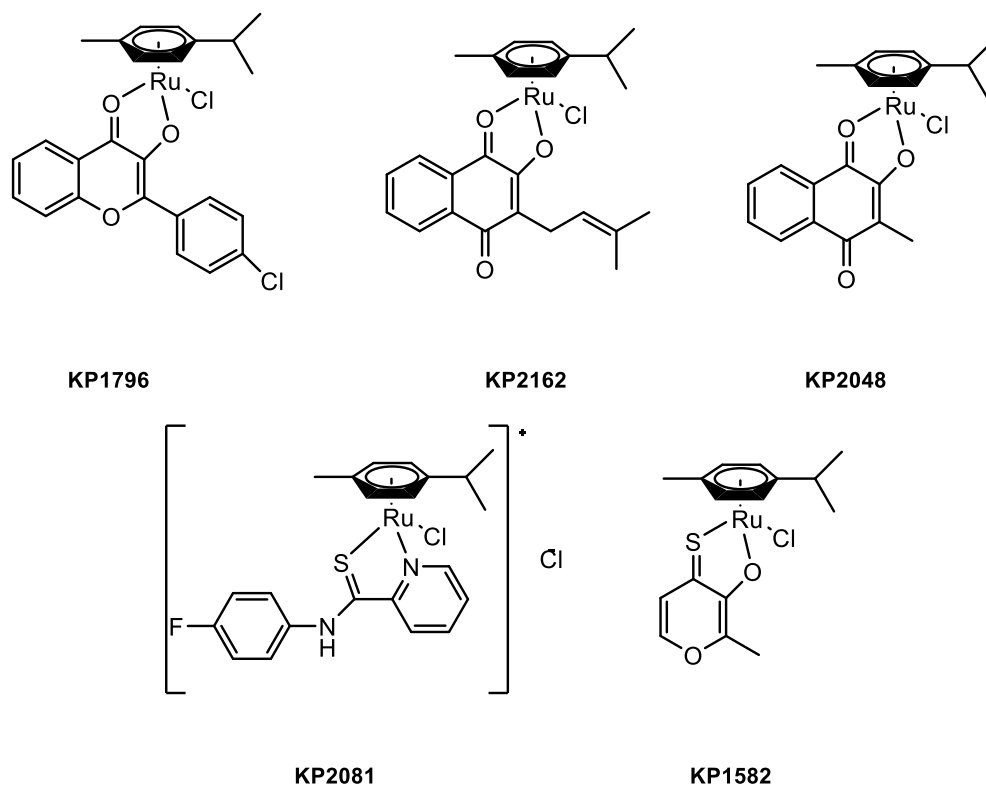
Increased levels of transferrin receptors in malignant cells, caused by a high demand for iron and promoted by hypoxia, would contribute to such a tumor-specific mode of action. For its analogue KP1019 the mode of action has been investigated extensively and binding of the substance to the iron binding sites in transferrin indeed occurs. Release of the substance in the endosomes is assumed. Tumor reducing qualities of KP1090, seen in *in vivo* experiments are highly influenced by the presence of transferrin receptors and its activation by reduction principle.<sup>41</sup>

The compound activates the intrinsic mitochondrial pathway and early onset of the mitochondrial membrane depolarization suggests direct interaction. This is influenced by the capacity of the compound to generate reactive oxygen species (ROS), since addition of antioxidant reduces depolarization and decreases cytotoxicity. However, other studies found a sensitization to KP1339 by inhibition of DNA repair pathways. Processing of the induced DNA lesions seems different from those induced by cisplatin.<sup>41</sup>

Induction of ER (endoplasmic reticulum) stress is another relevant factor in its cytotoxic properties, caused by the presence of a high number of damaged and misfolded proteins leading to the unfolded protein response (UPR). UPR leads to an antiapoptotic or a proapoptotic response if the unfolded protein accumulation exceeds a threshold, which can be caused by high levels of ROS. KP1339 also downregulates GRP78 on the protein level, suggesting an ER associated protein degradation.<sup>42</sup> GRP78 is upregulated in tumors and associated with drug resistance and tumor progression.

Despite its low cytotoxicity the compound KP1339 showed promising results in first clinical studies. A phase I study showed high tolerability and safety of the drug. Due to the effect on GRP78, combination with other drugs could be beneficial and is proposed for further studies.<sup>43</sup>

### 1.4.3.2 Ru(II)-arene complexes



**Figure 9:** Structures of used Ru(II)-arene compounds.

The arene moiety of these complexes provides enough lipophilicity for cell accumulation (cyclopentadienyl or para-cymene ligands are often used), whilst the hydrophilic metal center contributes to its solubility.<sup>44</sup> Various organometallic substances, shown in Figure 9, with potentially intercalating or DNA groove binding ligands have been synthesized and tested for their anti-tumor activity.

**KP1582** - Chlorido[3-(oxo-κO)-2-methyl-pyran-4(1H)-thionato-κS4](η<sup>6</sup>-p-cymene)ruthenium(II)

In a series of Ru(II)-cymene complexes with a variety of pyrone ligands, the thiomaltol complex KP1582 showed the highest activity *in vitro*. This correlates with the higher lipophilicity of thiomaltol compared to maltol. The position of the methyl group within thiomaltol also influences the activity of the complex. Due to the results *in vitro* and since it is a potentially prototypic

structure for derivatization of the thiomaltol moiety this organometallic compound was chosen for further investigation *in vivo*.<sup>45</sup>

**KP1796** – Chlorido[3-(oxo-κO)-2-(4-chlorophenyl)-chromen-4(1*H*)-onato-κO](η<sup>6</sup>-*p*-cymene)-ruthenium(II)

Using a flavonoid as a ligand in this Ru(II)-arene complex creates a structure that is capable of interacting with topoisomerase IIα, an enzyme essential for DNA replication. Compared to other tested substances with a flavonoid ligand, this compound showed the highest ability to inhibit topoisomerase IIα, correlating with its activity *in vitro*. The *in vitro* activity of this complex is comparable to cisplatin in SW480 and in the low micromolar range for CH1 and A549, which is outstanding for Ru(II) compounds. Due to its ability not only to inhibit topoisomerase but also to bind DNA with its metal center it is a candidate for overcoming acquired resistance to compounds such as cisplatin.<sup>46</sup>

**KP2048** - Chlorido(2-hydroxy-3-methyl-1,4-naphthoquinato)(η<sup>6</sup>-*p*-cymene)ruthenium(II)

The design of this drug is also based on the promising findings of Ru(II) half-sandwich complexes. It showed higher activity *in vitro* than KP1339 and first *in vivo* experiments in CT26 tumor models in mice were promising as well.<sup>47</sup>

**KP2081** - Chlorido(η<sup>6</sup>-*p*-cymene)(*N*-{4-fluorophenyl}-2-pyridinecarbothioamide)ruthenium(II)] chloride / **plecstatin-1**

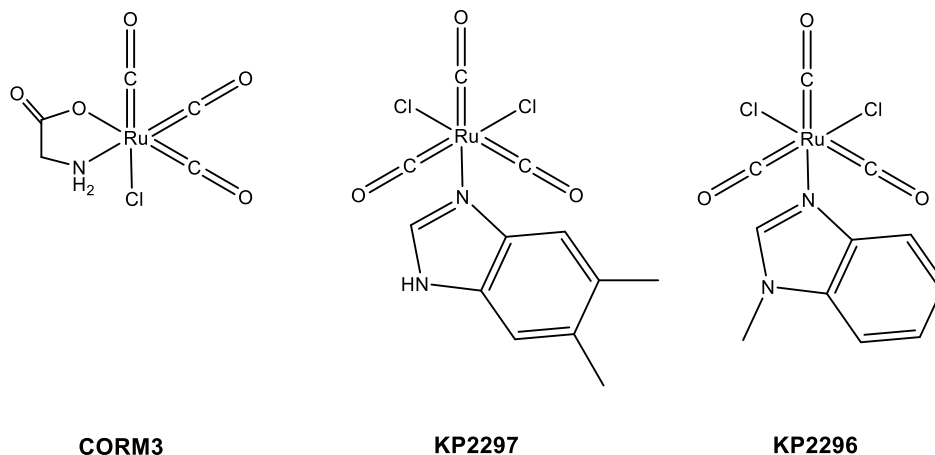
*N*-substituted 2-pyridinecarbothiamide (PCA) compounds exhibit a low acute toxicity and are known for their gastric mucosal protecting properties, making them suitable ligands for orally administered drugs since there are reports of ligand cleavage from the metal center for some donor atom systems. In a series of similar Ru(II) compounds, plecstatin-1 showed the highest cytotoxicity *in vitro* and high stability under acidic conditions, which encouraged its testing *in vivo*.<sup>48</sup> Upon oral administration to mice it showed activity in the CT26 solid tumor model and even higher antitumor activity against B16 melanoma. Plectin, a structural protein involved in cytoskeleton organization and in cellular motility, was found to be the main target of this drug.<sup>49</sup>

**KP2162** - Chlorido[(3-(3-methylbut-2-enyl)-2-oxo-κO)-[1,4]-naphthoquinonato-κO](η<sup>6</sup>-*p*-cymene)ruthenium(II)

With a similar intention as for KP1796, integration of a bioactive ligand into an anticancer metal complex led to the design of a Ru(II)-arene complex with a lapachol ligand. The antibiotic and

anticancer properties of lapachol reported by other authors led to this choice of ligand. It hydrolyses fast to the active aqua complex and shows  $IC_{50}$  values in the low micromolar range *in vitro*.<sup>50</sup>

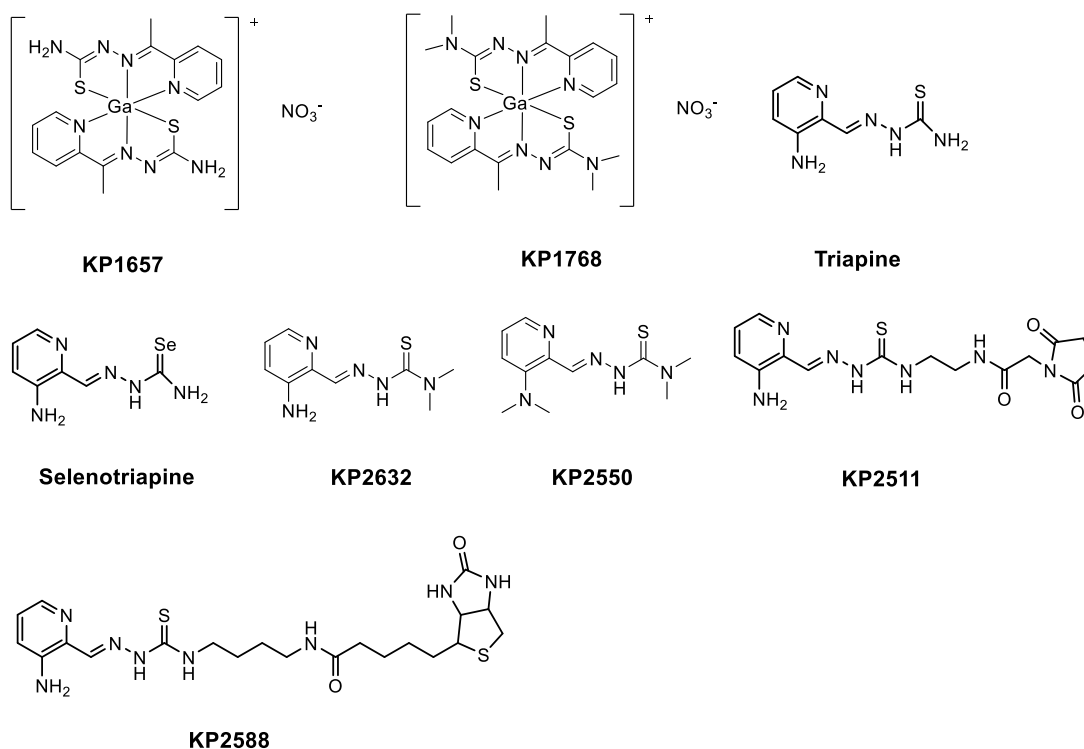
#### 1.4.3.3 Ru(II)-CO complexes (2296, 2297, CORM-3)



**Figure 10:** Structures of used Ru(II)-CO complexes.

CO-releasing molecules such as **CORM3** (tricarboxylchlorido(glycinato)ruthenium(II)) have shown beneficial effects in inflammatory diseases and sepsis. CORM3 can improve renal function after cisplatin-induced nephrotoxicity or acute renal failure and reduce injury from myocardial infarction in mice.<sup>51</sup> To gain knowledge about the anticancer properties of this substance class, **KP2296** - *fac*-[Ru(II)(CO)<sub>3</sub>Cl<sub>2</sub> (N-methylbenzimidazole)] and **KP2297** - *fac*-[Ru(II)(CO)<sub>3</sub>Cl<sub>2</sub> (5,6-dimethylbenzimidazole)] were synthesized and tested *in vitro* and *in vivo* in murine colon carcinoma models (Figure 10).<sup>52</sup>

## 1.4.4 Thiosemicarbazones



**Figure 11:** Structures of used thiosemicarbazones.

This class of organic substances (Figure 11) comprises inhibitors of ribonucleotide reductase (RR). RR is an enzyme responsible for the conversion of ribonucleotides into deoxyribonucleotides, therefore providing the resources for DNA synthesis and repair. The R1 subunit of the enzyme binds the substrates, while the R2 subunit contains the components for its catalytic activity - a tyrosyl radical stabilized by an iron center. Especially  $\alpha$ -N-heterocyclic thiosemicarbazones, known tridentate iron chelators, are potent inhibitors of RR activity, which is essential for cell proliferation.<sup>53</sup>

### **Triapine/KP1690** - 3-Aminopyridine-2-carboxaldehyde thiosemicarbazone

Triapine has entered phase I and II of clinical trials as an antitumor agent. The presence of iron is essential for its antiproliferative activity and the iron complex of triapine is likely to be the active species, to generate ROS (reactive oxygen species) and to destroy the tyrosyl radical.<sup>54,55</sup> Due to

its fluorescent properties, it was possible to monitor its intracellular distribution, showing a strong affinity of triapine towards the nuclear membrane<sup>56</sup>. Furthermore, accumulation in the endoplasmic reticulum (ER) and/or the mitochondria and induction of ER stress could be demonstrated. Triapine induces proapoptotic signaling of the UPR, independent of ROS generation.<sup>57</sup>

**KP2550** - 3-(Dimethylamino)pyridine-2-carbaldehyde-*N,N*-dimethylthiosemicarbazone

Research to find compounds with an increased cytotoxicity compared to triapine showed that increased activity correlates with terminal dimethylation. This fully methylated derivative shows a tremendously decreased IC<sub>50</sub> value (from the micromolar to nanomolar range) *in vitro* and was active in triapine-resistant SW480 cells.<sup>58</sup>

**KP2632** - 3-Aminopyridine-2-carboxaldehyde-*N,N*-dimethylthiosemicarbazone hydrochloride

This compound also shows the tendency of an increased cytotoxicity *in vitro* seen in terminally dimethylated triapine derivatives, although the effect is not as significant as for KP2550. However, this compound was also able to overcome triapine resistance.<sup>58</sup>

**Selenotriapine / KP2634** - 3-Aminopyridine-2-carboxaldehyde selenosemicarbazone

Selenium compounds have been found less toxic in comparison to their thiosemicarbazone analogues, they also exhibit higher antiproliferative and antimicrobial activity and show better selectivity toward neoplastic cells compared to normal cells. Apoptosis induction and toxicity profile were superior in the selenium analogue compared to triapine.<sup>59</sup>

**BioTriapine/KP2588** - (*E*)-*N*-(4-(2-((3-aminopyridin-2-yl)methylene)hydrazine-1-carbothioamido)butyl)-5-(2-oxohexahydro-1*H*-thieno[3,4-*d*]imidazol-4-yl)pentanamide

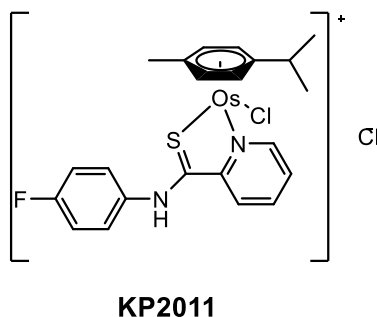
In an attempt to increase tumor targeting in triapine, the drug was linked to biotin. This is a common strategy since cancer cells often overexpress receptors for biomolecules such as biotin. The sodium-dependent multivitamin transporter, largely responsible for the import of biotin, is overexpressed in many cancer cells, making biotin a suitable carrier for an increased uptake and accumulation in tumor tissue. However *in vitro* and *in vivo* studies showed no significant change in cytotoxicity or tumor growth inhibition.<sup>60</sup>

**KP2511** - (*E*)-*N*-(2-(2-((3-aminopyridin-2-yl)methylene)hydrazine-1-carbothioamido)ethyl)-3-(2,5-dioxopyrrolidin-1-yl)propanamide

This succinimide derivative of triapine showed decreased cytotoxicity *in vitro* and promoted tumor growth *in vivo*.

In addition to the mentioned metal complexes gallium(III) complexes such as KP46 are investigated for their antitumor activity. Due to the similarities to  $\text{Fe}^{3+}$ ,  $\text{Ga}^{3+}$  can bind to transferrin, thereby increasing cellular uptake of these compounds. One of the targets of gallium complexes is RR, in which it replaces the iron ion of the R2 subunit. The destabilization of the tyrosyl radical by  $\text{Ga}^{3+}$  leads to the inhibition of this enzyme.<sup>6</sup> Thiosemicarbazones can serve as tridentate ligands for  $\text{Ga}^{3+}$ , resulting in increased cytotoxicity levels due to the synergistic action of central metal and ligand. Although the cytotoxic effects are mainly attributed to the thiosemicarbazone ligands, complexation to gallium(III) seems beneficial especially compared with iron(III) complexes.<sup>61</sup> Complexes such as **KP1657** - [bis(2-acetylpyridinethiosemicarbazonato)-*N,N,S*-gallium(III)] nitrate<sup>54</sup> with  $\text{IC}_{50}$  values in the micromolar range or **KP1768** - [bis(2-acetylpyridine *N,N*-dimethylthiosemicarbazonato)-*N,N,S*-gallium(III)] nitrate<sup>61</sup> with  $\text{IC}_{50}$  values in the nanomolar range were synthesized and tested to determine structure-activity relationships for this substance class. Compounds with such a high cytotoxicity may have the drawback of a small therapeutic window.

### 1.4.5 Osmium



**Figure 12:** Structure of KP2011, the osmium(II) analogue of KP2081

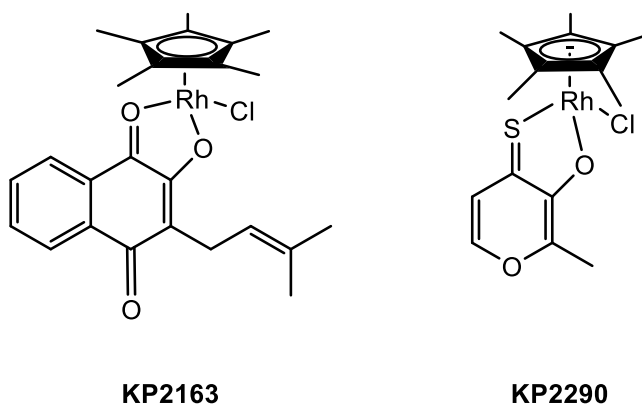
The antitumor properties of this heavier iron and ruthenium congener have been discovered upon the synthesis of Os(II) arene complexes, which showed cytotoxicity levels comparable to cisplatin. Earlier osmium complexes were often too inert. The synthesis of Os(II) analogues to ruthenium

compounds is just one of many branches in current research for chemotherapeutic osmium compounds.<sup>44</sup>

**KP2011** - Chlorido( $\eta^6$ -*p*-cymene)(*N*-{4-fluorophenyl}-2-pyridinecarbothioamide)osmium(II)] chloride

This compound (Figure 12) is the osmium(II) analogue of KP2081 and, due to the changed metal center, it has a slightly higher lipophilicity and altered cytotoxic profile. It can undergo S→O exchange and the metal coordination changes from N,S- to N,N-bidentate, facilitating DNA binding and suggesting a dual mode of action.<sup>48</sup>

### 1.4.6 Rhodium



**Figure 13:** Structures of used Rh(III) complexes.

Research into rhodium complexes as anticancer drugs started in the 1970s. Complexes of various oxidation states (Rh(I), Rh(II) and Rh(III)) as well as mono- and dinuclear compounds were synthesized. This often resulted in unreactive compounds due to the inertness of the metal. Research into organorhodium(III) compounds, however, produced promising substances that are often analogues to ruthenium(II) compounds. The anionic (pentamethyl)cyclopentadienyl ligand is often used to provide a lipophilic moiety whilst three sites for hydrophilic ligands remain. The structure of two of these complexes are depicted in Figure 13. The cytotoxicity of these complexes can be mainly explained via DNA interaction.<sup>44</sup>

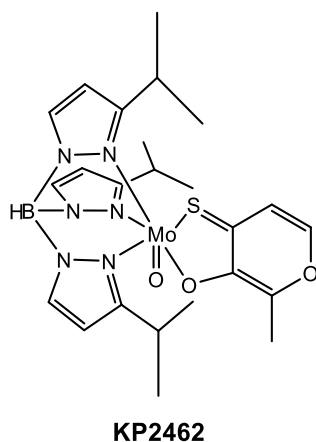
**KP2163** - Chlorido[(3-(3-methylbut-2-enyl)-2-oxo- $\kappa$ O)-[1,4]-naphthoquinonato- $\kappa$ O] ( $\eta^5$ -pentamethylcyclopentadienyl)rhodium(III)

This Rh(III) complex is an analogue to the Ru(II) complex KP2162. The arene consists of  $\eta^5$ -pentamethylcyclopentadiene instead of an  $\eta^6$ -*p*-cymene. Although *in vitro* activity was lower in the standard monolayer cultures for KP2163 than for KP2162 *in vivo* it showed a higher activity.<sup>50</sup>

**KP2290** - Chlorido{3-(oxo- $\kappa$ O)-2-methyl-pyran-4(1*H*)-thionato- $\kappa$ S}( $\eta^5$ -1,2,3,4,5-pentamethylcyclopentadienyl)rhodium(III)

This Rh(III) analogue of the aforementioned KP1582 - a ruthenium arene complex with a thiomaltol ligand - was synthesized and compared to the ruthenium(II) compound, it showed lower IC<sub>50</sub> values.<sup>62</sup>

### 1.4.7 Molybdenum



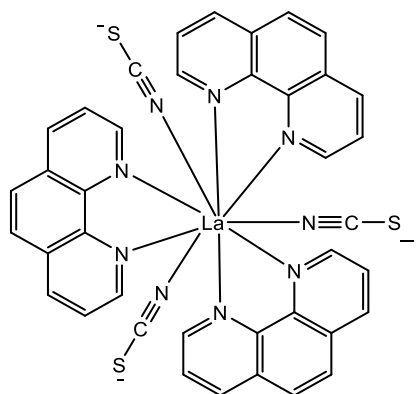
**Figure 14:** The structure of KP2462, the only investigated Mo(IV) compound.

Several molybdenum containing compounds that show carcinostatic activity have been discovered. Some of them are for example: Na<sub>2</sub>MoO<sub>4</sub><sup>63</sup>, heteropolyacidic Mo salts and polyoxomolybdates<sup>64</sup>. Molybdenum is also an essential trace metal for organisms and plays an important role as a cofactor for many enzymes. In organisms it is transported and excreted mainly as the anion [MoO<sub>4</sub>]<sup>2-</sup> with low toxicity, making it possible to use molybdenum containing complexes as therapeutic agents<sup>65</sup>. However, the mechanisms of action for most organometallic complexes of molybdenum are still not completely known but may well be related to DNA damage.

Possible explanations would include a direct interaction with DNA (e.g. intercalation into the double helix) or the oxidative action of oxygen free radicals generated by the chemical agents.<sup>66</sup>

**KP2462** - Hydrotris(3-isopropyl-1*H*-pyrazolyl)boro[2-methyl-3-(oxo- $\kappa$ O)-4*H*-pyran-4-thioato- $\kappa$ S]oxomolybdenum(IV) is a substance that showed high cytotoxicity *in vitro*.

### 1.4.8 Lanthanum



**KP772**

**Figure 15:** The structure of KP772, the only investigated La(III) compound.

Lanthanide (Ln) compounds have long been investigated for their anti-tumor properties.  $\text{Ln}^{3+}$  ions can bind to  $\text{Ca}^{2+}$  binding sites in biomolecules due to their similarity.<sup>67</sup> Antitumor properties are increased by complexation. Complexes with phenanthroline ligands induce cell cycle arrest in the G0/G1 phase.<sup>68</sup>

**KP772** - Tris(1,10-phenanthroline)tris(thiocyanato- $\kappa$ N)lanthanum(III)

This compound has shown activity against several cancer cell lines in monolayer and spheroid cultures. Activity in spheroids was not decreased by hypoxia.<sup>29</sup> *In vivo* results show activity against a colon carcinoma xenograft model.<sup>69</sup> No resistances against KP772 are acquired and research suggests activity against drug-resistant tumor types, which is why it has been proposed as a second-line treatment.

## 2 Aims

There is a divergence between compounds that show high activity *in vitro* and those that exert this activity *in vivo* in animal models. This is especially true for colon cancer. *In vivo* efficacy is influenced by more factors than flat monolayer cell culture can provide. Pharmacokinetic effects and toxicity are evaluated *in vivo* and determine the likelihood of a compound becoming a drug<sup>13</sup>. *In vitro* testing should provide a preselection of the countless synthesized compounds for several reasons. This includes ethical reason as well as cost efficacy. *In vitro* testing provides a more economical way to test substances in high throughput, using minimal substance amounts. In contrast to animal experiments, test conditions are more standardized, and results can be quantified easily.<sup>12</sup> Drug testing in spheroids is proclaimed to bridge the gap between *in vitro* and *in vivo* testing due to their similarities with tumor tissue.<sup>17</sup> Past experiments have shown the presence of a hypoxic core and a quiescent zone in spheroids, as well as a necrotic core in larger spheroids (diameter > 500  $\mu\text{m}$ ).<sup>28</sup> Cells that are arranged in a 3D manner resemble their tissue of origin more closely regarding their morphology. This provides the basis for studying drugs affected by hypoxia in tumor tissue, drug penetration in a model similar to avascular micrometastases and more complex experiments involving co-culture systems including other cell types.<sup>16</sup>

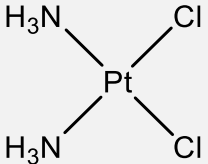
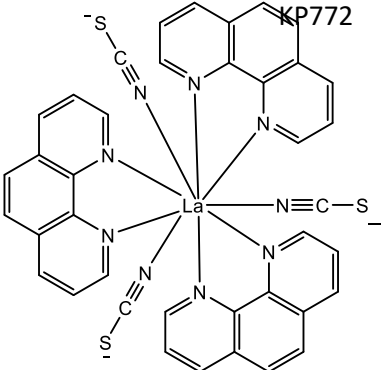
The aim of this thesis was to verify whether cytotoxicity testing in spheroids has a higher predictivity for *in vivo* efficacy than the classic 2D monolayer cell culture. For this purpose, a system had to be established that allowed drug testing in 2D and 3D in parallel. The used spheroid models had to be checked for proper conditions but also optimized for cytotoxicity testing with an appropriate throughput. After gaining *in vitro* data, statistical analysis to compare with the available *in vivo* data had to be carried out. Finding the most efficient testing system that allows better predictivity for *in vivo* efficacy (but ultimately for effectiveness in patients) would allow to cut time and costs in the search for anticancer drugs.

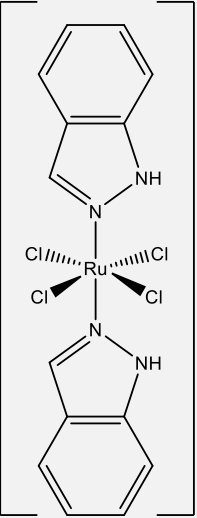
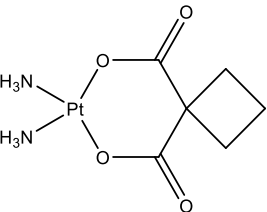
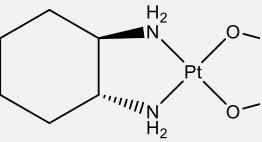
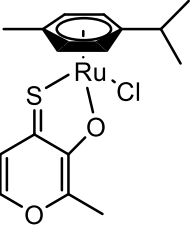
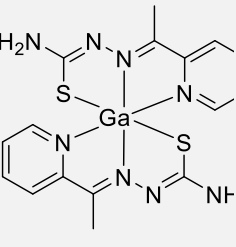
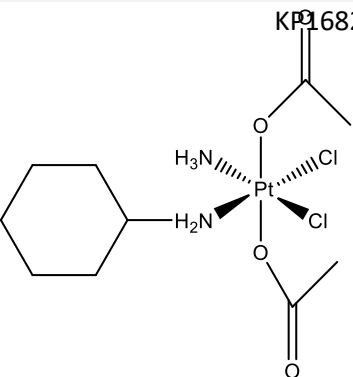
## 3 Material and Methods

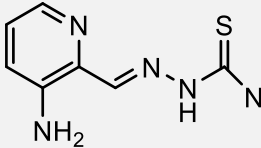
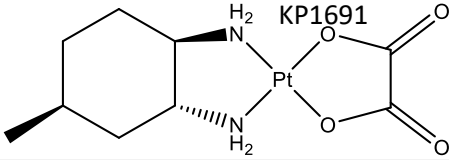

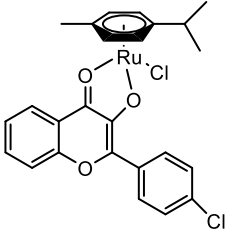
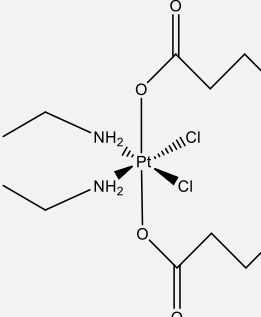
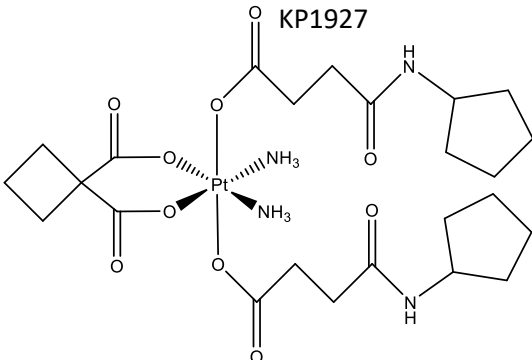
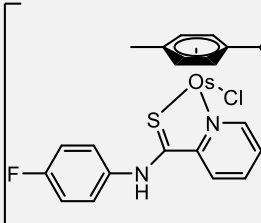
### 3.1 Substances

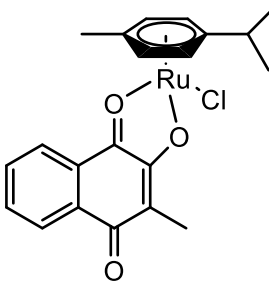
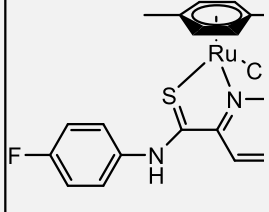
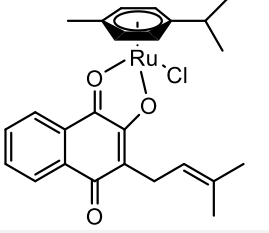
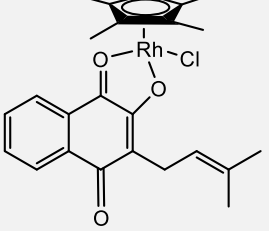
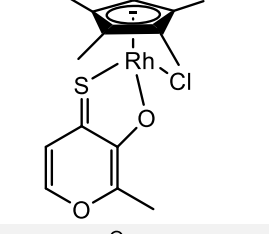
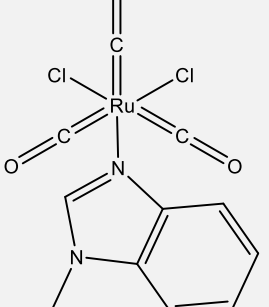
All used compounds were synthesized at the Institute of Inorganic Chemistry of the University of Vienna, except for CORM-3, which was purchased from Sigma-Aldrich. Table 1 gives the results of the *in vivo* testing of these substances, kindly provided by Dr. Petra Heffeter, Institute of Cancer Research, Medical University of Vienna. IC<sub>50</sub> values (obtained by MTT assays in SW480 cells) that were available from the Institute of Inorganic Chemistry prior to this master thesis are listed as well (with references to publications whenever available).

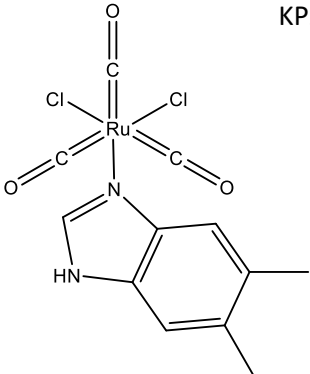
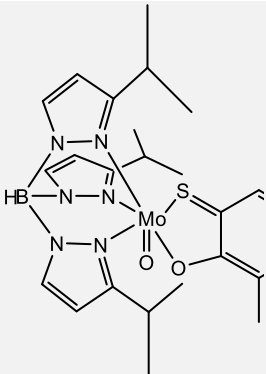
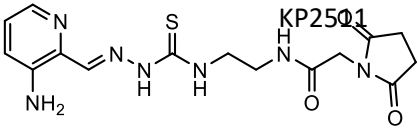
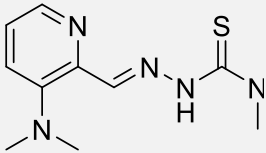
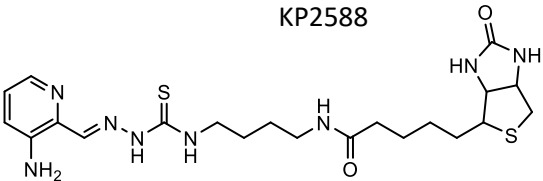
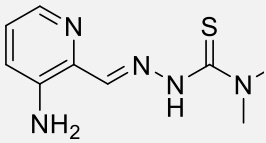
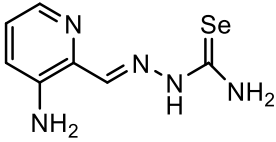
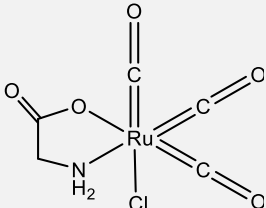
**Table 1:** Provided *in vivo* and *in vitro* data for all tested substances.

IUPAC Name	Substances	Central Ion	IC <sub>50</sub> (μM) in SW480 Cells
	Cisplatin	Pt(II)	3.3 ± 0.2 <sup>70</sup>
		La(III)	2.1 ± 0.3

	KP1339	Ru(III)	89 ± 19
	KP1342 = Carboplatin	Pt(II)	42 ± 10
	KP1343 = Oxaliplatin	Pt(II)	0.30 ± 0.08 <sup>34</sup>
	KP1582	Ru(II)	5.1 ± 0.5 <sup>45</sup>
	KP1657	Ga(III)	
	KP1682 = Satraplatin	Pt(IV)	1.5 ± 0.1 <sup>70</sup>

	KP1690 = Triapine	-	$0.55 \pm 0.2^{71}$
	KP1691	Pt(II)	$0.33 \pm 0.14^{34}$
	KP1768	Ga(III)	
	KP1796	Ru(II)	$3.8 \pm 0.5^{46}$
	KP1819	Pt(IV)	$0.30 \pm 0.05^{39}$
	KP1927	Pt(IV)	$500^{+40}$
	KP2011	Os(II)	$10 \pm 2^{48}$

	KP2048	Ru(II)	$15 \pm 3^{47}$
	KP2081	Ru(II)	$4.3 \pm 1.2^{48}$
	KP2162	Ru(II)	$4.1 \pm 1.5^{50}$
	KP2163	Rh(III)	$39 \pm 12^{50}$
	KP2290	Rh(III)	$1.0 \pm 0.1^{62}$
	KP2296	Ru(II)	$48 \pm 4^{52}$

	KP2297	Ru(II)	$44 \pm 7^{52}$
	KP2462	Mo(IV)	$0.46 \pm 0.34^{72}$
	KP2501	-	-
	KP2550	-	-
	KP2588	-	-
	KP2632	-	-
	KP2634 = Seleno-Triapine	-	-
	CORM3	Ru(II)	

## 3.2 Cell lines

In **Table 2** the used cell lines in this thesis are summarized. All cell lines were provided by the Institute of Cancer Research, Medical University of Vienna, checked for absence of mycoplasma contamination and authenticated by Multiplexion Inc. (Heidelberg, Germany).

**Table 2:** Used cell lines.

<i>Name</i>	<i>Species</i>	<i>Tissue/Organ</i>	<i>Tumor</i>
SW480 <sup>73</sup>	human	colon	adenocarcinoma
HCT116 <sup>74</sup>	human	colon	carcinoma
CT26 <sup>75</sup>	mouse	colon	carcinoma

## 3.3 Media

Table 3 shows the used cell culture media. All media were supplemented with 10% heat-inactivated fetal bovine serum (FBS, BioWest) and 4 mM L-glutamine (Sigma-Aldrich). MEM was supplemented with 1% MEM Non-Essential Amino Acid Solution (Sigma-Aldrich) and 1 mM sodium pyruvate (Sigma-Aldrich). Further mentions of medium will refer to supplemented medium, unless stated otherwise.

**Table 3:** Used cell culture media.

<i>Cell culture medium</i>	<i>Abbreviation</i>	<i>Provider</i>
R5886 RPMI-1640 (HEPES Modification)	RPMI-1640	Sigma-Aldrich
M2279 Minimum Essential Medium Eagle	MEM	Sigma-Aldrich
51448C Dulbecco's Modified Eagle's Medium/Ham's Nutrient Mixture F12	DMEM/Ham F12	Sigma-Aldrich

## 3.4 Other Chemicals and Solutions

Listed below in Table 4 are all not otherwise stated chemicals and solutions used.

**Table 4:** Further chemicals and solutions.

<i>Name</i>	<i>Abbreviation</i>	<i>Provider</i>
<i>Ethanol, 96%</i>		Roth
<i>Ethanol, 70%</i>		-
<i>Dimethyl sulfoxide</i>	DMSO	Fisher Chemicals
<i>Dulbecco's Phosphate Buffered Saline</i>	PBS	Sigma-Aldrich
<i>Dulbecco's Phosphate Buffered Saline powder</i>	PBS powder	Gibco
<i>Paraformaldehyde 32%, EM Grade</i>	PFA	VWR
<i>Pimonidazole</i>		Hypoxypore
<i>ProLong™ Gold Antifade Mountant with DAPI</i>	Mountant with DAPI	Thermo Fisher Scientific
<i>Triton X</i>		Sigma-Aldrich
<i>Trypsin – EDTA</i>	Trypsin	Sigma-Aldrich
<i>Thiazolyl Blue</i>	MTT	Sigma-Aldrich
<i>Tetrazolium Bromide</i>		
<i>0.25 g MTT in 50 mL PBS</i>	MTT solution	
<i>Trypan blue</i>		Sigma-Aldrich

## 3.5 Instruments and Labware

All used instruments and labware are listed in Table 5 below.

**Table 5:** Used instruments and labware.

75 cm <sup>2</sup> Cell culture flasks (CytoOne™, Starlab)
10 µL, 200 µL, 1,000 µL Pipettes (Eppendorf) and matching tips (autoclaved)
Multipipette E3 and 1 mL Combitips (Eppendorf)
Accu-jet® Pro (BRAND®)
Serological pipettes (Starlab)
<b>Petri dishes (Thermo-Fisher Scientific)</b>
2 mL Tubes (Eppendorf)

15 mL Centrifuge tubes (Starlab)
Megafuge 1.0R (Heraeus)
Neubauer cell counting chamber (Hecht)
Inverted microscope (Euromex)
Vortex mixer (LabDancer, IKA™)
SuperFrost Plus™ Adhesion slides (Thermo-Fisher Scientific)
Coverslips 24 x 50 mm (Menzel)
PAP pen for immunostaining (Vector Laboratories)
Cryostat microtome CM3050S (Leica)
Microtome blades (Leica)
Confocal laser-scanning microscope LSM 800 (Zeiss)

### 3.6 Culture Conditions

Frozen aliquots of the cells were thawed at 37 °C for several minutes and then transferred to a 15 mL tube containing 10 mL of medium. After centrifugation at 1200 g (3 min) the cell pellet was resuspended in 3 mL fresh medium. This cell suspension was added to 10 mL medium in a 75 cm<sup>2</sup> culture flask. After 24 h the medium was changed. For further use the adherent cells were kept at 37 °C, 5% CO<sub>2</sub> and a humidified atmosphere for 2 to 4 days before passaging. For subculturing the medium was removed, cells were washed with 5 mL PBS and 2 mL trypsin were added to the flask. After 3 min of incubation at 37 °C the detachment of cells was checked under the microscope and helped by gently tapping the flask if necessary. Trypsin was deactivated by addition of 5 mL fresh medium. To gain single cell suspensions the cell suspension was repeatedly pipetted up and down. Depending on the previously noted confluence of the cell line, 10–30% of the suspension were left in the flask and mixed with 10 mL of fresh medium.

For seeding cells, the cell suspension was centrifuged in a 15 mL tube at 1200 g for 3 min. The cell pellet was resuspended in 2 to 5 mL fresh medium and the number of cells/mL was determined by mixing the suspension 1:10 with trypan blue (100 µL, half diluted) and counting viable cells with a Neubauer chamber. The cell suspension was diluted to the desired density of cells/mL and mixed using a multichannel pipette.

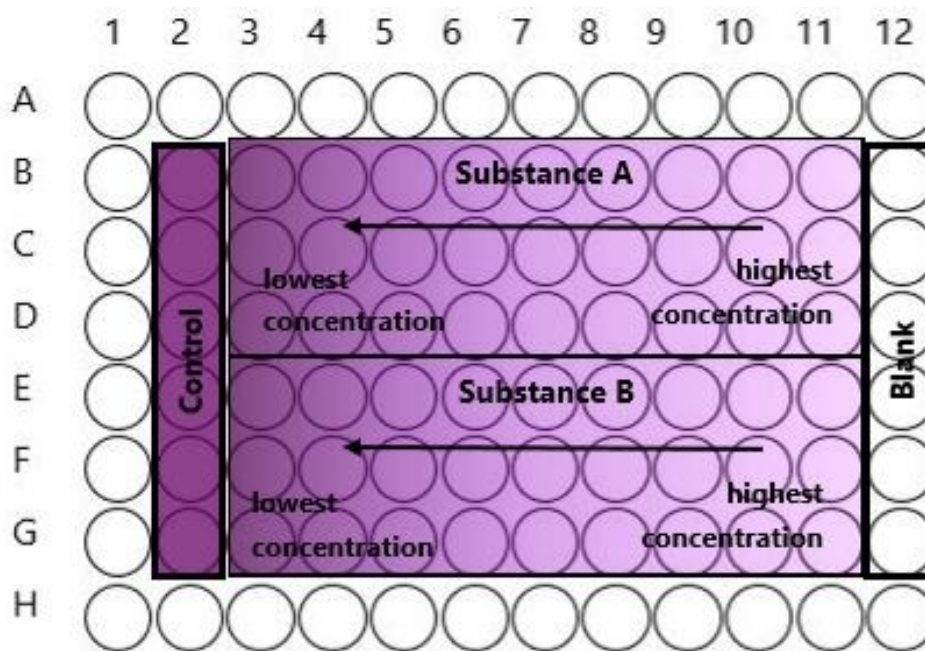
## 3.7 MTT Testing

### 3.7.1 Principle

MTT testing is usually carried out in 96-well plates, containing cells that are treated with increasing concentrations of the investigated compound. After an incubation time span of 24 to 96 h 3-(4,5-dimethylthiazol-2-yl)-2,5-diphenyltetrazolium bromide (MTT), a yellow dye, is dissolved in PBS and added to the wells. This dye can penetrate cells and is transformed to the water insoluble violet formazan crystals. MTT is reduced to formazan by enzymes using NADH, so the amount of formed formazan correlates to cell metabolism and therefore can also be related to cell viability. After incubation of 4 h the medium in the wells is removed and replaced with DMSO to dissolve the formazan crystals. Absorption by formazan can be measured at 550 nm (close to its absorption maximum) with a plate reader against a reference wavelength of 660 nm. The measured optical density (OD) in relation to that of the untreated control is transformed to cell viability in percent. A concentration-effect curve obtained from such measurements will give the  $IC_{50}$  value, the (inhibitory) concentration at which the OD value is at 50% of the untreated control.<sup>16</sup>

### 3.7.2 Procedure

SW480 cells were seeded in 100  $\mu$ L MEM with a density of  $2 \cdot 10^3$  cells/100  $\mu$ L. (12 wells on the  $T_0$  plate were seeded in parallel. Their OD was measured the same day the substances were applied.) After a recovery time of 24 h at 37 °C, nine 1:2 dilutions of the substances (dissolved in 100  $\mu$ L medium per well) were added to three wells per concentration and experiment (Figure 16). Substances were either dissolved directly in medium (CORM-3) or in DMSO first and diluted in medium to give a maximum concentration of 1% DMSO on the cells. Dilutions were prepared in 15 mL tubes by 1:2 dilution steps with MEM. Table 6 shows the maximum concentration applied to the cells.



**Figure 16:** Configuration of a 96-well plate used in the MTT assay. 2 substances per plate can be tested with this design. 6 wells were used for the untreated control. 3 wells per concentration and substance were used, enabling the testing of 9 different concentrations per substance. 6 wells are used as blank (DMSO only).

**Table 6:** Substances tested with the MTT assay and their maximum applied concentration.

Substance	Max. concentration ( $\mu\text{M}$ )	Substance	Max. concentration ( $\mu\text{M}$ )
KP1657	25	KP1768	0.0125
KP2511	100	KP2550	0.025
KP2588	12.5	KP2632	6.25
KP2634	12.5	CORM-3	800

100  $\mu\text{L}$  MEM were added to the control wells. After 96 h of incubation at 37  $^{\circ}\text{C}$  the medium was discarded and replaced with 100  $\mu\text{L}$  of MTT solution/RPMI-1640 medium (1:7). The cells were incubated for 4 h at 37  $^{\circ}\text{C}$  and 5%  $\text{CO}_2$  and the dyeing solution was replaced with 150  $\mu\text{L}$  DMSO to dissolve the formazan crystals. The absorption was measured at 550 nm against the reference wavelength of 690 nm with a BioTek microplate spectrophotometer ELx808 operated with Gen5 2.09 software. The cell viability was calculated in percent of the untreated control and the mean value of three technical replicates was taken into account for the concentration-effect curve and  $\text{IC}_{50}$  calculations. The experiment was repeated three times independently, except for weighing the

water insoluble substances and dissolving in DMSO. These three experiments were used to create the curve for concentration dependency of cytotoxicity and a mean IC<sub>50</sub>.

## 3.8 Optimization of CT26 Cell Number for Cytotoxicity Test in Monolayer Cultures

Literature recommends seeding of 2,000 or 4,500 CT26 cells per well with a substance exposure time of up to 72 h.<sup>76,77</sup> To optimize the setting for future substance testing on CT26 cells in 96 well plates, experiments have been carried out to choose a cell number for seeding (and the preferred medium). Cell line CT26 was subcultured in RPMI-1640 medium and DMEM/HAM F12, as described above. In either medium, CT26 cells have been seeded in the following densities:

### Experiment 1 (only CT26 in RPMI-1640):

1. 40,000 cells/mL
2. 30,000 cells/mL
3. 20,000 cells/mL (*via* 1:2 dilution of 1.)
4. 15,000 cells/mL (*via* 1:2 dilution of 2.)
5. 10,000 cells/mL (*via* 1:2 dilution of 3.)
6. 5,000 cells/mL (*via* 1:2 dilution of 5.)

### Experiments 2 and 3:

1. 80,000 cells/mL
2. 40,000 cells/mL (*via* 1:2 dilution of 1.)
3. 20,000 cells/mL (*via* 1:2 dilution of 2.)
4. 10,000 cells/mL (*via* 1:2 dilution of 3.)
5. 5,000 cells/mL (*via* 1:2 dilution of 4.)

Cells were seeded in 12 wells per concentration, 4 plates were prepared for CT26 (RPMI-1640) and CT26 (DMEM/HAM F12), each to be measured on days 1, 4, 5 and 6. The growth was measured *via* MTT assay, as described above (without application of substances).

### 3.9 Microscopy and Spheroid Measuring

For further experiments CT26 spheroids of a diameter between 300 and 600  $\mu\text{m}$ , 4 days after seeding were required. To obtain spheroids in this size range CT26 cells (in RPMI-1640 medium) were seeded in various numbers (see Table 7) into ultra-low attachment round-bottom 96 well plates (Costar) and diameters of the resulting spheroids measured on days 4 to 6. In another experiment CT26 cells were seeded in two different media (DMEM/HAM F12 and RPMI-1640) to compare growth. The diameter of three different spheroids per seeded cell number was measured twice using the Olympus CKx41 inverted microscope with ColorView camera and Cell<sup>^</sup>F software. HCT116 spheroids (previously in RPMI-1640 medium) were subcultured in DMEM/HAM F12 and seeded in the same numbers as in CT26 experiments 2 and 3 (see above) into round-bottom 96 well plates, using a quarter of a plate (24 wells) for each cell line/medium. The diameter of four spheroids per cell number, cell line and medium was measured four times each. In a final experiment only CT26 cells in DMEM/HAM F12 were seeded at a cell number of 400 per well. After the trypsin solution was neutralized, each cell suspension was split in half and each part centrifuged and resuspended separately. Cells counting and preparation of the 4,000 cells/mL suspension was also carried out independently for these cells (referred to as CT26 DMEM/HAM F12 2(1) and CT26 DMEM/HAM F12 2(2)).

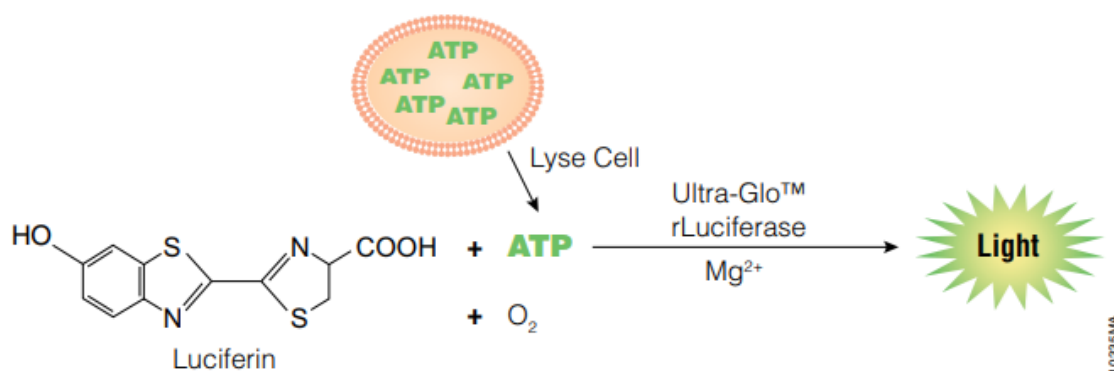
**Table 7:** Seeded cell numbers for determination of growth curves of CT26 spheroids in RPMI-1640.

<i>Cells/mL</i>	<i>Preparation</i>	<i>Total volume (mL)</i>
40,000	Directly via dilution from the resuspended cell pellet after trypsinization.	20
30,000	Directly via dilution from the resuspended cell pellet after trypsinization.	10
20,000	Via 1:2 dilution of the 40,000 cells/mL suspension.	30
15,000	Via 1:2 dilution of the 30,000 cells/mL suspension.	20
10,000	Via 1:2 dilution of the 20,000 cells/mL suspension.	20
5,000	Via 1:2 dilution of the 10,000 cells/mL suspension.	10

## 3.10 Cytotoxicity Testing Using the CellTiter-Glo® 2.0 Assay in Monolayer Cultures and CellTiter-Glo® 3D in Spheroids

### 3.10.1 Principle

CellTiter-Glo® (from Promega) is a pre-mixed reagent that indicates ATP content, resulting in luminescence by using luciferase. Cellular ATP and the used Ultra-Glo™ rLuciferase convert Luciferin to Oxyluciferin, as shown in Figure 17. The measured luminescence is directly proportional to the number of viable cells in the tested sample. For cell culture purposes, CellTiter-Glo® 2.0 for monolayer testing and CellTiter-Glo® 3D for spheroid testing are provided. A lysing agent is added for 3D experiments, to ensure equal distribution over all cells present. This sensitive reagent is frequently used in cytotoxicity testing with spheroids.<sup>31,78,79</sup>



**Figure 17:** Generation of light emission in viable cells using the CellTiter-Glo® reagents.

### 3.10.2 Procedure for Monolayer Cell Culture

CT26 cells and HCT116 cells were seeded in 100 µL DMEM/HAM F12 per well with a density of  $1.5 \cdot 10^3$  cells/100 µL into black, flat-bottom 96-well plates (Falcon). After a recovery period of 24 h at 37 °C and 5% CO<sub>2</sub>, six 1:2 dilutions of the substances (dissolved in 100 µL medium) were added to three wells per concentration and experiment (Figure 18). Substances were either dissolved directly in medium or in DMSO and further diluted in medium to give a maximum concentration of 1% DMSO on the cells. Dilutions were prepared in 15 mL tubes by 1:2 dilution steps with

DMEM/HAM F12 giving a total volume of 4 mL. Table 8 shows the maximum concentrations applied to the cells. 100  $\mu$ L DMEM/HAM F12 were added to the control wells.

After 96 h of incubation at 37 °C and 5% CO<sub>2</sub> the plates were cooled down to room temperature. Half of the medium was discarded and replaced with 100  $\mu$ L of CellTiter-Glo® 2.0 reagent. The cells were placed on a shaker for 2 min and further incubated for 10 min at room temperature. The luminescence was recorded using a Synergy HT multimode microplate spectrophotometer (BioTek) operated with Gen5 2.09 software. The cell viability was calculated in percent of the untreated control and the mean value of three technical replicates was used for the concentration-effect curve and IC<sub>50</sub> calculations. The experiment was repeated three times independently, except for weighing of the organic substances and their dissolution in DMSO. These three experiments were averaged to create the concentration-effect curves of the substances and a mean IC<sub>50</sub>.

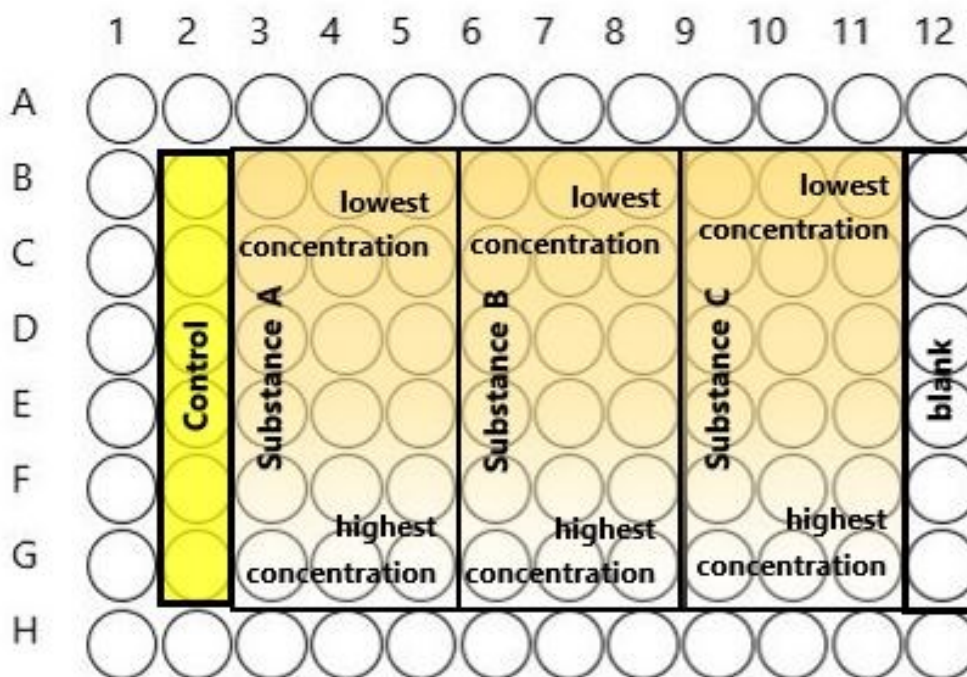
### 3.10.3 Procedure for Spheroids

CT26 cells and HCT116 cells were seeded in 100  $\mu$ L DMEM/HAM F12 per well with a density of  $4 \cdot 10^2$  cells/100  $\mu$ L into black, round-bottom 96-well plates with ULA coating (Costar®). After incubation for 96 h at 37 °C and 5% CO<sub>2</sub>, the size and shape of the formed spheroids was checked and six 1:2 dilutions of the substances (dissolved in 100  $\mu$ L medium) were added to three wells per concentration and experiment (Figure 18). Substances were dissolved and diluted as described above. 100  $\mu$ L DMEM/HAM F12 were added to the control wells.

After 96 h of incubation at 37 °C and 5% CO<sub>2</sub> the plates were cooled down to room temperature. Half of the medium was discarded and replaced with 100  $\mu$ L of CellTiter-Glo® 3D reagent. The cells were placed on a shaker for 5 min and further incubated for 25 min at room temperature. The luminescence was recorded and data from three independent experiments were evaluated as described above.

**Table 8:** Substances tested with the CellTiter-Glo® assay and their maximum applied concentration.

KP number	Maximum applied concentration (µM)			
	Monolayer		Spheroids	
	HCT116	CT26	HCT116	CT26
<i>Cisplatin</i>	25	3.125	100	12.5
1339	800	800	800	800
1342 = <i>Carboplatin</i>	100	50	400	200
1343 = <i>Oxaliplatin</i>	3.125	3.125	12.5	25
1582	50	100	800	800
1657	6.25	6.25	6.25	6.25
1682 = <i>Satraplatin</i>	12.5	12.5	50	25
1690 = <i>Triapine</i>	3.125	3.125	6.25	6.25
1691	3.125	6.25	6.25	12.5
1768	0.00625	0.0125	1.6	1.6
1796	25	25	50	50
1819	12.5	50	12.5	25
1927	800	800	800	800
2011	200	200	400	400
2048	200	400	400	800
2081	100	50	800	800
2162	100	100	200	200
2163	200	200	400	200
2290	6.25	6.25	800	800
2296	400	400	800	800
2297	400	400	800	800
2462	25	25	400	400
2511	100	800	100	800
2550	0.0125	0.025	1.6	6.4
2588	6.25	25	25	50
2632	3.125	2.4	3.125	3.125
2634 = <i>Seleno-Triapine</i>	6.25	12.5	12.5	12.5
CORM3	800	800	800	800



**Figure 18:** Configuration of a 96-well plate used in the CellTiter-Glo® assay. 3 substances per plate were used. 6 wells were used for the untreated control. 3 wells per concentration and substance were used for 6 different concentrations per substance. 6 wells were used as blank (DMSO only).

### 3.11 In-vivo data

Data from experiments in the subcutaneous CT26 murine colon carcinoma model in Balb/c mice, conducted at the Institute of Cancer Research, Department of Medicine I, Medical University of Vienna, Austria, were kindly provided by Petra Heffeter and Walter Berger. All experiments had been approved by the local ethics commission and carried out according to the Austrian and FELASA guidelines for animal care and protection.

Test compounds were administered to animals over a treatment period of at least two weeks at least twice weekly in the first two weeks. For further details of experiment performance and outcomes – as far as available - see Table 9. Note that drug vehicles, routes of administration (intraperitoneal, intravenous or oral) and dosing schedules (4–11 drug applications within a two-week treatment period) may differ from compound to compound, according to developmental rationales and drug properties (such as solubility and toxicity, determining the maximum applicable and tolerable doses, respectively).

Quantitative comparisons of the daily average tumor volume in treated and vehicle control groups, each consisting of at least four animals, were the basis for calculation of the *in-vivo* parameters used herein. In those few cases where more than one schedule or route of administration had been studied for a test compound, data from the setting yielding the highest therapeutic efficacy were chosen for all evaluations below.

**Table 9:** *Provided in vivo data for used substances, including references for published in vivo data.*

Substances	Central Ion	Best Dose & Route	Growth Inhibition (%) on Day 15*	Average Difference in Tumor Volume (mm <sup>3</sup> )**	References
KP1 / Cisplatin	Pt(II)	3 mg/kg x4 i.v.	40.8	98	
KP1339	Ru(III)		50.9	284	
KP1342 = Carboplatin	Pt(II)		-2.1	-54	
KP1343 = Oxaliplatin	Pt(II)	9 mg/kg x4 i.v.	59.4	174	Jungwirth, 2012 <sup>80</sup>
KP1582	Ru(II)	10 mg/kg x10 i.p.	10.6	8	Hackl, 2017 <sup>47</sup>
KP1657	Ga(III)	2.5 mg/kg x11 i.v.	67.4	318	
KP1682 = Satraplatin	Pt(IV)	40 mg/kg x4 p.o.	4.6	35	
KP1690 = Triapine	-	5 mg/kg x11 i.v.	79.9	158	Kallus, 2019 <sup>60</sup>
KP1768	Ga(III)	1.25 mg/kg x11 i.v.	54.8	325	
KP1796	Ru(II)	20 mg/kg x10 i.p.	-19.1	-82	Hackl, 2017 <sup>47</sup>
KP1819	Pt(IV)	51.7 mg/kg x4 p.o.	36.4	139	
KP1927	Pt(IV)	40 mg/kg x4 p.o.	23.1	185	
KP2011	Os(II)	30 mg/kg x10 p.o.	35.7	172	Klose, 2018 <sup>81</sup>
KP2048	Ru(II)	30 mg/kg x10 i.p.	32.3	68	Hackl, 2017 <sup>47</sup>
KP2081	Ru(II)	30 mg/kg x10 p.o.	29.3	84	Klose, 2018 <sup>81</sup>
KP2162	Ru(II)	20 mg/kg x9 p.o.	-13.4	-59	
KP2163	Rh(III)	30 mg/kg x9 p.o.	28.4	46	

<b>KP2290</b>	Rh(III)	10 mg/kg x10 i.p.	-14.6	-3	Hackl, 2017 <sup>47</sup>
<b>KP2296</b>	Ru(II)	2.5 mg/kg x8 i.p.	-12.8	-13	Tamasi, 2017 <sup>52</sup>
<b>KP2297</b>	Ru(II)	2.5 mg/kg x8 i.p.	28.3	29	Tamasi, 2017 <sup>52</sup>
<b>KP2462</b>	Mo(IV)		12.2	25.0	Berasaluce, 2020 <sup>72</sup>
<b>KP2511</b>	-		-15.8	-51.0	
<b>KP2550</b>	-		-16.5	-13	
<b>KP2588</b>	-		36.0	132	Kallus, 2019
<b>KP2632</b>	-		67.3	83.0	
<b>KP2634 = Seleno-Triapine</b>	-		73.1	429	
<b>CORM3</b>	Ru(II)		-72.0	-205	Tamasi, 2017 <sup>52</sup>

### 3.12 Statistical Analysis of the Data

Statistical analysis of the data was performed in GraphPad Prism, Version 8. For the plotting of the concentration-effect curves a logarithmic scale was used. Before further analysis IC<sub>50</sub> values in millimolar were logarithmically (base 10) transformed. The (few) substances that were insufficiently active up to a maximum tested concentration of 0.8 mM were attributed a dummy IC<sub>50</sub> value of 1 mM to include them in the calculations. Shapiro-Wilk normality test showed non-normal distribution for IC<sub>50</sub> values in SW480, CT26 and HCT116 spheroids. Distribution of IC<sub>50</sub> values (positive growth inhibition only) and IC<sub>50</sub> values (positive tumor volume reduction) of CT26 spheroids had a non-normal distribution as well. The same applied for the distribution of the 3D/2D quotients. Therefore, the Spearman's rank correlation coefficient *r* was chosen to calculate correlation. Linear regression was calculated and plotted with a 95% confidence interval (CI).

### 3.13 Spheroid Characterization Using Immuno-fluorescence

Untreated spheroids of HCT116 cells and spheroids of CT26 cells were grown in 96-well plates as described above for 4 and 8 days to mimic their condition at the beginning and at the end of

cytotoxicity tests, respectively. 6 to 10 spheroids were harvested using a 1 mL tip with an Eppendorf pipette and placed close to the bottom of sample holders (Sakura) filled with Tissue-Tek (Sakura). The samples were stored at -80 °C. The frozen samples were cut into 5 µm thin slices using a cryostat microtome at -20 °C. Several of these sections were mounted onto SuperFrost slides and stored at -20 °C. The cells on these slides were fixed with 4% PFA for 30 min. The slides were washed twice with PBS and incubated for 10 min with 0.1% Triton X (in PBS). Another washing step was followed by blocking of the slides for 45 min with a solution of 10% goat serum and 2% BSA in PBS. The next washing step was preceded by encircling the samples with a liquid blocker and application of the primary antibody (Table 10 shows the dilutions). Incubation took place overnight at 4 °C and was followed by rinsing thrice with PBS. The secondary antibody was applied for 45 min and washed off by rinsing three times with PBS. Mountant with DAPI was applied to the samples and a coverslip placed on top. After a drying period of 2–3 days the fluorescence of the samples was imaged with a confocal laser-scanning microscope (Zeiss LSM800) using a 200x magnification.

**Table 10:** Antibodies used for immunofluorescence experiments.

<i>Antibody (Product number)</i>	<i>Species</i>	<i>Provider</i>	<i>Dilution</i>
<i>Anti-Ki-67 (D3B5)</i>	Rabbit	Cell Signaling Technology (CST)	1:400
<i>Anti-cleaved caspase 3 (5A1E)</i>	Rabbit	Cell Signaling Technology (CST)	1:400
<i>Anti-cyclophilin <math>\alpha</math> (ab42408)</i>	Rabbit	Abcam	1:1000
<i>Anti-pimonidazole – FITC (FITC-MAb1)</i>	Mouse	Hypoxypore Inc.	1:100
<i>Goat Anti-Rabbit IgG H&amp;L (Alexa Fluor® 594) preadsorbed (ab150088)</i>	Goat	Abcam	1:1000

To image hypoxia, treatment with 100 µM pimonidazole-HCl (2 h incubation at 37 °C and 5% CO<sub>2</sub>) was carried out before proceeding with harvesting of the spheroids. The blocking solution for these spheroids contained no goat serum and the first antibody used, anti-pimonidazole, was

already tagged with FITC (fluorescein isothiocyanate), hence no secondary antibody was used. Incubation with the primary antibody was performed at room temperature for 1 h.

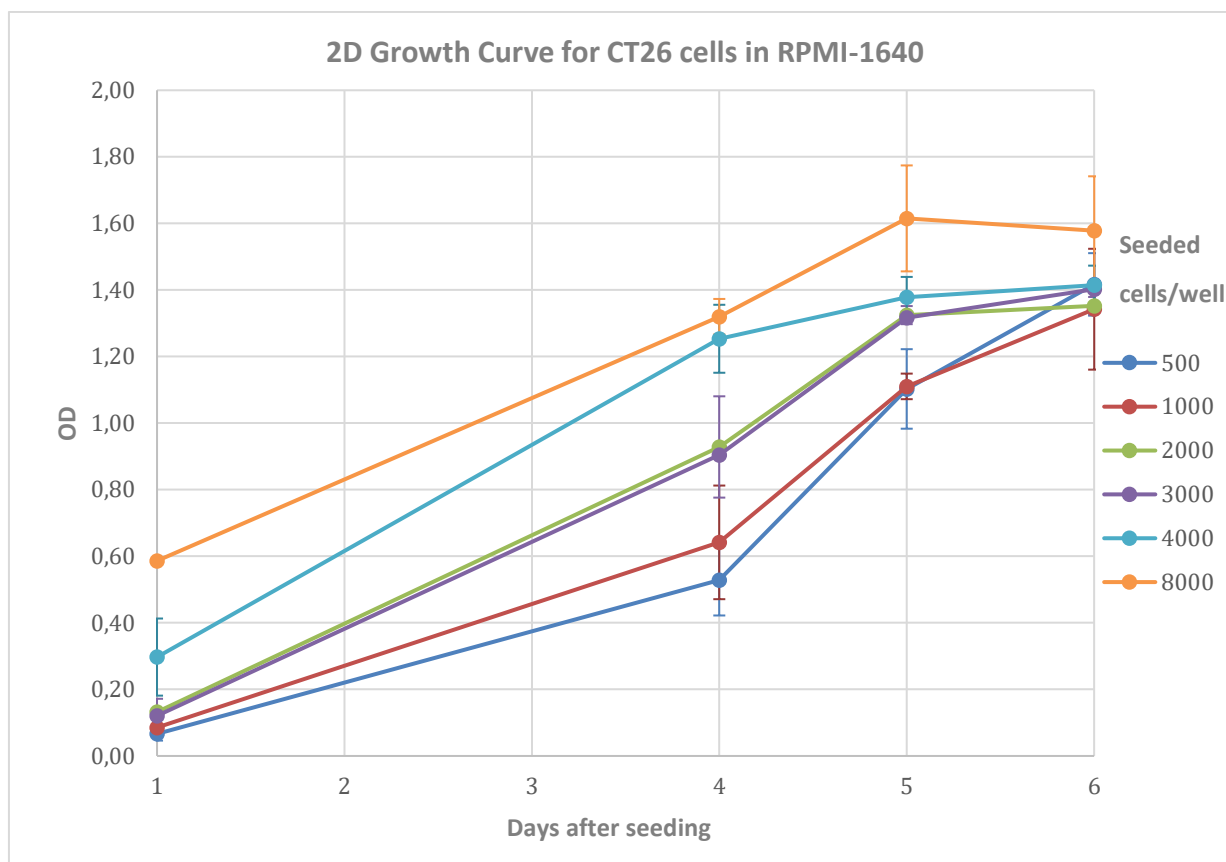
## 4 Results & Discussion

### 4.1 Optimization of CT26 Cell Number

Different cell numbers of CT26 cells in DMEM/HAM F12 and RPMI-1640 medium were seeded and MTT-stained, and their OD was measured on days 1, 4, 5 and 6. In further experiments these cells would be left to recover 24 h after seeding and incubated with substances for another 96 h, ending the experiment on day 5. Towards the end of this timespan, cells are required to be still in the stage of exponential growth and their degree of confluence should still increase. Cells in RPMI-1640 medium only did show an OD slightly higher than 1.5 on day 5 for a seeding number of 8,000 cells/well, as shown in Figure 19 and Table 11, whereas cells in DMEM/HAM F12 had a suitable OD for every cell density used for seeding (Table 11, Figure 20). Seeding of 1,000 and 2,000 cells/well yielded sufficient degrees of confluence on day 5 (Figure 21) that still increased to day 6 (Figure 22). They had an OD close to 2 and their OD increased twice and 1.7 times from day 4 to day 5. Based on these results a seeding number of 1,500 cells/well in DMEM/HAM F12 was chosen.

**Table 11:** Dependence of measured ODs by day on the cell number initially seeded, using MTT staining for CT26 cells in RPMI-1640 medium. \*3,000 cells/well were seeded only in one experiment.

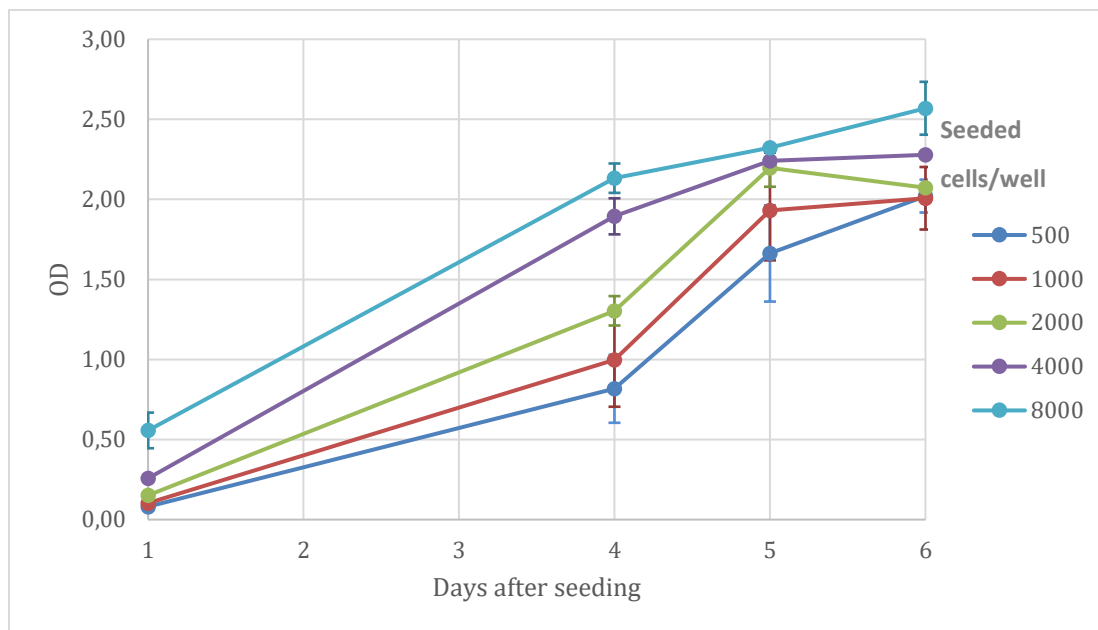
		Seeded cells/well	500	1000	2000	3000*	4000	8000
Days after seeding	day 1		0.07	0.09	0.13	0.12	0.30	0.59
	day 2							
	day 3							
	day 4		0.53	0.64	0.93	0.90	1.25	1.32
	day 5		1.10	1.11	1.32	1.32	1.38	1.62
	day 6		1.42	1.34	1.35	1.40	1.41	1.58
		Measured OD						



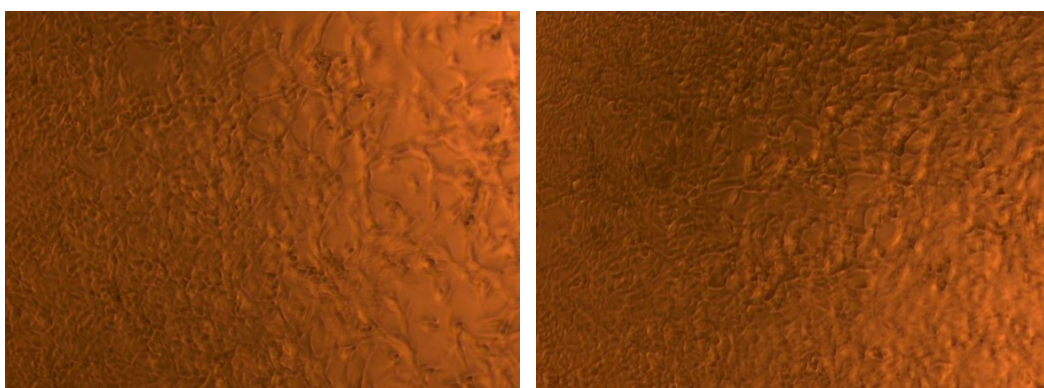
**Figure 19**

**Table 12:** Dependence of measured ODs by day on the cell number initially seeded, using MTT staining for CT26 cells in DMEM/HAM F12.

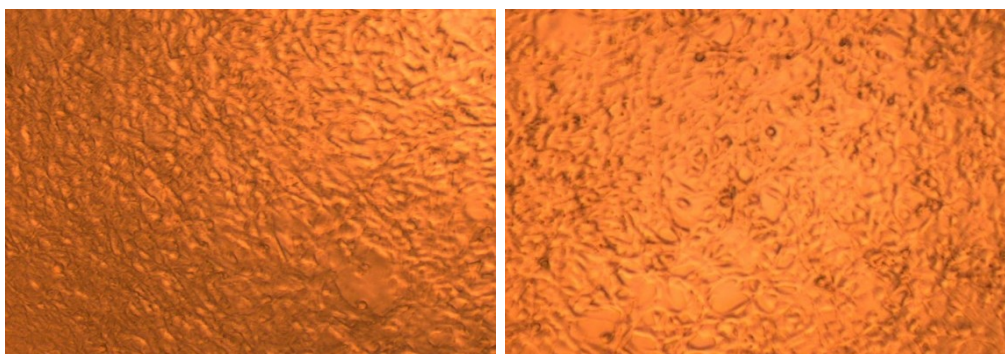
Seeded cells/well		500	1000	2000	4000	8000
Days after seeding	day 1	0.08	0.10	0.15	0.25	0.52
	day 2					
	day 3					
	day 4	0.74	0.89	1.27	1.85	2.10
	day 5	1.56	1.82	2.15	2.22	2.32
	day 6	1.98	1.94	2.07	2.28	2.51
Measured OD						



**Figure 20** 2D growth curve for CT26 cells in DMEM/HAM F12



**Figure 21:** Confluence of CT26 cells in DMEM/HAM F12 on day 5. Left: 1,000 seeded cells/well; Right: 2,000 seeded cells/well. Areas without cells are well discernible for 1,000 seeded cells/well.



**Figure 22:** Confluence of CT26 cells in DMEM/HAM F12 on day 6. Left: 1,000 seeded cells/well; Right: 2,000 seeded cells/well.

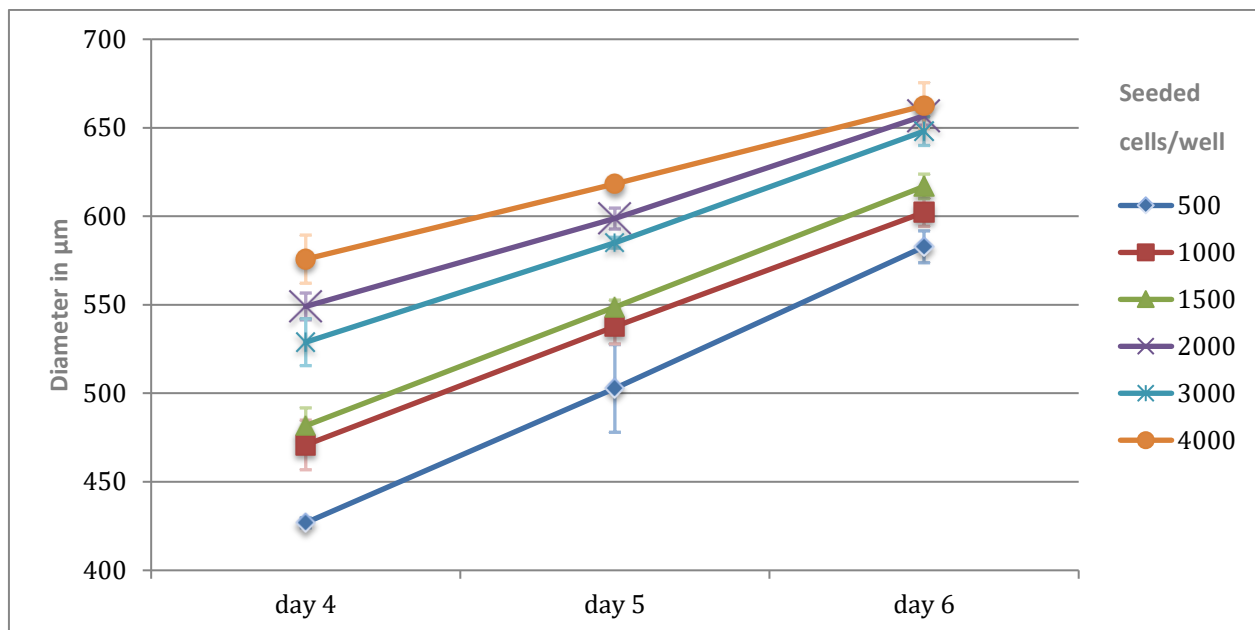
## 4.2 Spheroid Growth Curve

### 4.2.1 Optimization of Cell Number for CT26 Spheroids

Spheroids grown from CT26 cells (in RPMI-1640 medium) show an appropriate diameter for cytotoxicity tests within a wide range of cell numbers seeded (Table 13, Figure 23). Spheroids with a diameter < 300  $\mu\text{m}$  will most likely have no hypoxic regions and are therefore less desirable as tumor models.<sup>23</sup> With increasing size, on the other hand, higher drug concentrations are usually required for comparable effect. Since some compounds have a low solubility, smaller diameters are favorable. Therefore, spheroid sizes in a range of 350 to 500  $\mu\text{m}$  on the fourth day after seeding are preferred. To make future experiments more comparable with experiments on HCT116 spheroids, which are seeded using a number of 400 cells/well, the same number was chosen for CT26 cells. The diameter of CT26 spheroids (in DMEM/Ham F12) was measured four days after seeding of 400 cells/well. To make sure that diameters > 300  $\mu\text{m}$  are reproducible, a second experiment was carried out, preparing two independent cell suspensions. Overall, these experiments yielded an average spheroid diameter of  $391 \pm 29 \mu\text{m}$  (Table 14, Figure 24). Four days after seeding, CT26 cells formed round spheroids with a defined shape (Figure 25). Due to these results, a seeding cell number of 400 cells/well for CT26 spheroids in DMEM/HAM F12 was chosen for further experiments.

**Table 13:** Measured diameters ( $\mu\text{m}$ ) of CT26 spheroids in RPMI-1640 medium after seeding of different cell numbers/well.

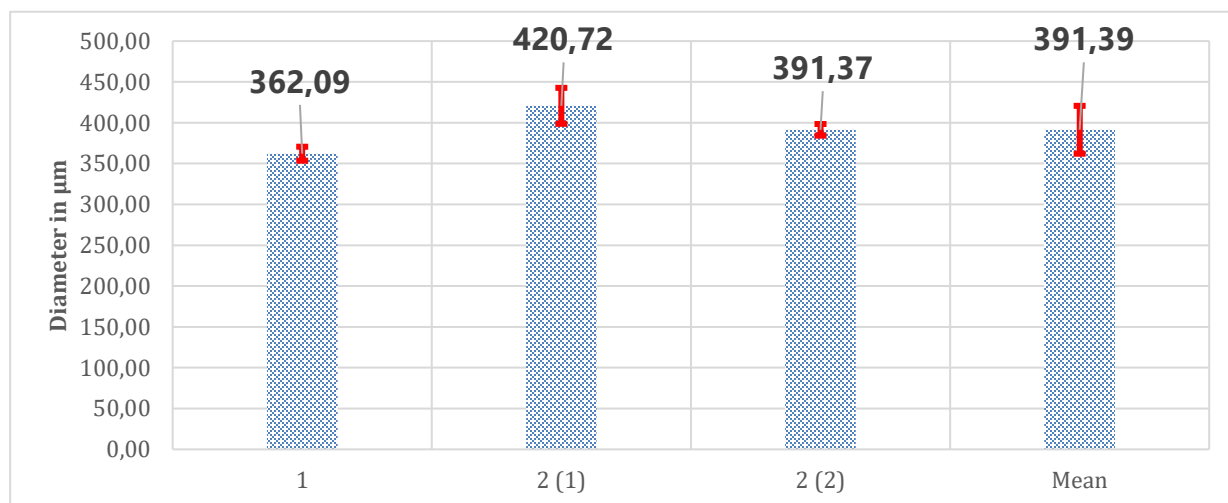
Seeded cells/well	500	1000	1500	2000	3000	4000
day 4	426.87	470.82	481.71	549.07	528.89	575.78
day 5	502.76	537.60	548.64	598.72	585.08	618.32
day 6	582.75	602.21	616.87	656.79	648.08	662.46
Measured diameters in $\mu\text{m}$						



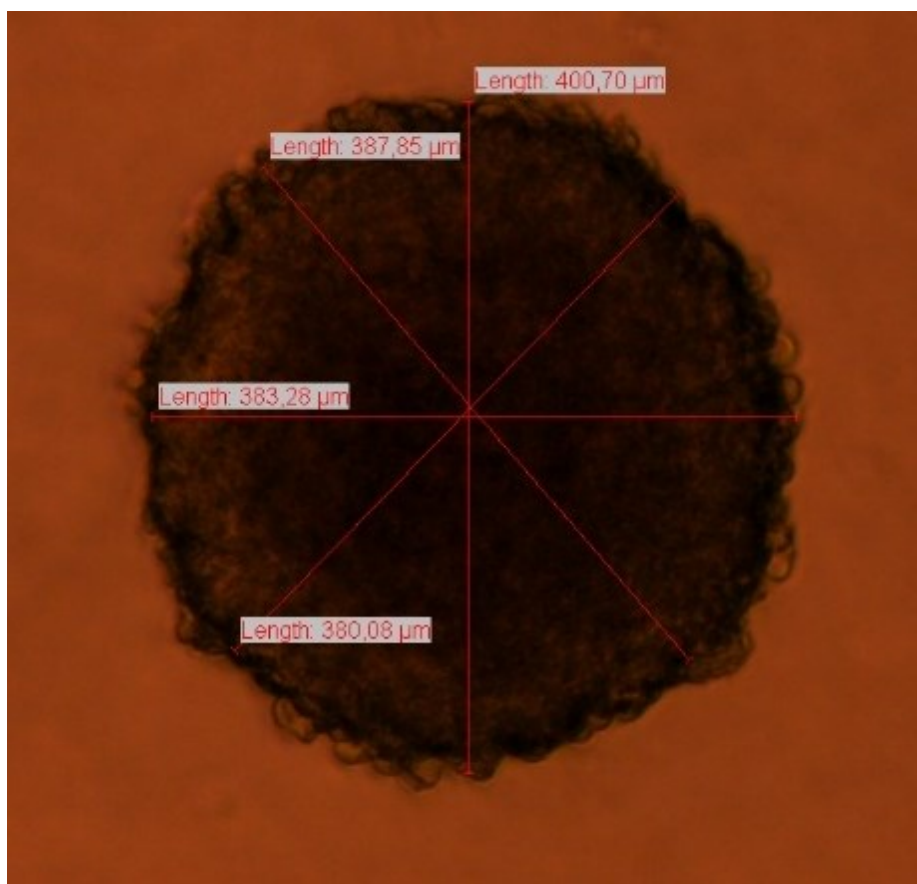
**Figure 23:** Spheroid growth curve for CT26 in RPMI-1640

**Table 14:** Diameter (μm) of CT26 spheroids in DMEM/HAM F12, measured 96 h after seeding of 400 cells/well.

	Experiment 1	Experiment 2 (1)	Experiment 2 (2)	Mean
Diameter (μm)	362.09	420.72	391.37	391.39
STDV	8.56	22.05	7.11	29.32



**Figure 24:** Comparison of diameter (μm) of CT26 (DMEM) spheroids after 96 h (400 cells/well seeded)



**Figure 25:** CT26 spheroid in DMEM/Ham F12, four days after seeding of 400 cells/well.

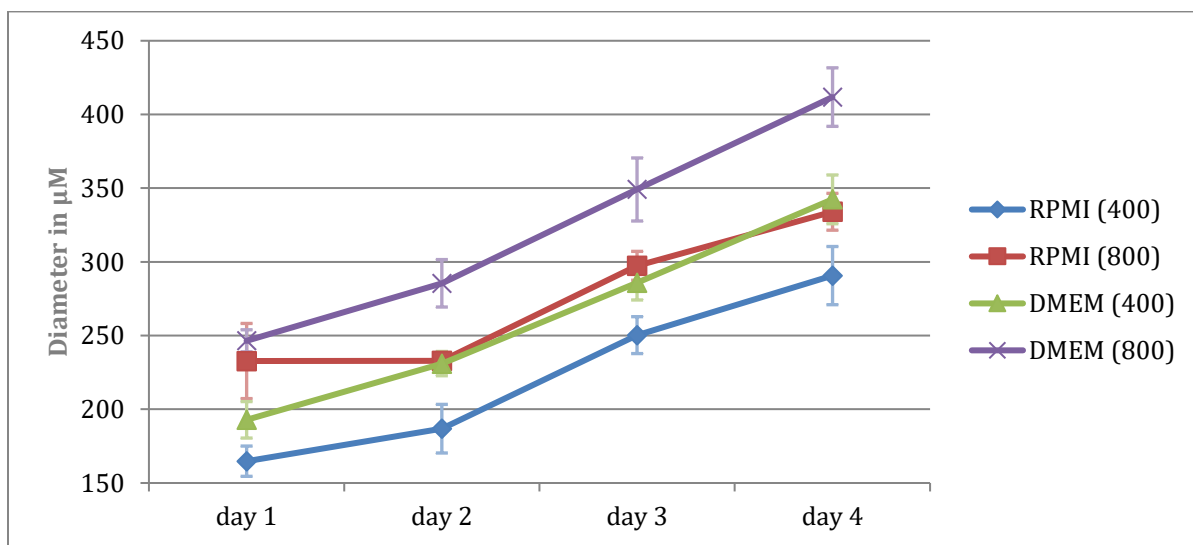
### 4.2.2 Choice of Medium

Since CT26 spheroids were to be used in parallel with HCT116 spheroids, which are seeded with a number of 400 cells/well, comparable cell numbers and the same medium for both cell lines are preferable. Therefore, both cell lines were seeded using 400 cells/well (as well as 800 cells/well for comparison) in DMEM/HAM F12 and RPMI-1640 medium, and spheroid growth curves were generated by measuring the diameter on days 1 to 4. Table 15 lists the measured diameters for HCT116 spheroids and Table 16 for CT26 spheroids. Their corresponding growth curves are shown in Figures 26 and 27. Both cell lines are known to grow in RPMI-1640 medium<sup>82,83</sup> and in DMEM/HAM F12<sup>84,85</sup>, but according to their growth curves they grow better in DMEM/HAM F12.

**Table 15:** Measured diameter ( $\mu\text{m}$ ) of HCT-116 spheroids in RPMI-1640 medium and DMEM/HAM F12 on days 1–4 after seeding of 400 or 800 cells/well.

seeded cells/well	RPMI-1640 (400)	RPMI-1640 (800)	DMEM/HAM F12 (400)	DMEM/HAM F12 (800)
day 1	164.79	232.74	192.85	246.45
day 2	186.84	232.82	231.00	285.46
day 3	250.31	297.33	285.89	349.12
day 4	290.68	333.99	342.41	411.77

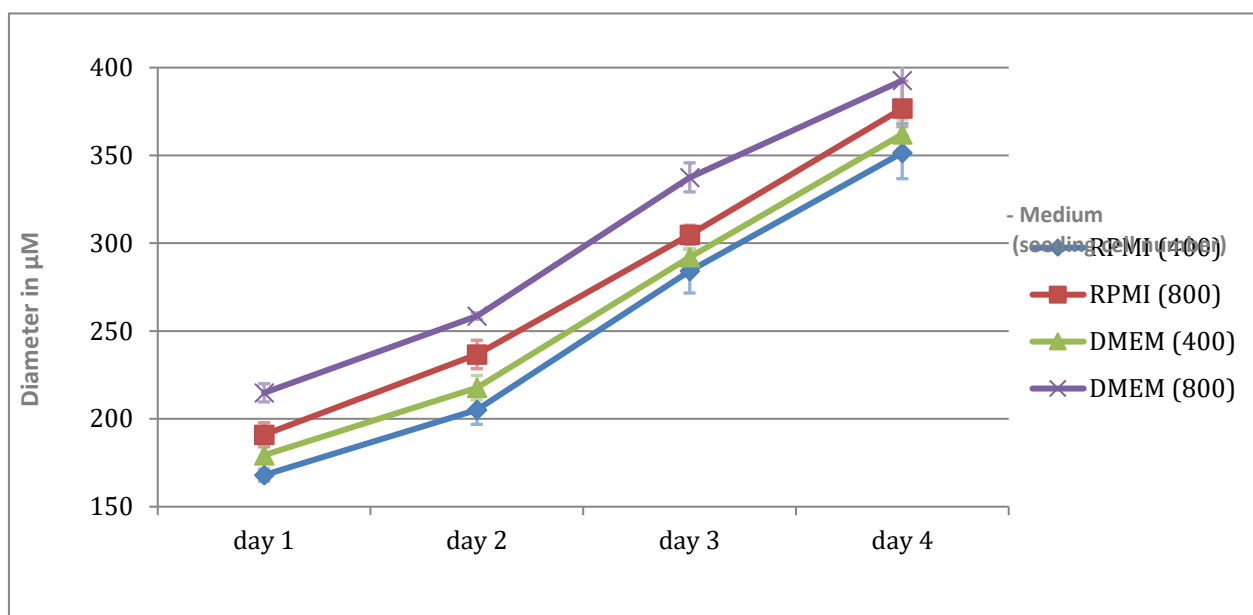
Measured diameters in  $\mu\text{m}$



**Figure 26:** Spheroid growth curve for HCT 116

**Table 16** Measured diameter ( $\mu\text{m}$ ) of CT26 spheroids in RPMI-1640 medium and DMEM/HAM F12 on days 1–4 after seeding of 400 or 800 cells/well.

seeded cells/well	RPMI-1640 (400)	RPMI-1640 (800)	DMEM/HAM F12 (400)	DMEM/HAM F12 (800)
day 1	168.00	190.95	179.32	214.83
day 2	205.16	236.65	217.73	258.56
day 3	284.16	304.80	291.97	337.48
day 4	351.53	376.72	362.09	392.66
Measured diameters in $\mu\text{m}$				



**Figure 27:** Spheroid growth curve for CT26

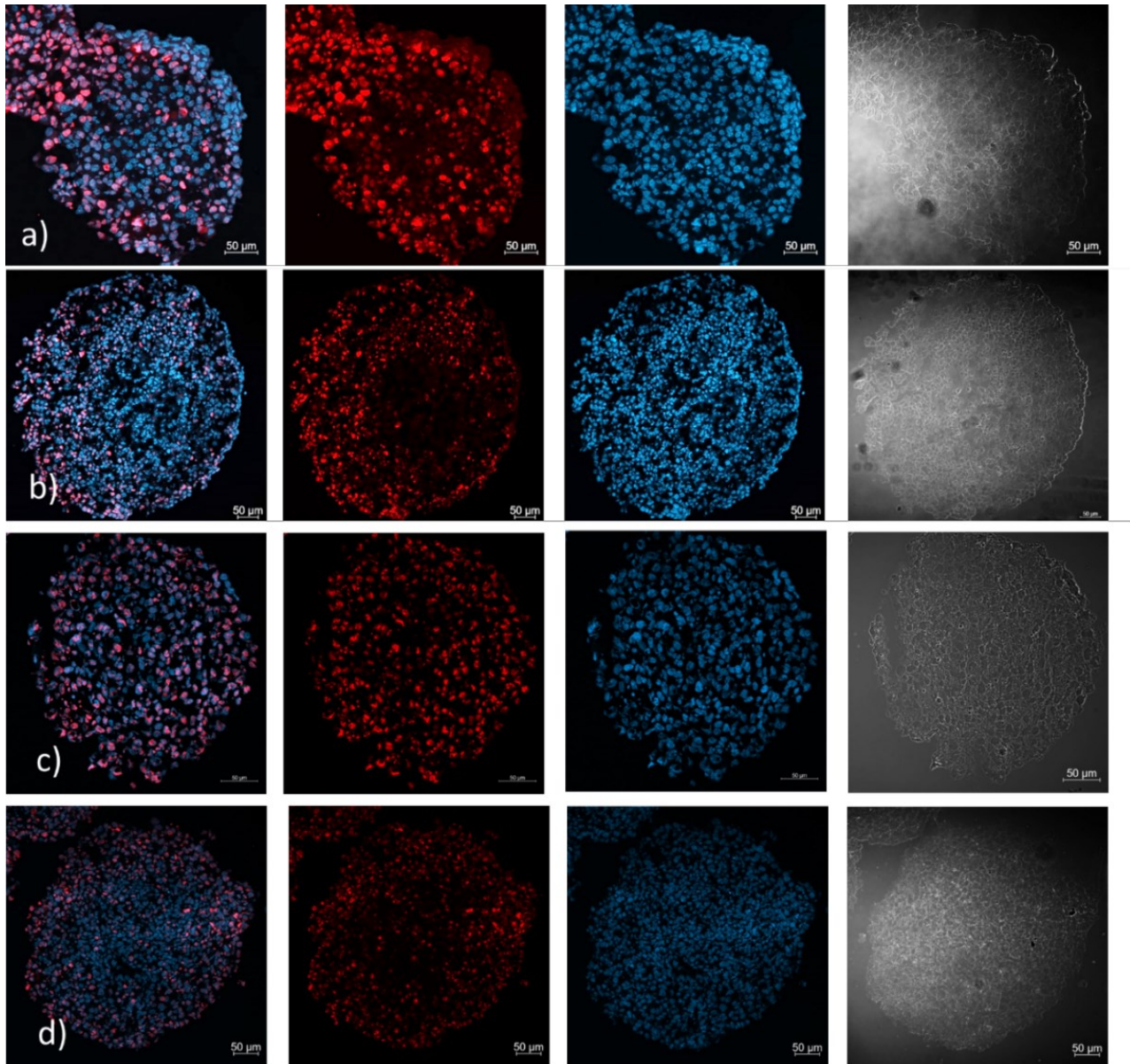
## 4.3 Spheroid Characterization via Immunofluorescence

To confirm that spheroids generated for this study do have a rim of proliferating cells, a quiescent zone and beginning necrosis in the core as found in the literature<sup>28</sup> and in previous experiments, they were characterized via immunofluorescence. These experiments were carried out in untreated CT26 and HCT116 spheroids harvested 96 h after seeding (corresponding to the time point when treatments were started), and 184 h after seeding (corresponding to the end of treatment).

### 4.3.1 Cell Proliferation

Cell proliferation was examined using Ki-67 antibodies. Ki-67 is a protein that is present in the nuclei of proliferating cells and missing in cells in the G0 phase. Thus, it is frequently used as a proliferation marker.<sup>28</sup> Figure 28 shows that untreated spheroids of both cell lines have a proliferating rim at both time points and a quiescent zone in the center of the spheroid towards the end of the treatment period. Whilst it is shown there are differences in intensity of the

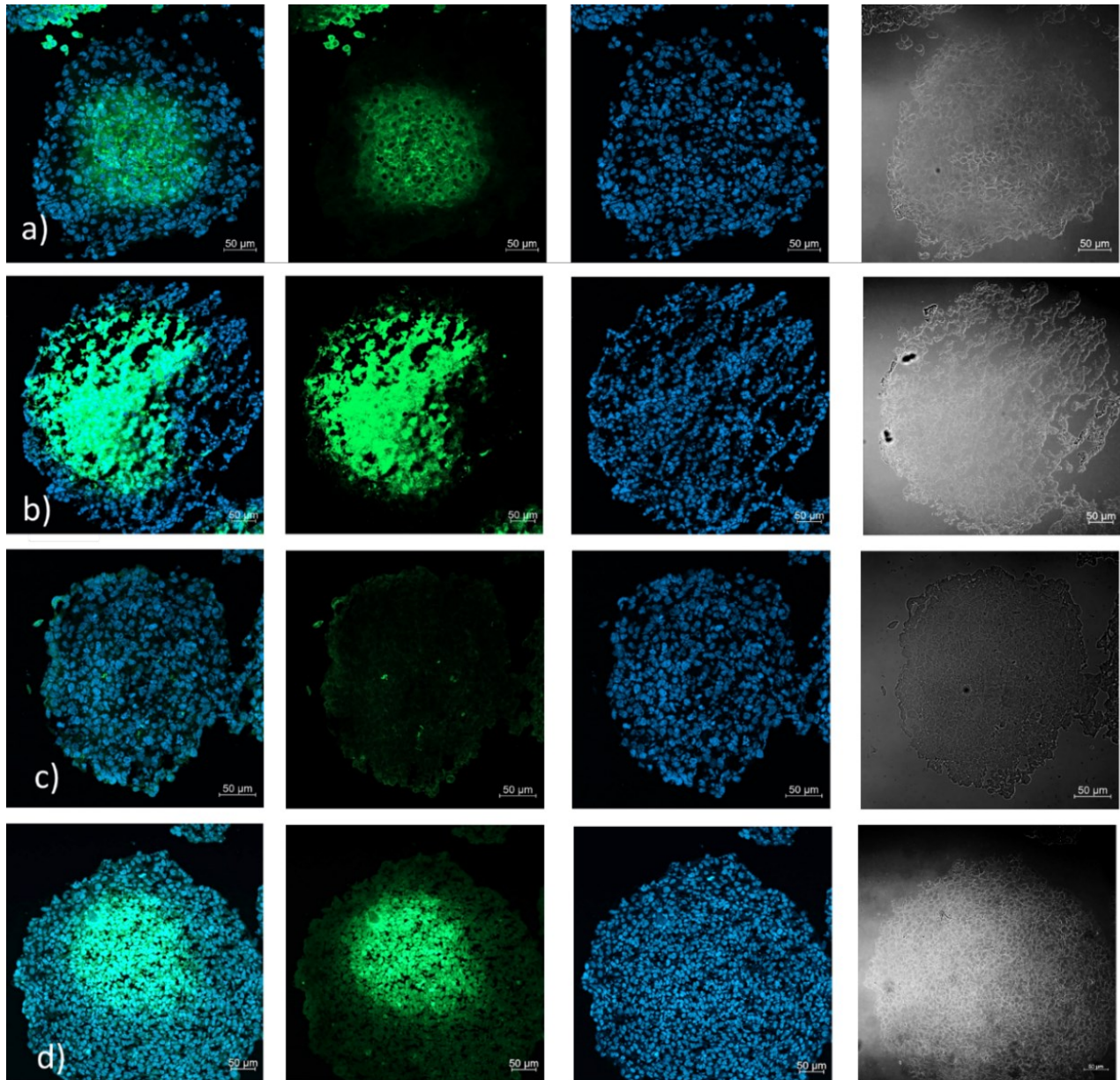
proliferation marker between outer and inner regions of the spheroids at the beginning of the treatment period, these differences are not yet as distinctive.



**Figure 28:** Representative confocal fluorescence micrographs of spheroid sections treated with an anti-Ki-67 antibody (red) and DAPI (blue), with an overlay of both stains (left) and brightfield images (right) for comparison; a) shows a 4 days old CT26 spheroid, b) an 8 days old CT26 spheroid, c) a 4 days old HCT116 spheroid, d) an 8 days old HCT116 spheroids. Scale bar indicates 50 µm.

### 4.3.2 Hypoxic Core Regions

To verify hypoxic conditions in the core region, pimonidazole was chosen as a marker. It penetrates spheroids and only forms covalent thiosulfate bonds in regions of hypoxia.<sup>28</sup> A FITC-anti-pimonidazole antibody was then used to detect the pimonidazole stained regions. Figure 29 shows intense staining in 8 days old spheroids and a distinctive hypoxic core region in 4 days old CT26 spheroids, whilst the staining in repetitive experiments of 4 days old HCT116 spheroids was faint and diffuse. This indicates that hypoxia is yet to commence at the beginning of the treatment period in HCT116 spheroids.

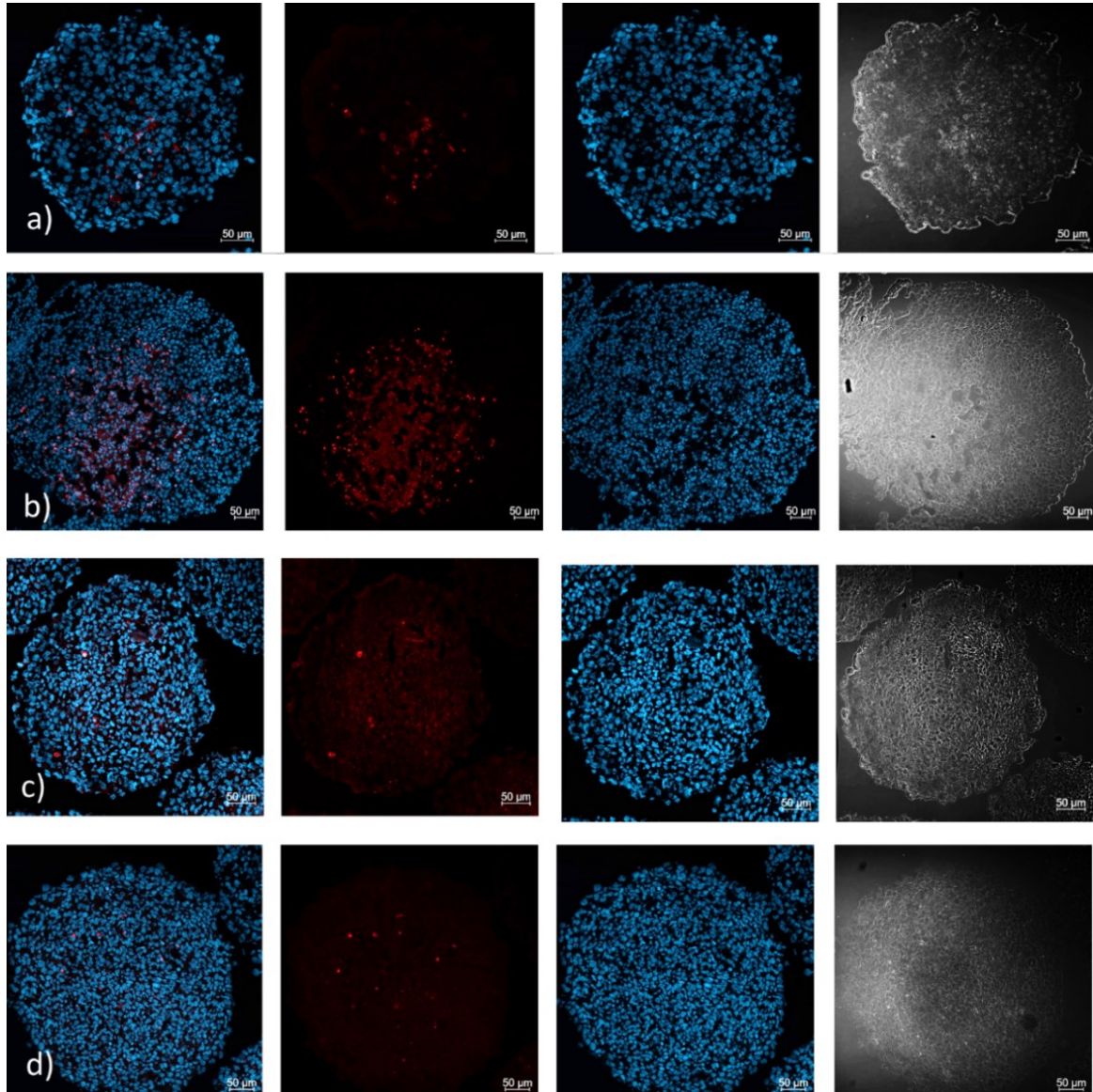


**Figure 29:** Representative confocal fluorescence micrographs of spheroid sections treated with an anti-pimonidazole antibody (green) and DAPI (blue), with an overlay of both stains (left) and brightfield images (right) for comparison; a) shows a 4 days old CT26 spheroid, b) an 8 days old CT26 spheroid, c) a 4 days old HCT116 spheroid, d) an 8 days old HCT116 spheroid. Scale bar indicates 50 µm.

### 4.3.3 Apoptosis

Cleaved caspase 3 was chosen as a marker for apoptosis. Caspase 3 is an enzyme activated by proteolytic processing during apoptosis. Therefore, cleaved caspase 3 is only present in apoptotic

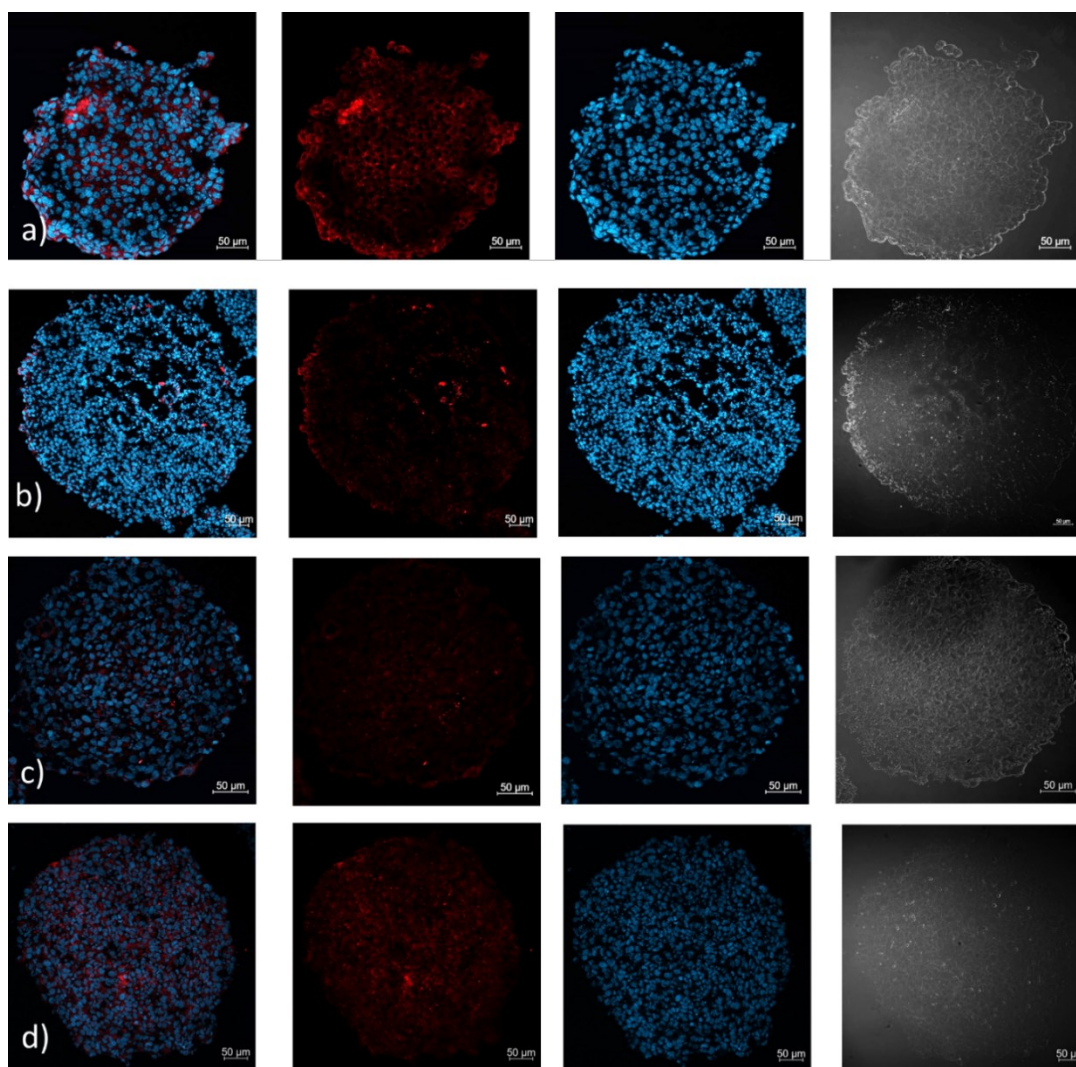
cells.<sup>28</sup> The main path for cell death in spheroids is necrosis, but often this is accompanied by apoptosis in the core region.<sup>28,86,87</sup> Figure 30 shows only few apoptotic cells in untreated spheroids.



**Figure 30:** Representative spheroid sections treated with an anti-cleaved caspase 3 antibody (red) and DAPI (blue), with an overlay of both stains (left) and brightfield images (right) for comparison; a) shows a 4 days old CT26 spheroid, b) an 8 days old CT26 spheroid, c) a 4 days old HCT116 spheroid, d) an 8 days old HCT116 spheroid. Scale bar indicates 50 µm.

### 4.3.4 Necrosis

It was reported that cyclophilin  $\alpha$  might be a suitable marker for necrotic cell death.<sup>86</sup> As shown in Figure 31, antibody detection was irregular and mostly faint. A different staining method or the use of a different antibody might be more suitable for this purpose. An in-depth investigation into staining methods for necrosis might be valuable for future experiments.



**Figure 31:** Representative confocal fluorescence micrographs of spheroid sections treated with an anti-cyclophilin  $\alpha$  antibody (red) and DAPI (blue), with an overlay of both stains (left) and brightfield images (right); a) shows a 4 days old CT26 spheroid, b) an 8 days old CT26 spheroid, c) a 4 days old HCT116 spheroid, d) an 8 days old HCT116 spheroid. Scale bar indicates 50  $\mu\text{m}$ .

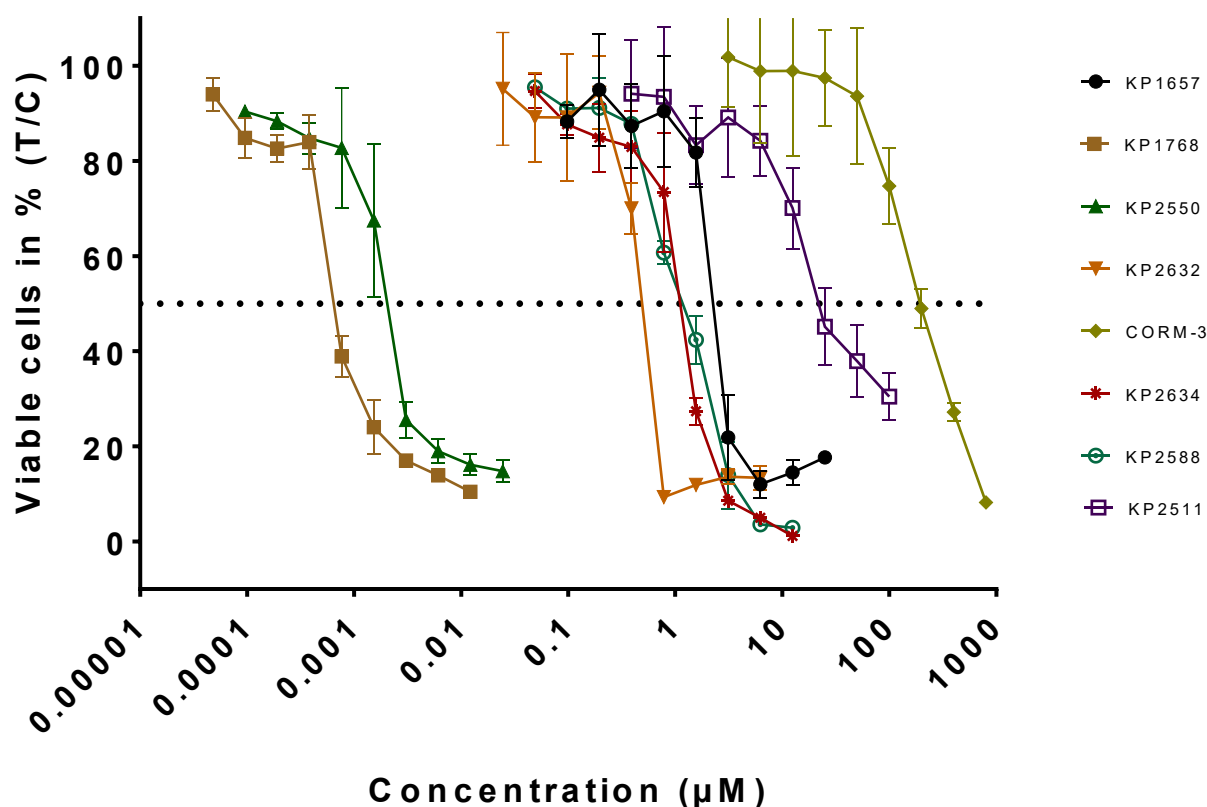
## 4.4 Cytotoxicity tests

### 4.4.1 MTT assay in SW480 Monolayer Cultures

Those IC<sub>50</sub> values in SW480 cells that had been missing in Table 1 have been measured using the MTT assay and are listed in **Table 17**: Measured IC<sub>50</sub> values in SW480 cells, obtained with the MTT assay (exposure time: 96 h). **Table 17**. Figure 32 summarizes all concentration-effect curves. Most compounds belong to the substance class of thiosemicarbazones (sulfur has been replaced with selenium in the case of KP2634), except for CORM-3. These concentration-effect curves of thiosemicarbazones have in common a steep slope, except for KP2511, succinimide-conjugated triapine. Four partially methylated substances (triapine, KP1657, KP2588, KP2632, KP2634) have IC<sub>50</sub> values in a similar, low  $\mu\text{M}$  range, whilst the fully methylated substances KP1768 and KP2550 have IC<sub>50</sub> values in the nM range. This correlates with previously published data for *in vitro* experiments in different cell lines.<sup>58</sup>

**Table 17:** Measured IC<sub>50</sub> values in SW480 cells, obtained with the MTT assay (exposure time: 96 h).

Substance	IC <sub>50</sub> ( $\mu\text{M}$ )
KP1657	2.3 $\pm$ 0.2
KP1768	0.00066 $\pm$ 0.00004
KP2511	24 $\pm$ 8
KP2550	0.0020 $\pm$ 0.0003
KP2588	1.2 $\pm$ 0.2
KP2632	0.49 $\pm$ 0.02
KP2634	1.1 $\pm$ 0.1
CORM-3	200 $\pm$ 20



**Figure 32:** Concentration-effect curves of substances tested in the MTT assay in SW480 (exposure time: 96 h).

#### 4.4.2 Cytotoxicity tests in HCT116 and CT26 Monolayer and Spheroid Cultures

Cytotoxicity in the cell lines HCT116 and CT26 was tested using the CellTiter-Glo® 2.0 and CellTiter-Glo® 3D as described above. CellTiter-Glo® 2.0 was used in an attempt to enhance comparability to the experiments carried out in spheroids, where usage of the MTT reagent was not feasible. Obtained  $IC_{50}$  values are given in Table 18 and the corresponding concentration-effect curves are shown in Figures 33–36 (sorted by substance class).

$IC_{50}$  results span six orders of magnitude in monolayer cultures and spheroid cultures. The median  $IC_{50}$  value of Ru(II)-CO complexes are among the least active, corresponding to the tumor promoting activities of CORM3 and KP2296 in vivo. In contrast to that, KP2297 showed tumor inhibition in vivo. KP2081 (plecstatin), and KP1339, substances already in clinical trials show high  $IC_{50}$  values as well. The  $IC_{50}$  values of the established drugs cisplatin and oxaliplatin are only slightly lower than the median in monolayer culture and about ten times lower than the median in 3D cell

culture. The IC<sub>50</sub> value of carboplatin is ten times higher than the median in HCT116 monolayer and spheroid cell culture, while its cytotoxicity is close to the average in CT26 monolayer and spheroid cell culture.

The thiosemicarbazones triapine, selenotriapine, KP2588, KP2632 and the gallium complex KP1657 show average cytotoxicity in monolayer culture, but are more effective in spheroid cell culture with IC<sub>50</sub> values ten to 100 times lower than the median.

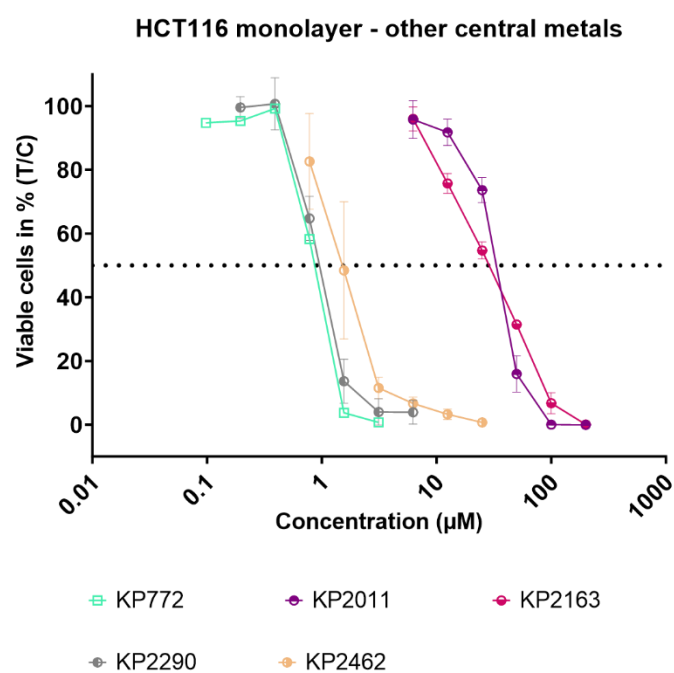
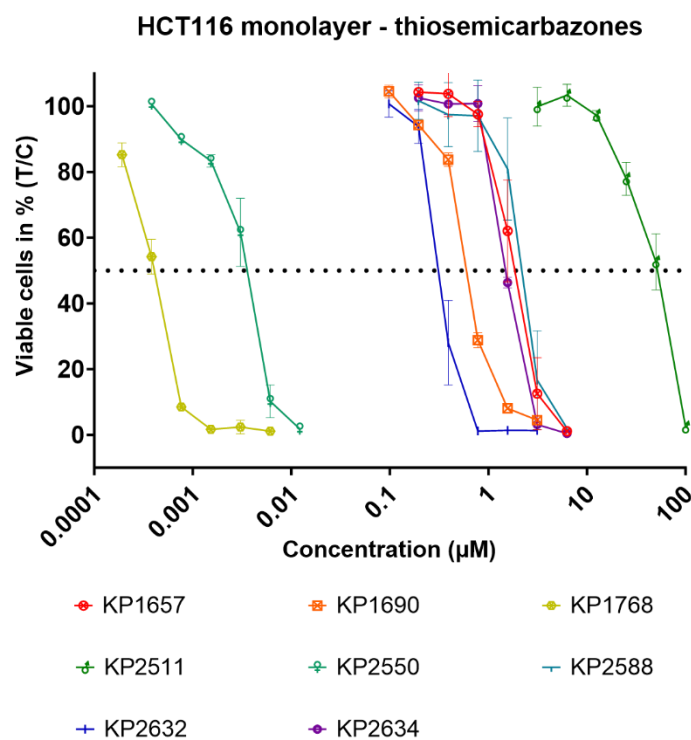
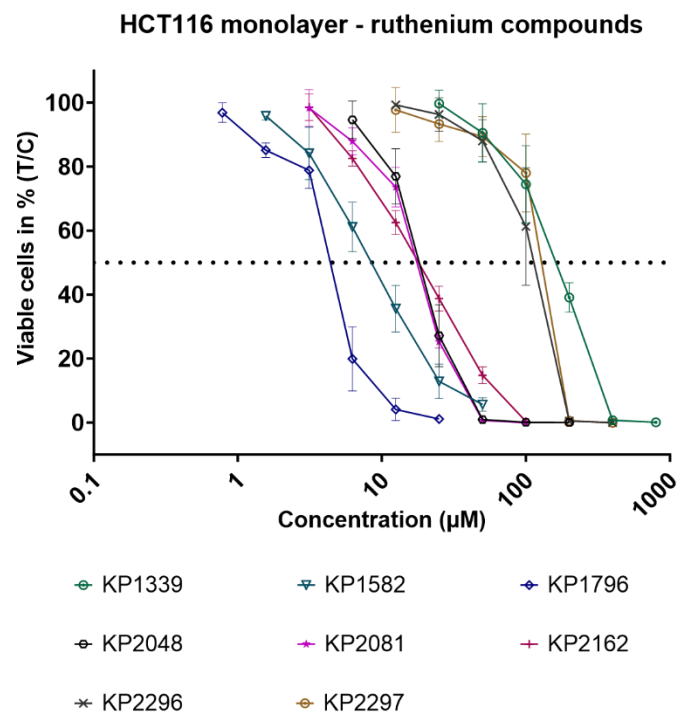
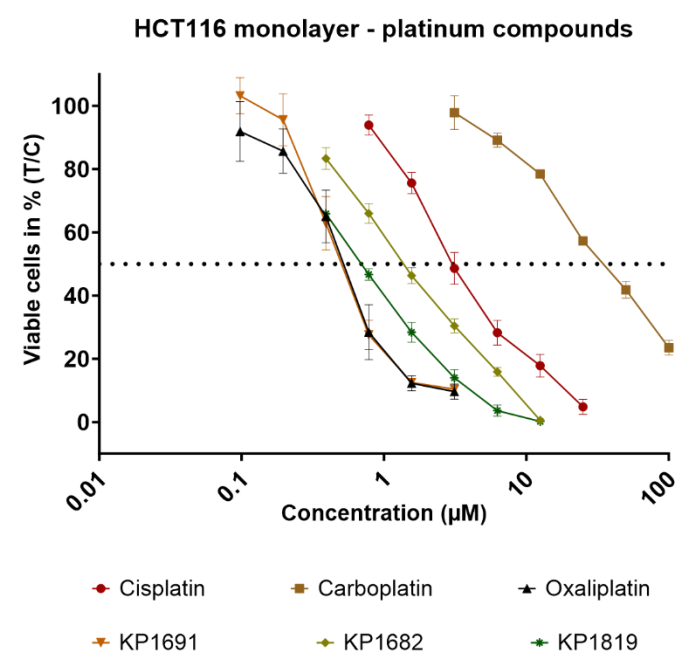
KP2550 and KP1768 are highly cytotoxic in monolayer cell culture, with IC<sub>50</sub> values in the nanomolar range. This unusually high cytotoxic effect was reduced significantly in spheroid cell culture, although IC<sub>50</sub> values were still 50 to 100 times lower than the median.

Table 18: Measured IC<sub>50</sub> values of all substances tested with the CellTiter-Glo® 2.0 and 3D assay.

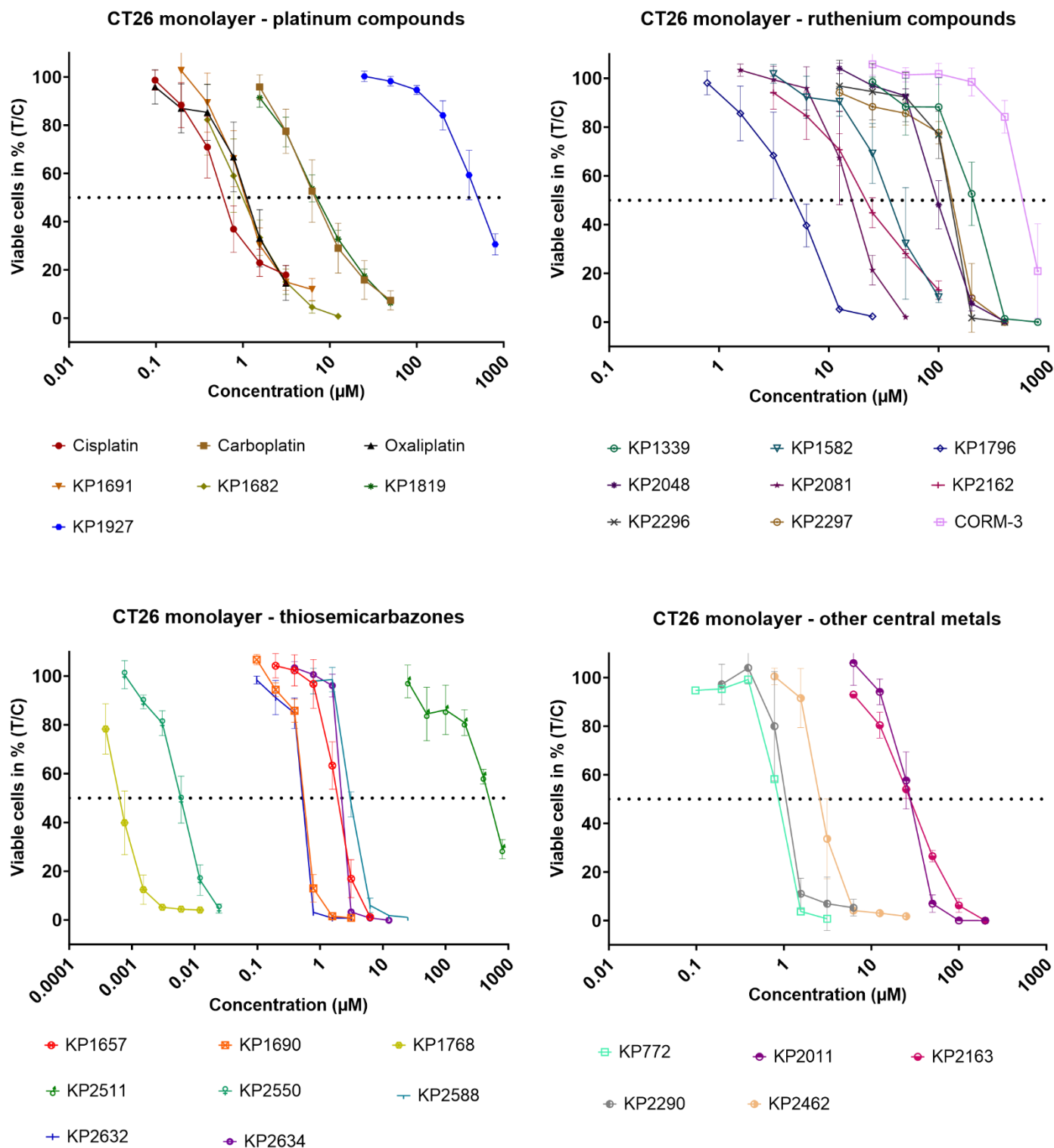
Substance	IC <sub>50</sub> (µM)			
	Monolayer		Spheroids	
	HCT116	CT26	HCT116	CT26
Cisplatin	3.1 ± 0.4	0.55 ± 0.20	18 ± 6	3.0 ± 1.6
KP1339	160 ± 20	200 ± 40	380 ± 70	350 ± 20
KP1342 = Carboplatin	35 ± 3	7.0 ± 2.5	200 ± 20	58 ± 32
KP1343 = Oxaliplatin	0.46 ± 0.05	1.1 ± 0.3	1.2 ± 0.6	4.4 ± 0.8
KP1582	8.5 ± 1.9	39 ± 14	620 ± 60	300 ± 60
KP1657	1.9 ± 0.4	1.9 ± 0.3	2.3 ± 0.3	1.3 ± 0.2
KP1682 = Satraplatin	1.4 ± 0.1	0.97 ± 0.31	4.1 ± 0.9	1.7 ± 0.7
KP1690 = Triapine	0.60 ± 0.01	0.55 ± 0.03	0.96 ± 0.18	0.47 ± 0.04
KP1691	0.50 ± 0.07	1.1 ± 0.2	0.93 ± 0.22	2.6 ± 0.3
KP1768	0.00042 ± 0.00003	0.00067 ± 0.00015	0.13 ± 0.03	0.33 ± 0.03
KP1796	4.4 ± 0.4	4.7 ± 1.6	9.7 ± 1.3	25 ± 8
KP1819	0.70 ± 0.04	7.1 ± 1.2	1.3 ± 0.3	3.9 ± 0.7
KP1927	*	500 ± 100	*	880 ± 110**
KP2011	33 ± 2	28 ± 4	240 ± 30	340 ± 60
KP2048	18 ± 2	98 ± 14	76 ± 5	120 ± 8
KP2081	18 ± 1	15 ± 3	370 ± 10	454 ± 7
KP2162	18 ± 2	22 ± 3	51 ± 9	74 ± 30
KP2163	29 ± 2	28 ± 3	108 ± 1	81 ± 14
KP2290	0.95 ± 0.08	1.0 ± 0.2	272 ± 6	210 ± 20
KP2296	110 ± 20	128 ± 7	400 ± 80	390 ± 30
KP2297	130 ± 10	130 ± 10	360 ± 40	310 ± 50
KP2462	2.6 ± 0.4	1.5 ± 0.5	84 ± 10	58 ± 7
KP2511	51 ± 6	490 ± 20	58 ± 3	590 ± 30
KP2550	0.0036 ± 0.0005	0.0062 ± 0.0012	0.58 ± 0.08	1.04 ± 0.08

KP2588	2.2 ± 0.4	3.0 ± 0.2	4.4 ± 1.4	6 ± .2
KP2632	0.32 ± 0.03	0.40 ± 0.01	0.41 ± 0.04	0.39 ± 0.06
KP2634 = Seleno-Triapine	1.49 ± 0.03	2.20 ± 0.04	2.13 ± 0.04	2.08 ± 0.02
CORM3	*	600 ± 100	*	*

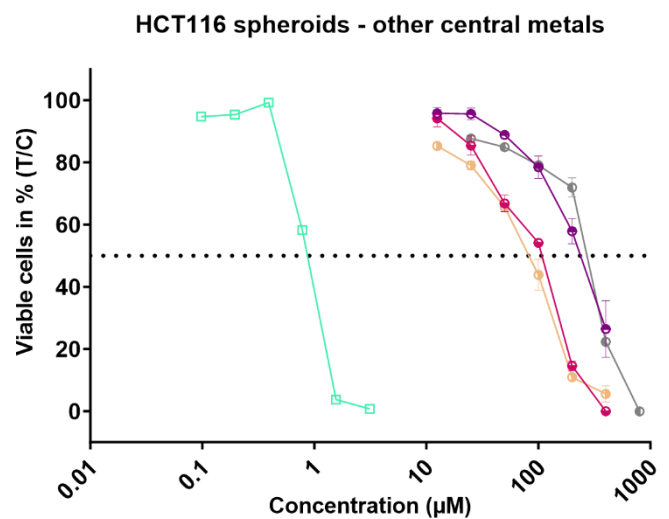
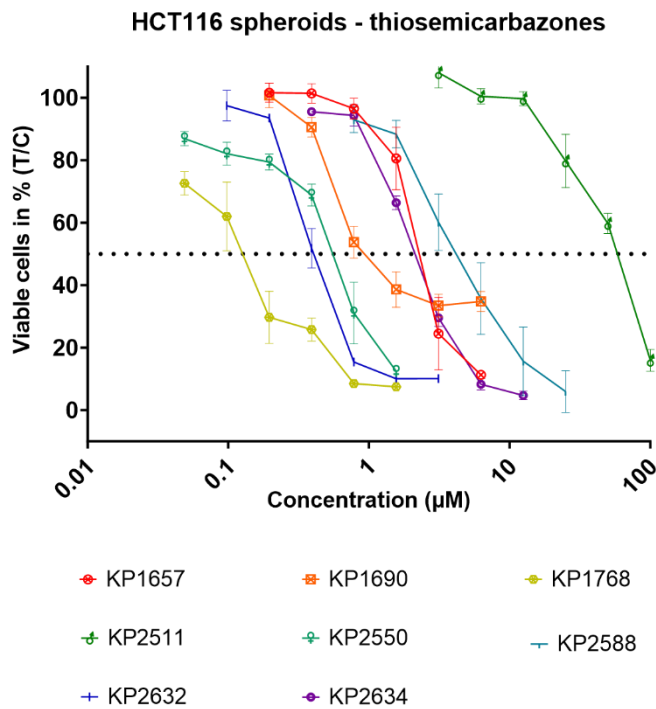
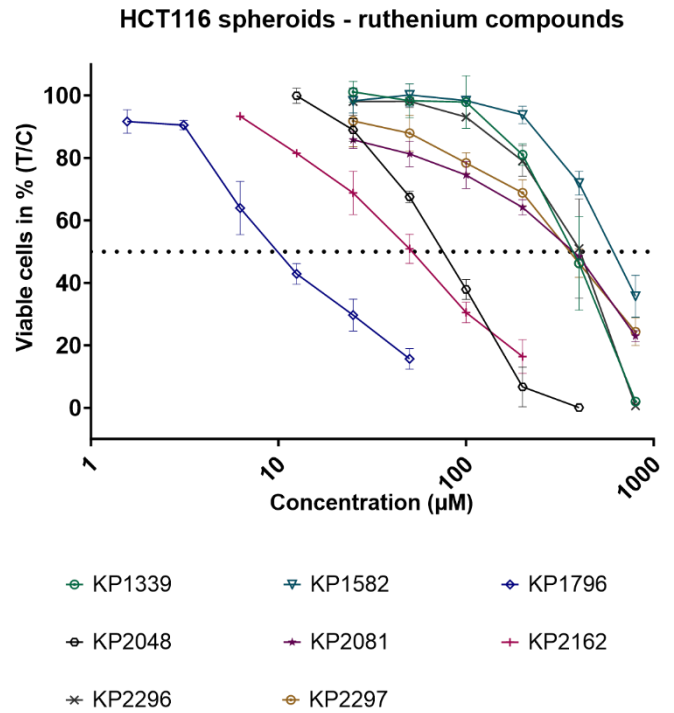
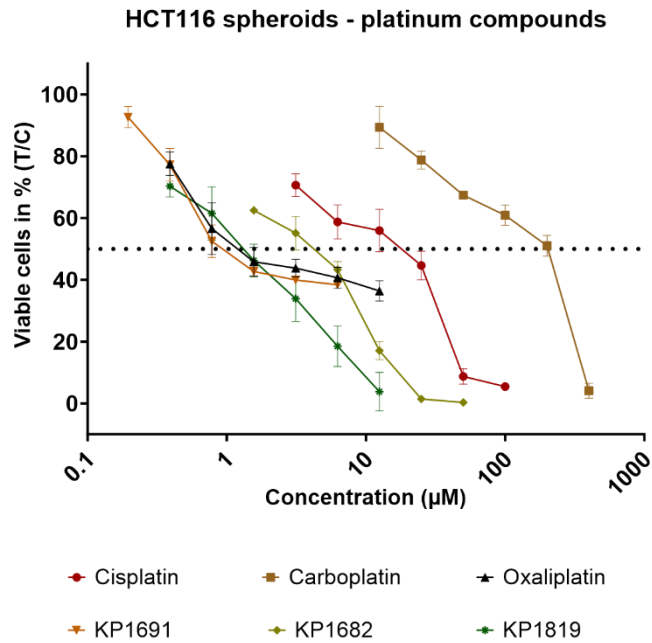
\*IC<sub>50</sub> value was > 800 µM; \*\* IC<sub>50</sub> value was > 800 µM but was extrapolated from data



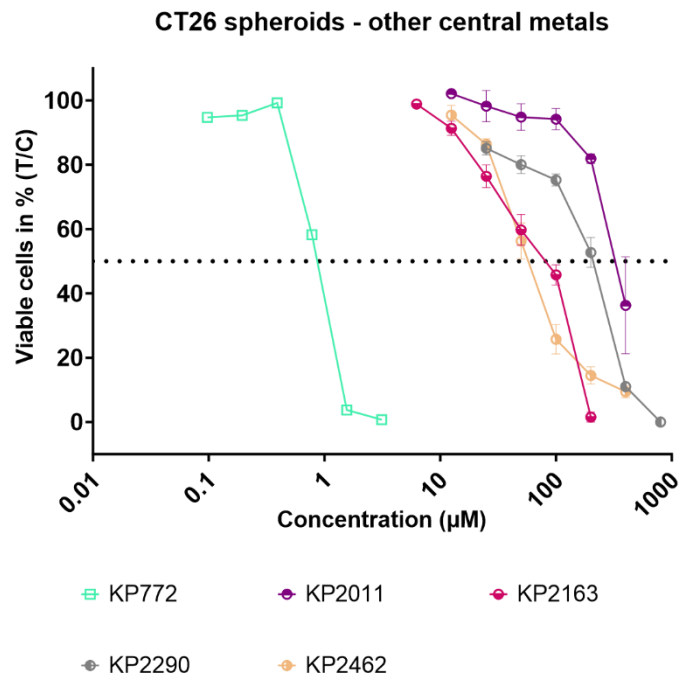
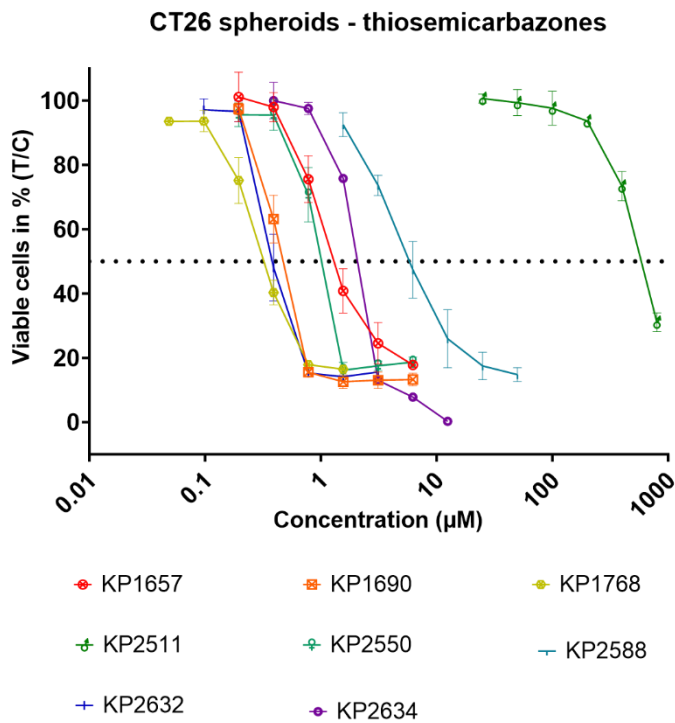
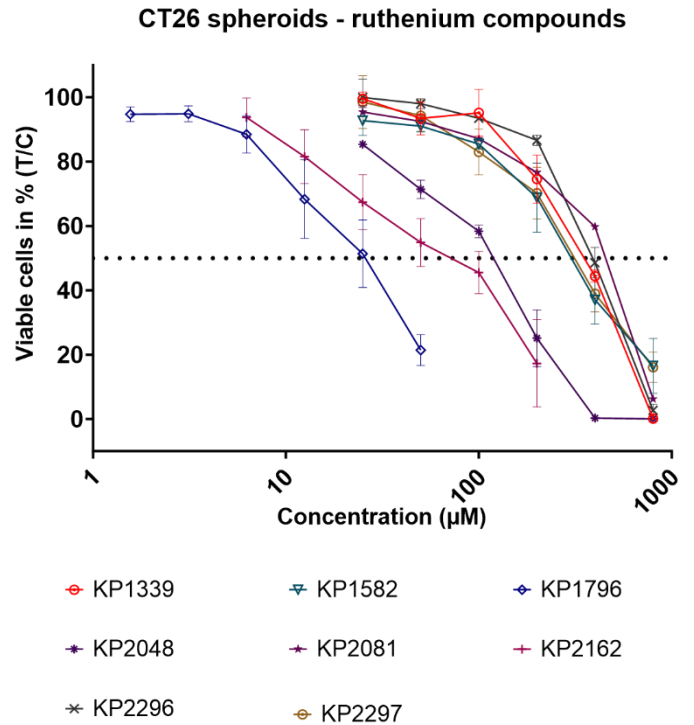
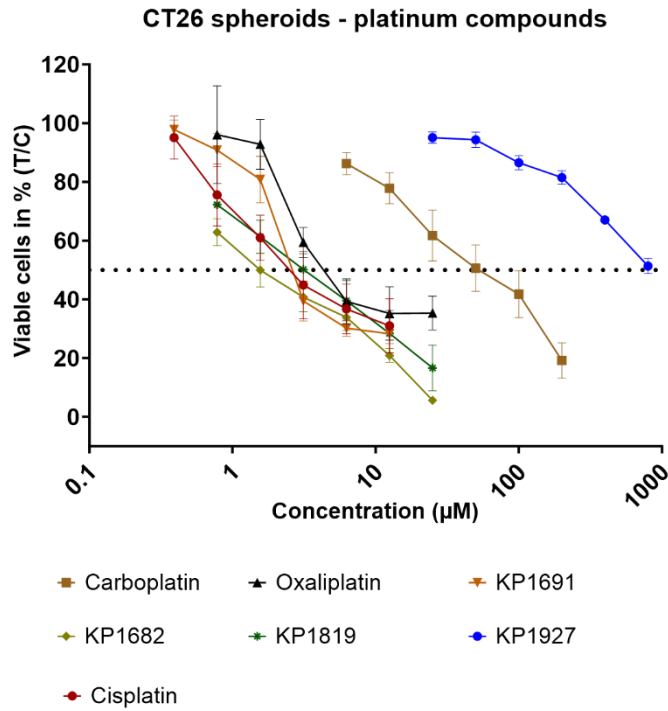
**Figure 33:** Concentration-effect curves of all substances tested with the CellTiter-Glo® 2.0 assay in HCT116 monolayer cell culture (exposure time: 96 h), separated by substance class.



**Figure 34:** Concentration-effect curves of all substances tested with the CellTiter-Glo® 2.0 assay in CT26 monolayer cell culture (exposure time: 96 h), separated by substance class.



**Figure 35:** Concentration-effect curves of all substances tested with the CellTiter-Glo® 3D assay in HCT116 spheroid cell culture (exposure time: 96 h), separated by substance class.



**Figure 36:** Concentration-effect curves of all substances tested with the CellTiter-Glo® 3D assay in CT26 spheroid cell culture (exposure time: 96 h), separated by substance class.

Table 19 lists the 3D/2D quotients for each substance to illustrate the differences in magnitude of cytotoxicity between these models. Compounds KP1768, KP2290 and KP2550 showed a 160- to 490-fold increase in IC<sub>50</sub> value. Their outstandingly low IC<sub>50</sub> values in monolayer cell culture were not paralleled in spheroids of the same cell line. These results, however, do not correlate with their performance *in vivo*. KP1768 had a tumor growth inhibition of 54.8 % on day 14 *in vivo*, which is above the median for all tumor-inhibiting substances (36 %). In contrast KP2250 and KP2290 were tumor-promoting *in vivo*. Several tumor-inhibiting substances showed almost no increase in IC<sub>50</sub> value (KP1657, triapine, KP1691, KP1819, KP1927, KP2632, selenotriapine). Their mechanism of action might not be influenced by the diffusion gradients, increased hypoxia and decreased cell cycle activity. Tumor-promoting substance KP2511 has similarly high IC<sub>50</sub> values in spheroid culture as in monolayer culture. CORM3 was almost completely inactive except for CT26 monolayer culture.

**Table 19:** 3D/2D quotients of IC<sub>50</sub> values in HCT116 and CT26 spheroids/monolayers.

Substance	Quotient of IC <sub>50</sub> values in 3D/2D	
	HCT116	CT26
Cisplatin	5.8	5.5
KP1339	2.4	1.7
KP1342 = Carboplatin	5.6	8.3
KP1343 = Oxaliplatin	2.7	3.9
KP1582	72	7.8
KP1657	1.2	0.69
KP1682 = Satraplatin	3.0	1.8
KP1690 = Triapine	1.6	0.85
KP1691	1.9	2.5
KP1768	310	490
KP1796	2.2	5.2
KP1819	1.9	0.55
KP1927	1.0	1.8
KP2011	7.3	12
KP2048	4.1	1.2
KP2081	21	31
KP2162	2.8	3.4
KP2163	3.8	2.9
KP2290	290	200
KP2296	3.6	3.1
KP2297	2.8	2.3
KP2462	32	38
KP2511	1.1	1.2

KP2550	160	170
KP2588	2.0	2.0
KP2632	1.3	0.96
KP2634 = Seleno- Triapine	1.4	0.95
CORM3	1.0	1.7

## 4.5 Statistical Analysis of the Data

To evaluate which cell culture model and which parameter are most predictive for activity in the *in vivo* CT26 solid tumor model in mice,  $IC_{50}$  values in monolayer (2D) and spheroid (3D) cultures as well as the quotients of the  $IC_{50}$  values (3D/2D) were calculated for each cell line.

*In-vivo* activity in the CT26 model was quantified by taking the percentages of tumor growth inhibition on day 15 (or day 14, if a value for day 15 was not available) of the respective experiment, *i.e.*, two weeks after the beginning of treatment. Although differences in tumor volume between treated and control groups usually increase with time and with repeated administration of active compounds, the percentage of tumor growth inhibition is not necessarily greatest on day 15 (day 14); hence, daily differences in tumor volume were averaged over the treatment period up to day 15 (or day 14, if a value for day 15 was not available; including interpolated values for days without data) and taken as an alternative measure of *in-vivo* activity.

Comparisons were carried out using all possible combinations of each of the two *in-vivo* parameters with each of the six *in-vitro* parameters of the following data sets:

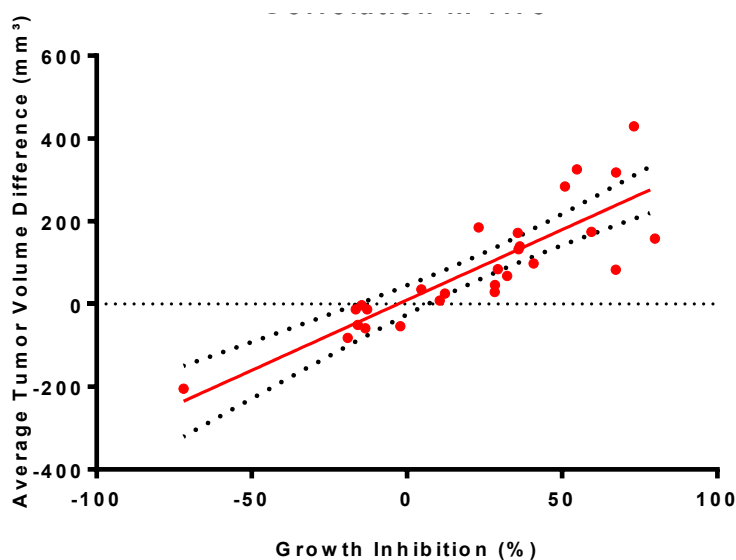
*In-vivo* parameters:

- Percentage of growth inhibition on day 15 (or day 14)
- Average daily difference in tumor volume from day 1 to day 15 (or day 14)

*In-vitro* parameters:

- $IC_{50}$  values in
  - HCT116 monolayers
  - HCT116 spheroids
  - CT26 monolayers
  - CT26 spheroids
- Quotients of the  $IC_{50}$  values (3D/2D) in the cell lines
  - HCT116
  - CT26

In addition to these 12 possible *in vivo* / *in vitro* combinations, the results in the standard cell line SW480 were also evaluated for their correlation with the growth inhibition and tumor volume difference. Figure 37 shows the linear regression of the two used *in vivo* evaluation methods.  $R^2=0.73$  for the formula  $y=3.40x+9.57$ . Significant correlation was calculated, giving a Pearson  $r=0.85$  ( $p<0.0001$ ).



**Figure 37:** Linear Regression of the two *in vivo* data evaluation methods used. Correlation analysis was carried out as well with  $r=0.8549$  [ $F=67.86$  (1, 25)  $p<0.0001$ ].

#### 4.5.1 Analysis of CT26 *in vivo* vs SW480 *in vitro* Data

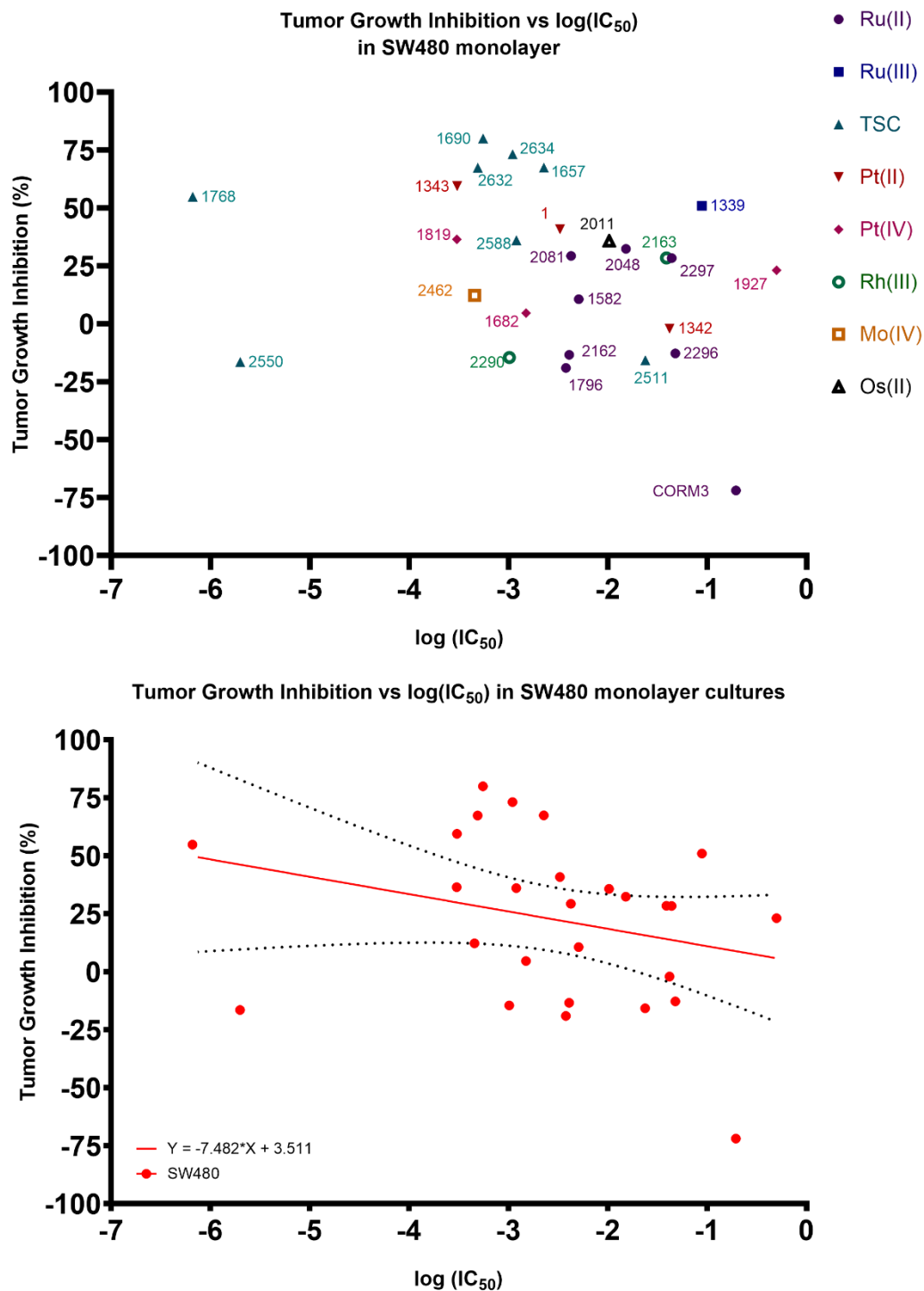
MTT assays in SW480 human colon carcinoma cells have been part of the primary substance screening practiced at this laboratory for more than two decades. Even though SW480 cells are unsuitable for scaffold-free spheroid production and hence not considered in the sections dealing with 3D cultures below, the correlation of their results with *in-vivo* outcomes in the CT26 murine colon carcinoma model represents a benchmark, upon which any alternative *in-vitro* methodology applied here should improve.

Figure 38 shows a scatter plot of IC<sub>50</sub> values in SW480 cells vs inhibition of CT26 tumor growth for all tested substances (27 data pairs). Linear regression was plotted with the formula  $y = -.48x + 3.51$  ( $R^2=0.08$ ;  $F(1, 25) = 2.09$ ,  $p = \text{n.s.}$ ). Correlation was not significant ( $r = -0.36$ ,  $p = \text{n.s.}$ ). In addition, the scatter plot of IC<sub>50</sub> values in SW480 cells vs average tumor volume difference is shown in Figure 39, as well as a plot of the corresponding linear regression with the formula  $y = -30.60x + 8.44$  ( $R^2 = 0.08$ ;  $F(1, 25) = 2.23$ ,  $p = \text{n.s.}$ ). Correlation was not significant ( $r = -0.27$ ,  $p = \text{n.s.}$ ). Nor do the scatter plots suggest any substantial non-linear correlation. This confirms the poor predictive power of monolayer cytotoxicity tests for *in vivo* results, as stated in literature especially for colon cancer cell lines.<sup>13</sup>

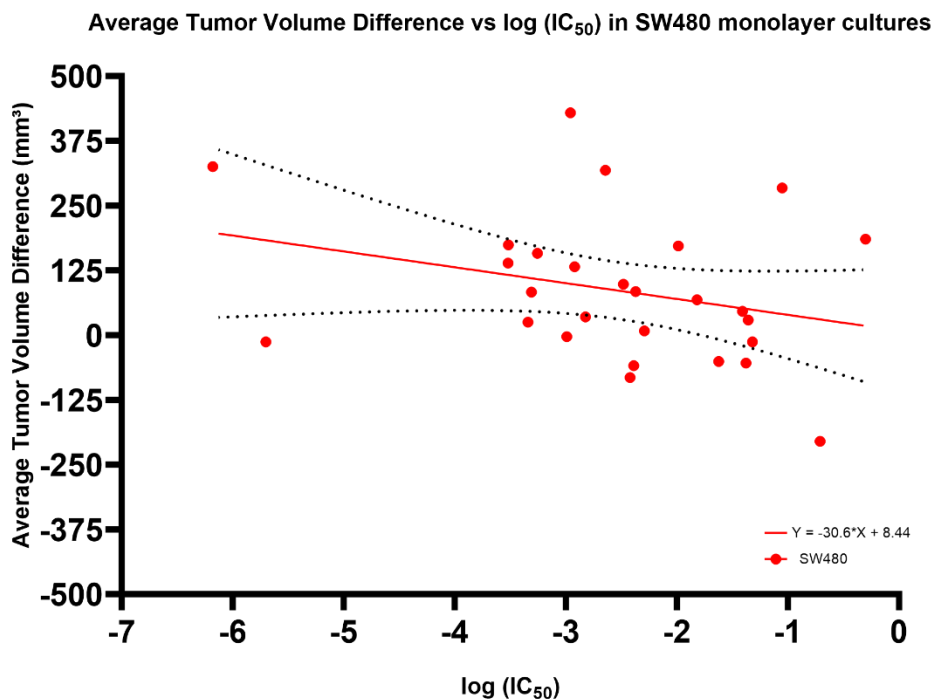
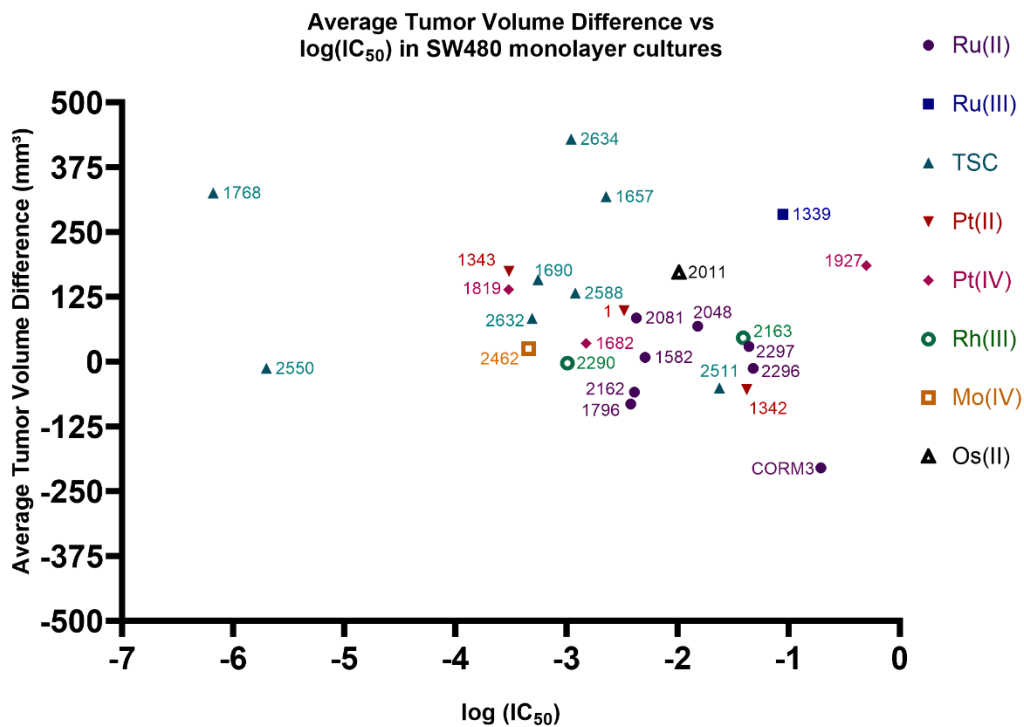
Evaluation by subgroup was also carried out. Plots of the linear regression for all Ru(II) and Ru(III) compounds (9 data pairs), all thiosemicarbazone compounds (8 data pairs) and for all Pt(II) and Pt(IV) compounds (6 data pairs) tested are shown in Figures 40 and 41. In addition, linear regression plots are shown, taking into account only positive values for tumor growth inhibition and average tumor volume difference, respectively (19 data pairs for each evaluation method); hence, only substances that had a tumor-inhibiting effect *in vivo* and thus were active in the CT26 tumor model were considered here. No analysis carried out within these subgroups showed a significant correlation. The significance of the slopes' deviation from 0 was checked with the *F*-test (Table 20). Deviation from 0 was not significant for any of these subgroups.

Table 20: Subgroup analysis of CT26 *in vivo* vs SW480 *in vitro* data.

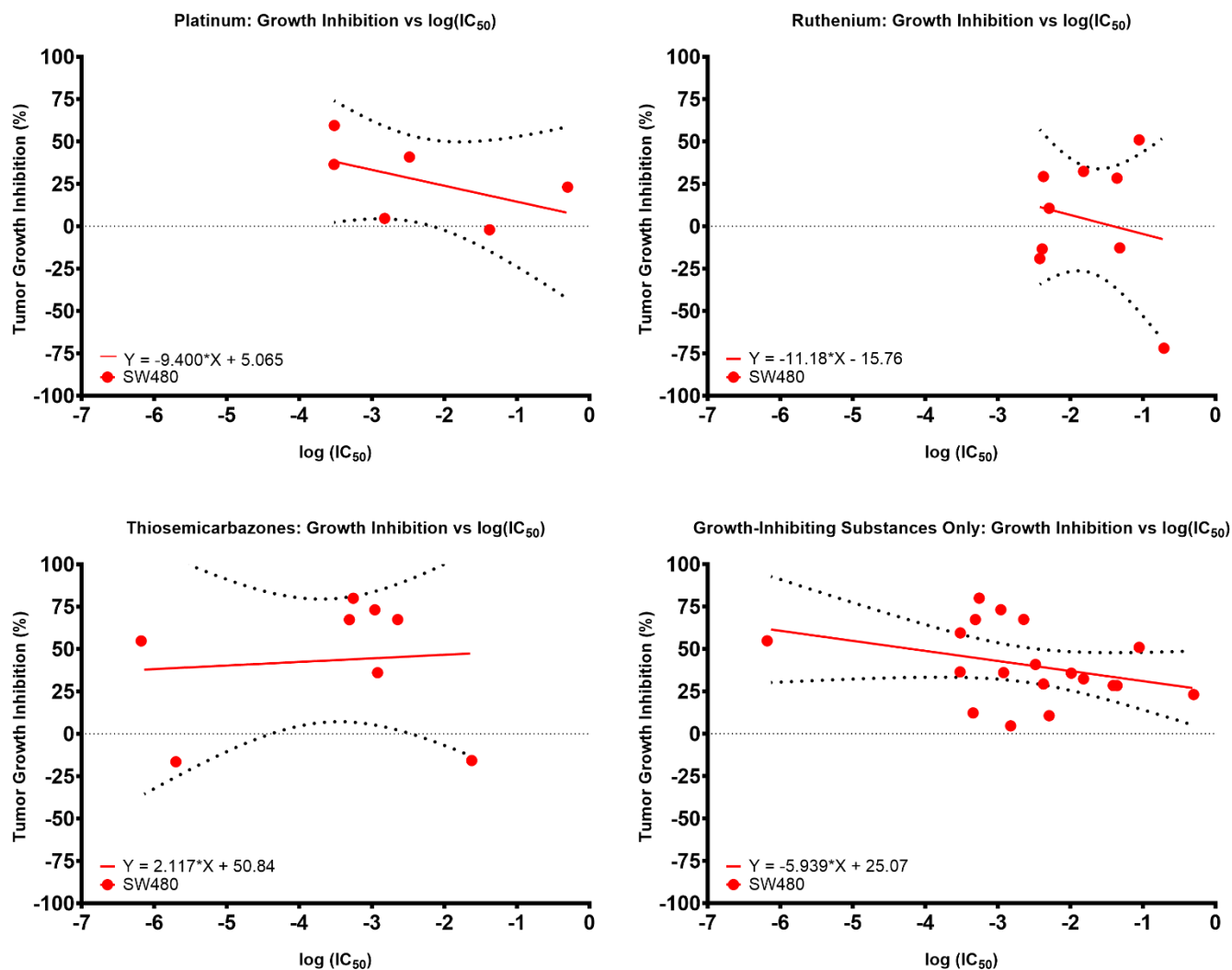
Analyzed subgroup	Correlation analysis		Linear Regression	
	Correlation coefficient <i>r</i>	<i>p</i> value	<i>Y</i> =	Statistical information
Pt(II) & Pt(IV) / tumor growth inhibition	-0.49	n.s.	-9.40x + 5.07	( $R^2=0.27$ $F(1, 4)=1.45$ , $p=\text{n.s.}$ )
Pt(II) & Pt(IV) / tumor volume difference	-0.03	n.s.	-9.37x + 74.27	( $R^2=0.02$ $F(1, 4)=0.07$ , $p=\text{n.s.}$ )
Ru(II) & Ru(III) / tumor growth inhibition	0.15	n.s.	-11.18x - 15.76	( $R^2=0.04$ $F(1, 7)=0.28$ , $p=\text{n.s.}$ )
Ru(II) & Ru(III) / tumor volume difference	0.12	n.s.	6.40x + 23.90	( $R^2=0.001$ $F(1, 7)=0.01$ , $p=\text{n.s.}$ )
TSCs / tumor growth inhibition	0.05	n.s.	2.12x + 50.84	( $R^2=0.01$ $F(1, 6)=0.04$ , $p=\text{n.s.}$ )
TSCs / tumor volume difference	-0.19	n.s.	-11.81x + 130.40	( $R^2=0.01$ $F(1, 6)=0.07$ , $p=\text{n.s.}$ )
Positive values only / tumor growth inhibition	-0.44	n.s.	-5.94x + 25.07	( $R^2=0.12$ $F(1, 17)=2.22$ , $p=\text{n.s.}$ )
Positive values only / tumor volume difference	-0.18	n.s.	-24.30x + 83.60	( $R^2=0.0663$ $F(1, 17)=1.21$ , $p=\text{n.s.}$ )



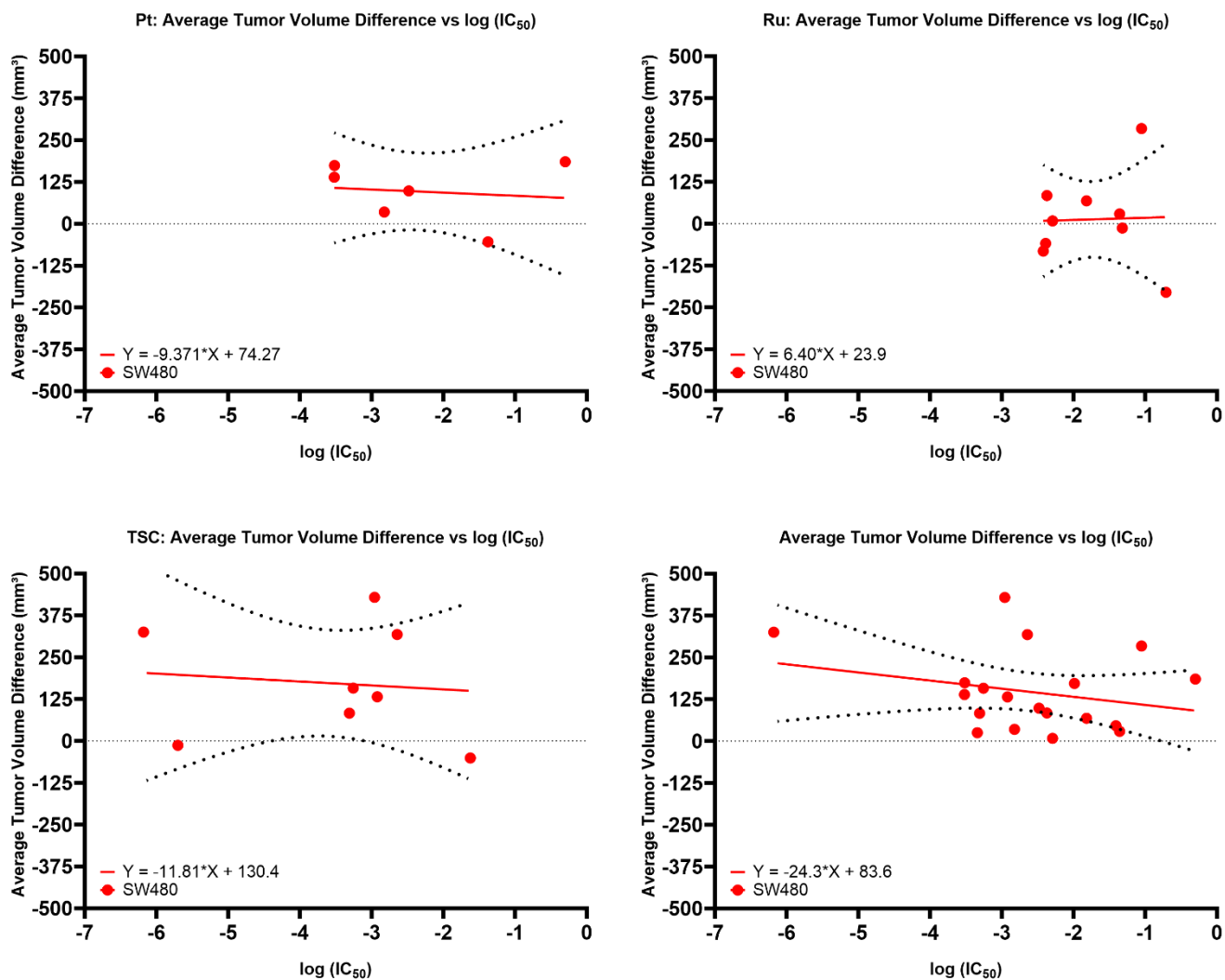
**Figure 38:** Correlation analysis of tumor growth inhibition in CT26 *in vivo* and SW480 monolayer *in vitro* data and linear regression.



**Figure 39** Correlation analysis of average tumor volume difference in CT26 *in vivo* and SW480 monolayer *in vitro* data and linear regression.



**Figure 40** Linear regression for subgroup analysis of tumor growth inhibition in CT26 *in vivo* and SW480 monolayer *in vitro* data.



**Figure 41** Linear regression for subgroup analysis of average tumor volume difference in CT26 *in vivo* and SW480 monolayer *in vitro* data.

## 4.5.2 Analysis of CT26 *in vivo* vs HCT116 Monolayer *in vitro* Data

Figure 42 shows a scatter plot of IC<sub>50</sub> values in HCT116 monolayer cultures vs inhibition of CT26 tumor growth for all tested substances (27 data pairs). Linear regression was plotted with the formula  $y = -8.52x + 2.71$  ( $R^2 = 0.12$ ;  $F(1, 25) = 3.29$ ,  $p = \text{n.s.}$ ). Correlation was significant ( **$r = -0.40$ ,  $p < 0.05$** ). In addition, the scatter plot of IC<sub>50</sub> values in HCT116 cells vs average tumor volume difference is shown in Figure 43, as well as a plot of the corresponding linear regression with the formula  $y = -32.80x + 10.00$  ( $R^2 = 0.11$ ;  $F(1, 25) = 3.05$ ,  $p = \text{n.s.}$ ). Correlation was not significant ( $r = -0.30$ ,  $p = \text{n.s.}$ ).

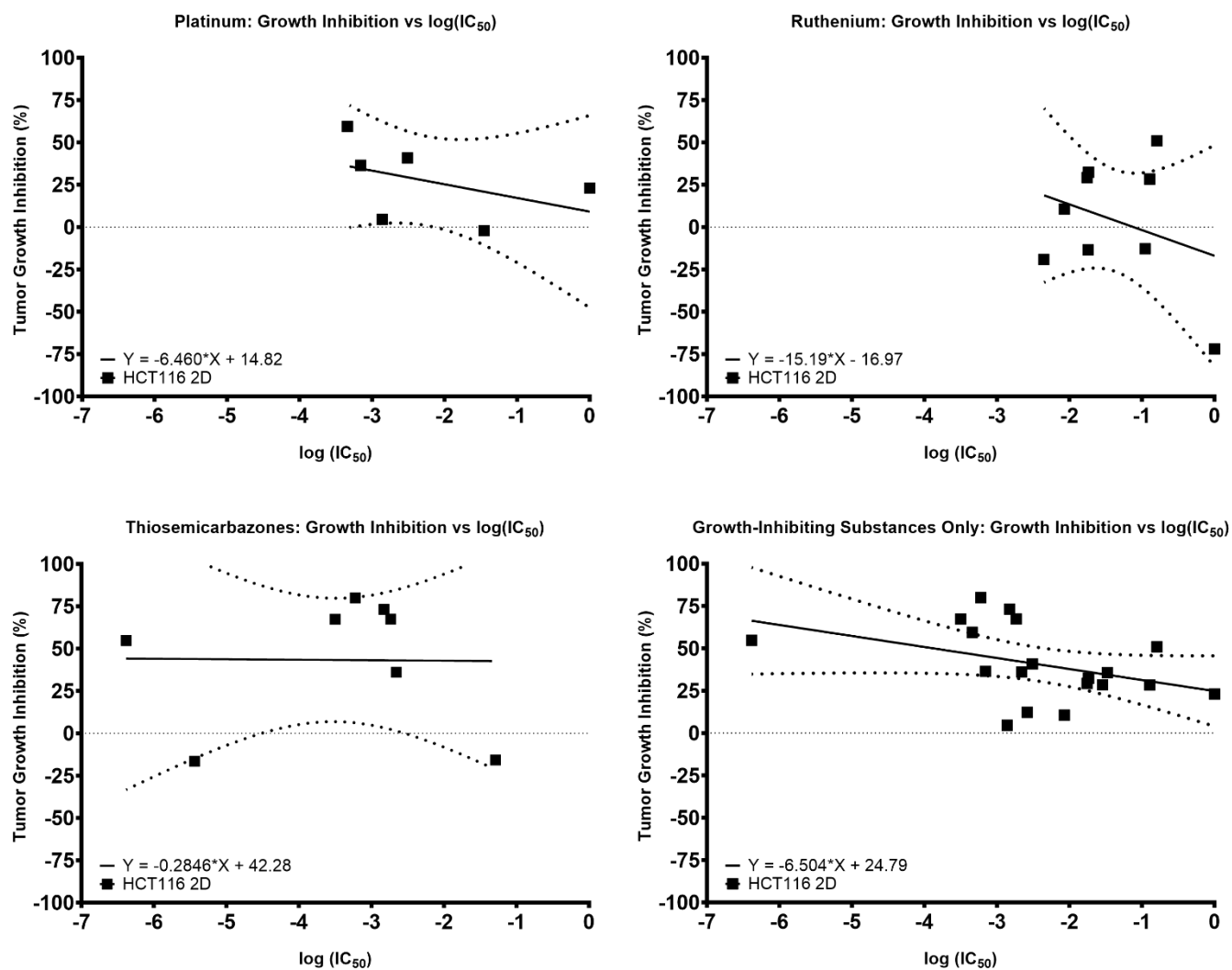
Evaluation by subgroup was also carried out. Plots of the linear regression for all Ru(II) and Ru(III) (9 data pairs), all thiosemicarbazone compounds (8 data pairs) and for all Pt(II) and Pt(IV) compounds (6 data pairs) tested are shown in Figures 44 and 45. In addition, linear regression plots are shown, taking into account only positive values for tumor growth inhibition and average tumor volume difference, respectively (19 data pairs for each evaluation method); hence, only substances that had a tumor-inhibiting effect *in vivo* and thus were active in the CT26 tumor model were considered here. Only one analysis carried out within these subgroups showed a significant correlation: When tumor-promoting substances were excluded, CT26 tumor growth inhibition vs IC<sub>50</sub> values in HCT116 monolayer cultures showed a correlation coefficient of  **$r = -0.53$** . The linear regression was checked with the F-test (Table 21), yielding no statistical significance, however.

Table 21: Subgroup analysis of CT26 *in vivo* vs HCT116 monolayer *in vitro* data.

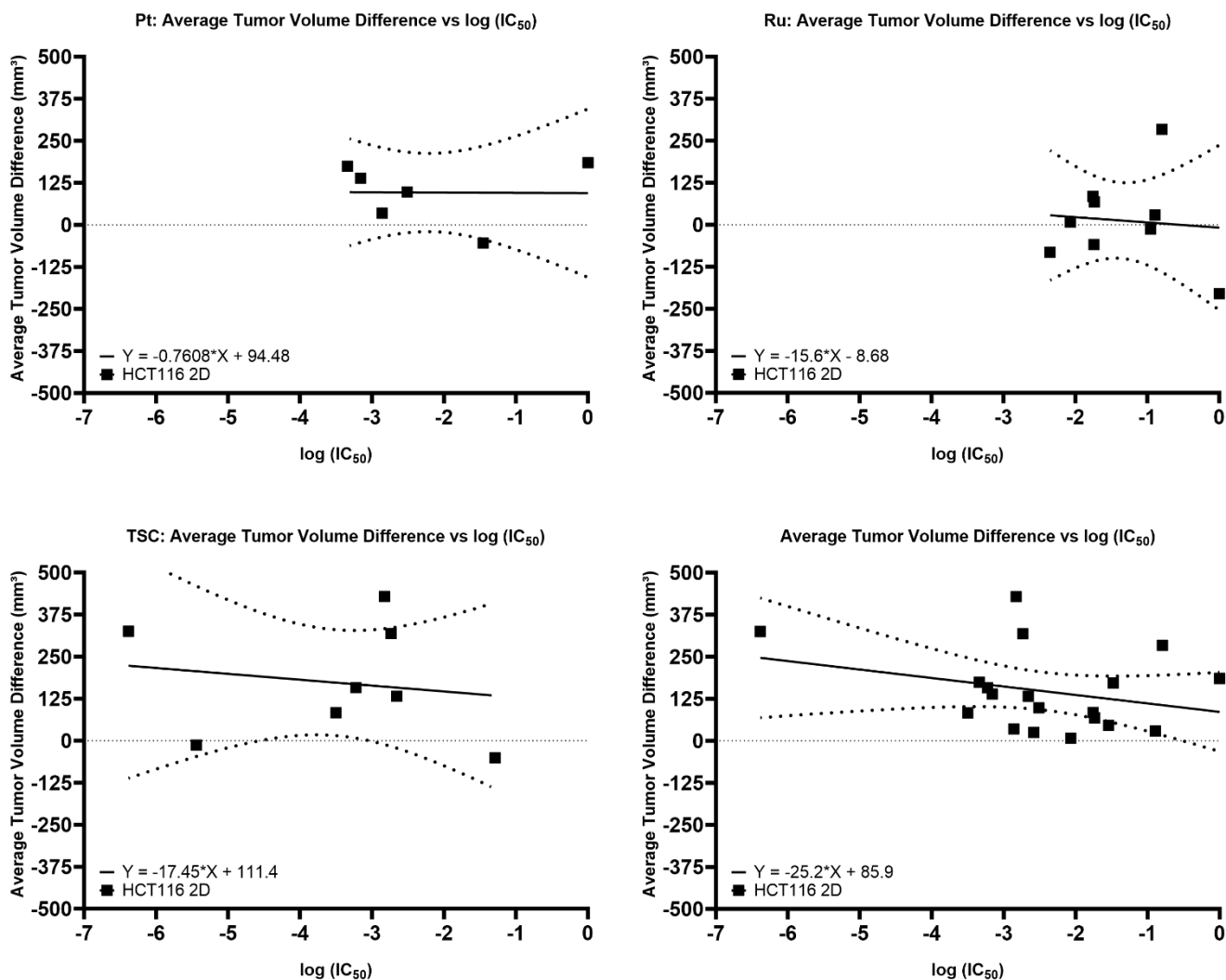
Analyzed subgroup	Correlation analysis		Linear Regression	
	Correlation coefficient $r$	$p$ -value	$Y=$	Statistical information
Pt(II) & Pt(IV) / tumor growth inhibition	-0.60	n.s.	$-8.07x + 9.12$	( $R^2=0.20$ $F(1, 4)=0.98$ , $p=\text{n.s.}$ )
Pt(II) & Pt(IV) / tumor volume difference	-0.09	n.s.	$-0.76x + 94.48$	( $R^2=0.0001$ $F(1, 4)=0.0004$ , $p=\text{n.s.}$ )
Ru(II) & Ru(III) / tumor growth inhibition	0.12	n.s.	$-15.19x - 16.97$	( $R^2=0.09$ $F(1, 7)=0.71$ , $p=\text{n.s.}$ )
Ru(II) & Ru(III) / tumor volume difference	0.08	n.s.	$-15.60x - 8.68$	( $R^2=0.01$ $F(1, 7)=0.05$ , $p=\text{n.s.}$ )
TSC / tumor growth inhibition	-0.02	n.s.	$-0.28x + 42.28$	( $R^2=0.0001$ $F(1, 6)=0.001$ , $p=\text{n.s.}$ )
TSC vs tumor volume difference	-0.24	n.s.	$-17.45x + 111.40$	( $R^2=0.03$ $F(1, 6)=0.17$ , $p=\text{n.s.}$ )
Positive values only / tumor growth inhibition	-0.53	<0.05	$-5.94x + 25.07$	( $R^2=0.12$ $F(1, 17)=2.22$ , $p=\text{n.s.}$ )
Positive values only / tumor volume difference	-0.20	n.s.	$-24.30x + 83.60$	( $R^2=0.0663$ $F(1, 17)=1.21$ , $p=\text{n.s.}$ )







**Figure 44:** Linear regression for subgroup analysis of tumor growth inhibition in CT26 *in vivo* and HCT116 monolayer *in vitro* data.



**Figure 45:** Linear regression for subgroup analysis of average tumor volume difference in CT26 *in vivo* and HCT116 monolayer *in vitro* data.

### 4.5.3 Analysis of CT26 *in vivo* vs CT26 Monolayer *in vitro* Data

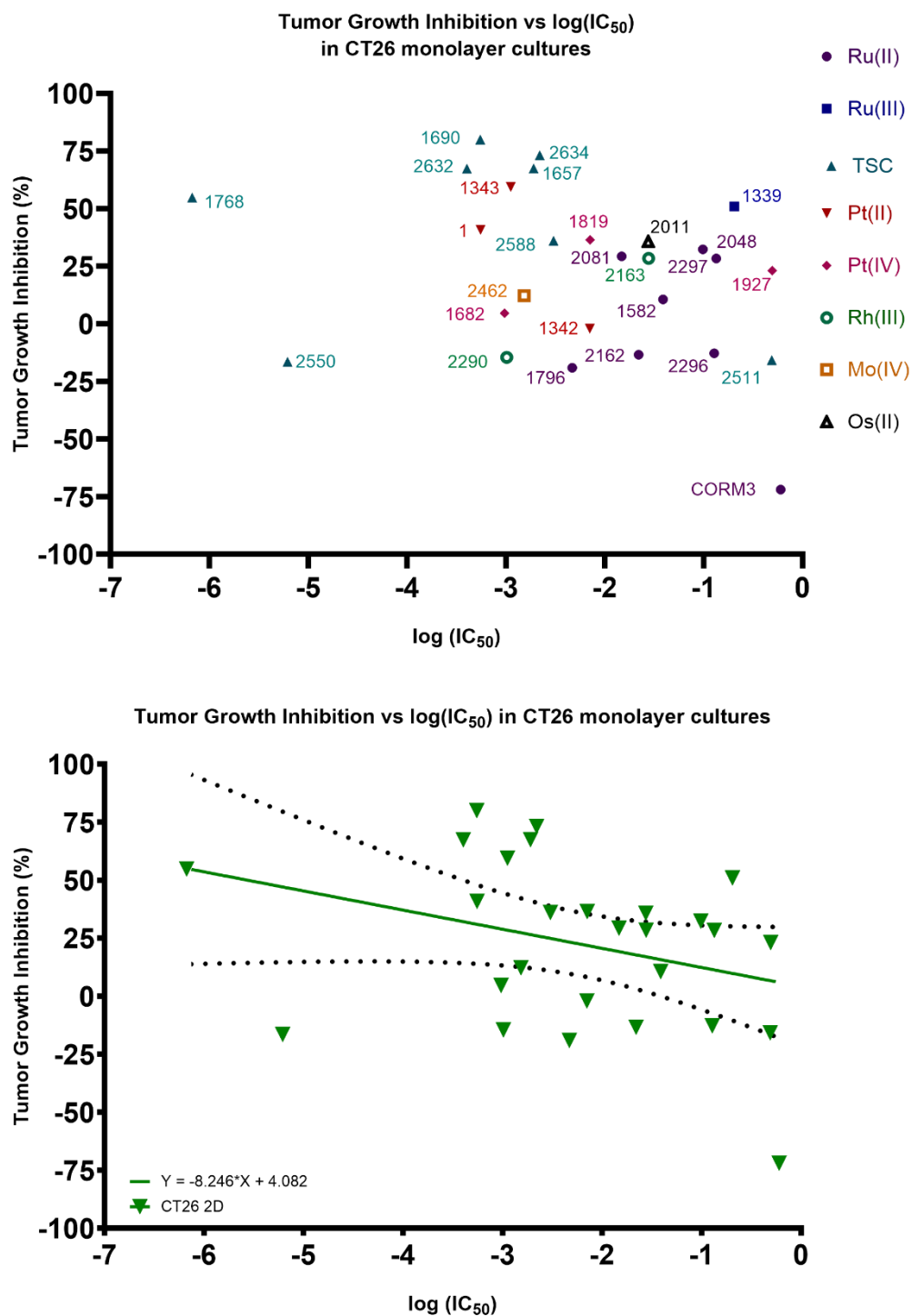
Figure 46 shows a scatter plot of IC<sub>50</sub> values in CT26 monolayer cultures vs inhibition of CT26 tumor growth for all tested substances (27 data pairs). Linear regression was plotted with the formula  $y = -8.52x + 2.71$  ( $R^2 = 0.12$ ;  $F(1, 25) = 3.29$ ,  $p = \text{n.s.}$ ). Correlation was not significant ( $r = -0.36$ ,  $p = \text{n.s.}$ ). In addition, the scatter plot of IC<sub>50</sub> values in CT26 cells vs average tumor volume difference is shown in Figure 47, as well as a plot of the corresponding linear regression with the formula  $y = -32.80x + 10.00$  ( $R^2=0.11$ ;  $F(1, 25)=3.05$ ,  $p=\text{n.s.}$ ). Correlation was not significant ( $r=-0.23$ ,  $p=\text{n.s.}$ ).

Evaluation by subgroup was also carried out. Plots of the linear regression for all Ru(II) and Ru(III) compounds (9 data pairs), all thiosemicarbazone compounds (8 data pairs) and for all Pt(II) and Pt(IV) compounds (6 data pairs) tested are shown in Figures 48 and 49. In addition, linear regression plots are shown, taking into account only positive values for tumor growth inhibition and average tumor volume difference, respectively (19 data pairs for each evaluation method); hence, only substances that had a tumor-inhibiting effect *in vivo* and thus were active in the CT26 tumor model were considered here. Only one analysis carried out within these subgroups showed a significant correlation. When tumor-promoting substances were excluded, CT26 tumor growth inhibition vs IC<sub>50</sub> values in CT26 monolayer cultures showed a correlation coefficient of  **$r=-0.48$** . The linear regression was checked with the F-test ( Table 22), yielding no statistical significance, however.

Table 22: Subgroup analysis of CT26 *in vivo* vs CT26 monolayer *in vitro* data.

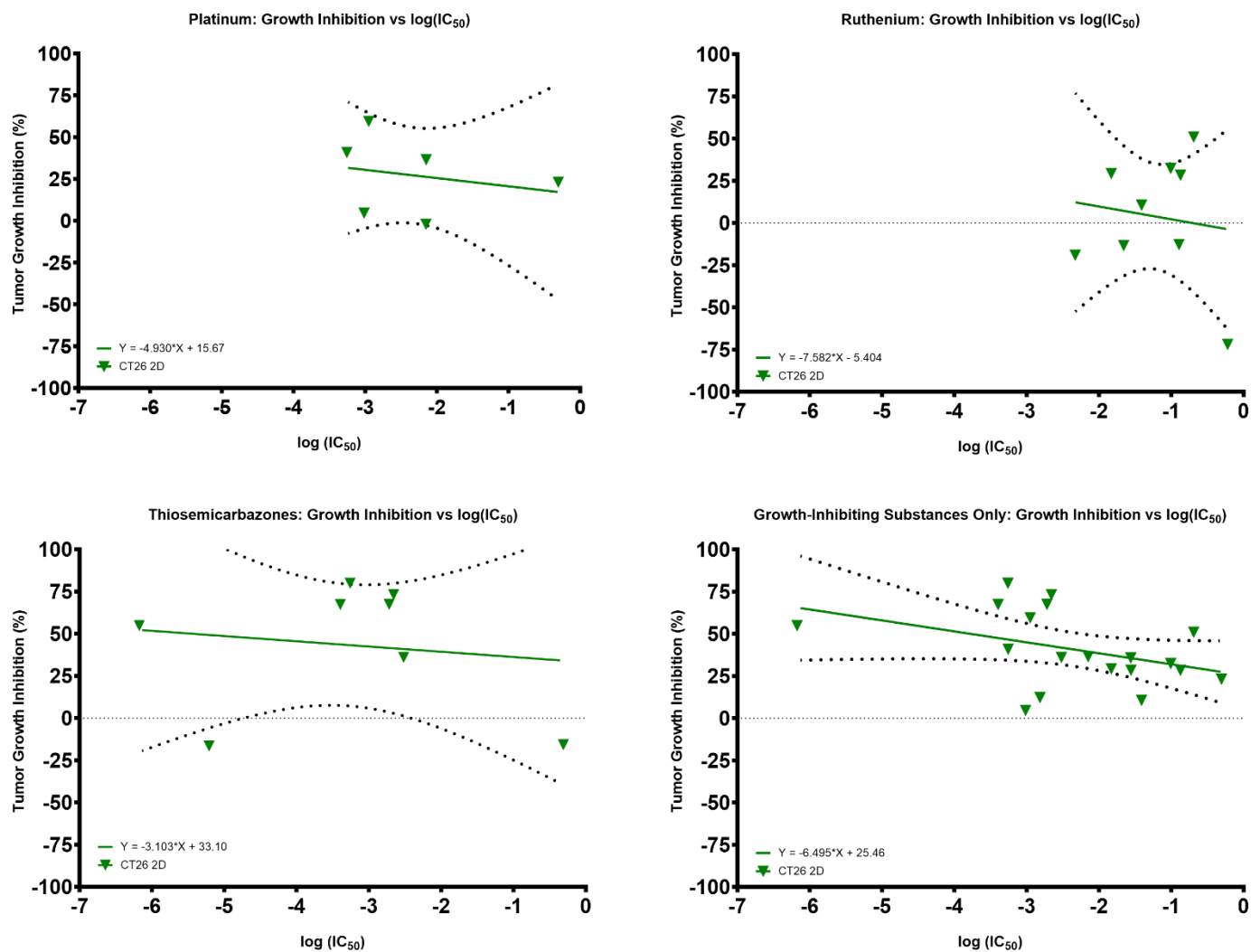
Analyzed subgroup	Correlation analysis		Linear Regression	
	Correlation coefficient $r$	$p$ -value	$Y=$	Statistical information
Pt(II) & Pt(IV) / tumor growth inhibition	-0.60	n.s.	$-4.93x + 15.67$	( $R^2=0.05$ $F(1, 4)=0.22$ , $p=\text{n.s.}$ )
Pt(II) & Pt(IV) / tumor volume difference	0.49	n.s.	$26.01x + 156.10$	( $R^2=0.09$ $F(1, 4)=0.42$ , $p=\text{n.s.}$ )
Ru(II) & Ru(III) / tumor growth inhibition	0.12	n.s.	$-7.58x - 5.40$	( $R^2=0.02$ $F(1, 7)=0.12$ , $p=\text{n.s.}$ )
Ru(II) & Ru(III) / tumor volume difference	0.07	n.s.	$8.54x + 23.00$	( $R^2=0.002$ $F(1, 7)=0.01$ , $p=\text{n.s.}$ )
TSC / tumor growth inhibition	0.00	n.s.	$-3.10x + 33.10$	( $R^2=0.02$ $F(1, 6)=0.12$ , $p= \text{n.s.}$ )
TSC / tumor volume difference	-0.19	n.s.	$-23.72x + 94.82$	( $R^2=0.06$ $F(1, 6)=0.39$ , $p=\text{n.s.}$ )
Positive values only / growth inhibition	-0.48	<0.05	$-6.50x + 25.46$	( $R^2=0.16$ $F(1, 17)=3.18$ , $p= \text{n.s.}$ )

Positive values only /s tumor volume difference	-0.14	n.s.	-25.40x + 88.00	( $R^2=0.08$ F(1, 17)=1.53, p= n.s.)
---	-------	------	-----------------	--------------------------------------

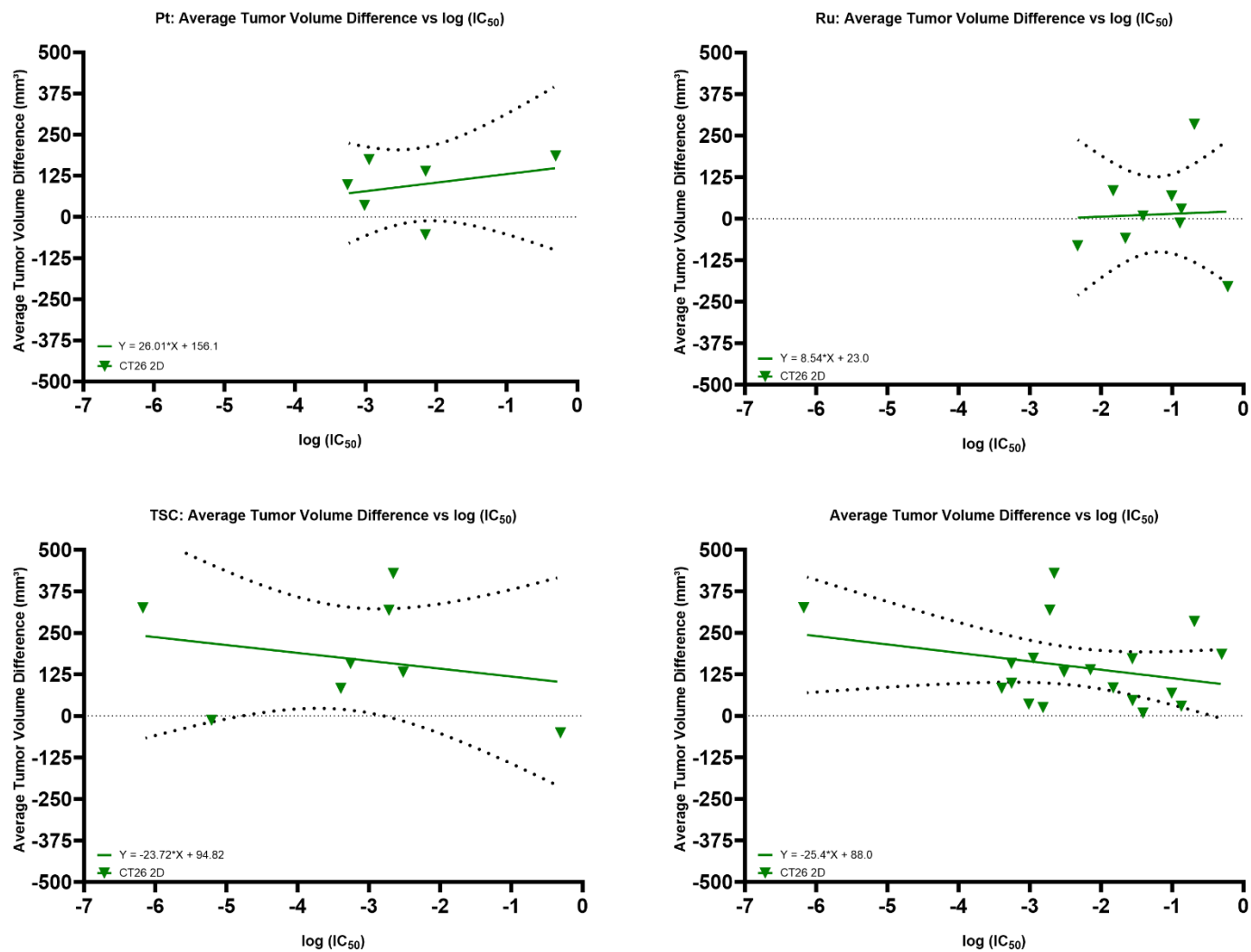


**Figure 46** Correlation analysis of tumor growth inhibition in CT26 *in vivo* and CT26 monolayer *in vitro* data and linear regression.





**Figure 48** Linear regression for subgroup analysis of tumor growth inhibition in CT26 *in vivo* and CT26 monolayer *in vitro* data.



**Figure 49** Linear regression for subgroup analysis of average tumor volume difference in CT26 *in vivo* and CT26 monolayer *in vitro* data.

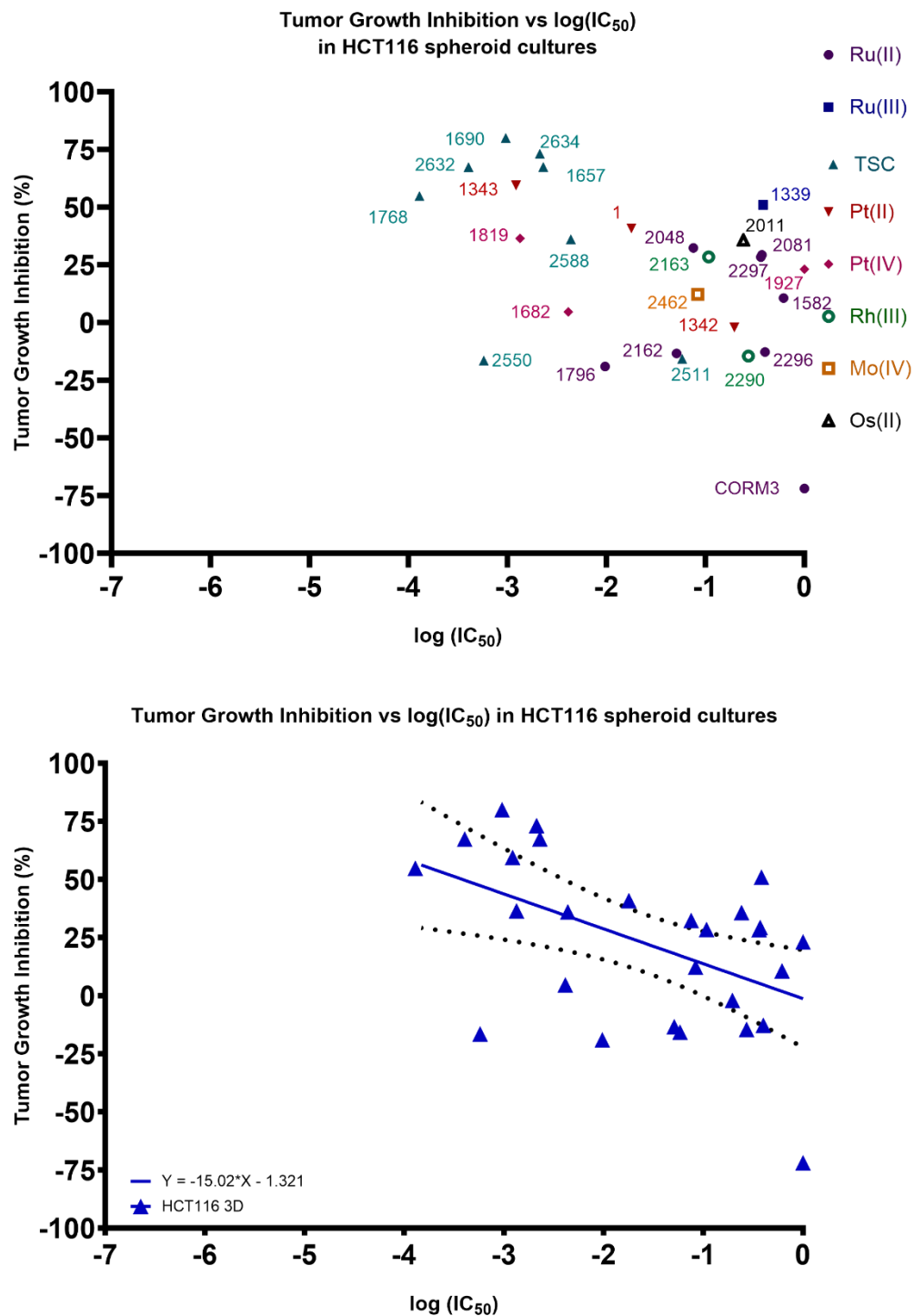
#### 4.5.4 Analysis of CT26 *in vivo* vs HCT116 Spheroid *in vitro* Data

Figure 50 shows a scatter plot of IC<sub>50</sub> values in HCT116 spheroid cultures vs inhibition of CT26 tumor growth for all tested substances (27 data pairs). Linear regression with was plotted with the formula  $y = -15.02x - 1.32$  ( $R^2 = 0.25$ ;  $F(1, 25) = 8.39$ ,  $p < 0.01$ ). Correlation was significant ( $r = -0.47$ ;  $p < 0.05$ ). In addition, the scatter plot of IC<sub>50</sub> values in HCT116 spheroids vs average tumor volume difference is shown in Figure 51, as well as a plot of the corresponding linear regression with the formula  $y = -50.80x + 5.50$  ( $R^2 = 0.18$ ;  $F(1, 25) = 5.55$ ,  $p < 0.05$ ). Correlation was not significant ( $r = -0.32$ ,  $p = \text{n.s.}$ ).

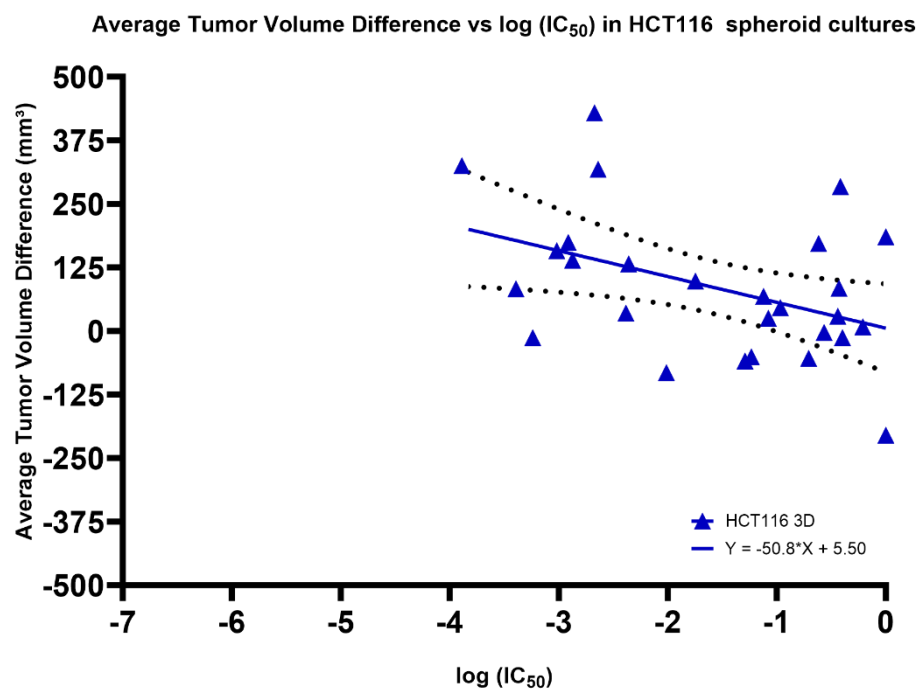
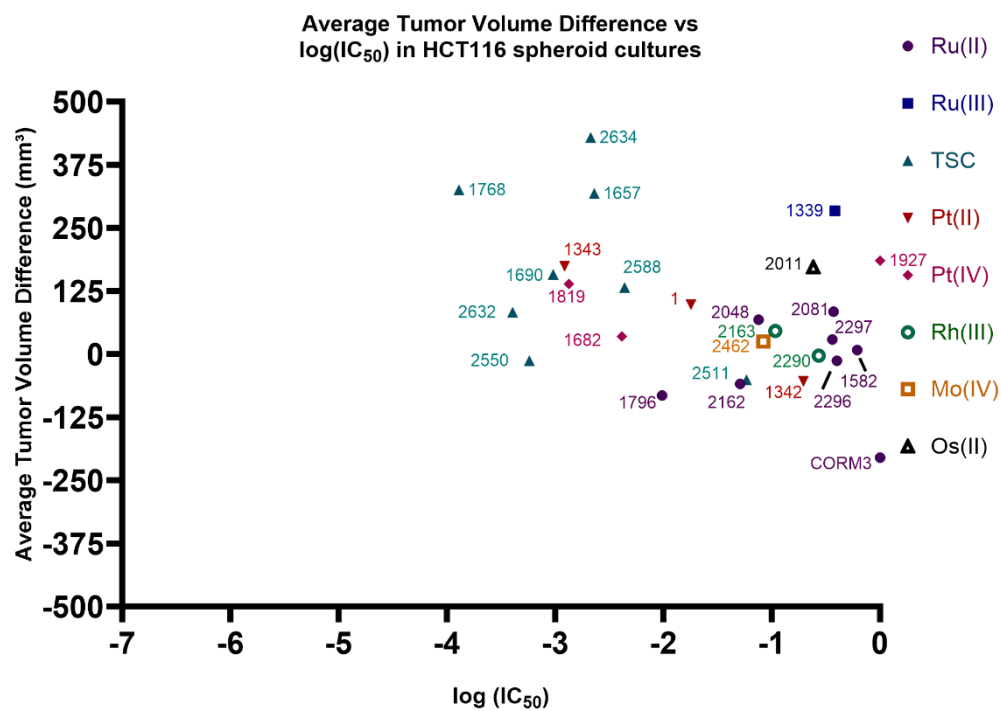
Evaluation by subgroup was also carried out. Plots of the linear regression for all Ru(II) and Ru(III) compounds (9 data pairs), all thiosemicarbazone compounds (8 data pairs) and for all Pt(II) and Pt(IV) compounds (6 data pairs) tested are shown in Figure 52 and 53. In addition, linear regression plots are shown, taking into account only positive values for tumor growth inhibition and average tumor volume difference, respectively (19 data pairs for each evaluation method); hence, only substances that had a tumor-inhibiting effect *in vivo* and thus were active in the CT26 tumor model were considered here. Only one analysis carried out within these subgroups showed a significant correlation – When tumor-promoting substances were excluded, CT26 tumor growth inhibition vs IC<sub>50</sub> values in HCT116 spheroid cultures showed a correlation coefficient of  $r = -0.68$ . The linear regression was checked with the F-test (Table 23), yielding a high significance for this model.

**Table 23:** Subgroup analysis of CT26 *in vivo* vs HCT116 spheroid *in vitro* data.

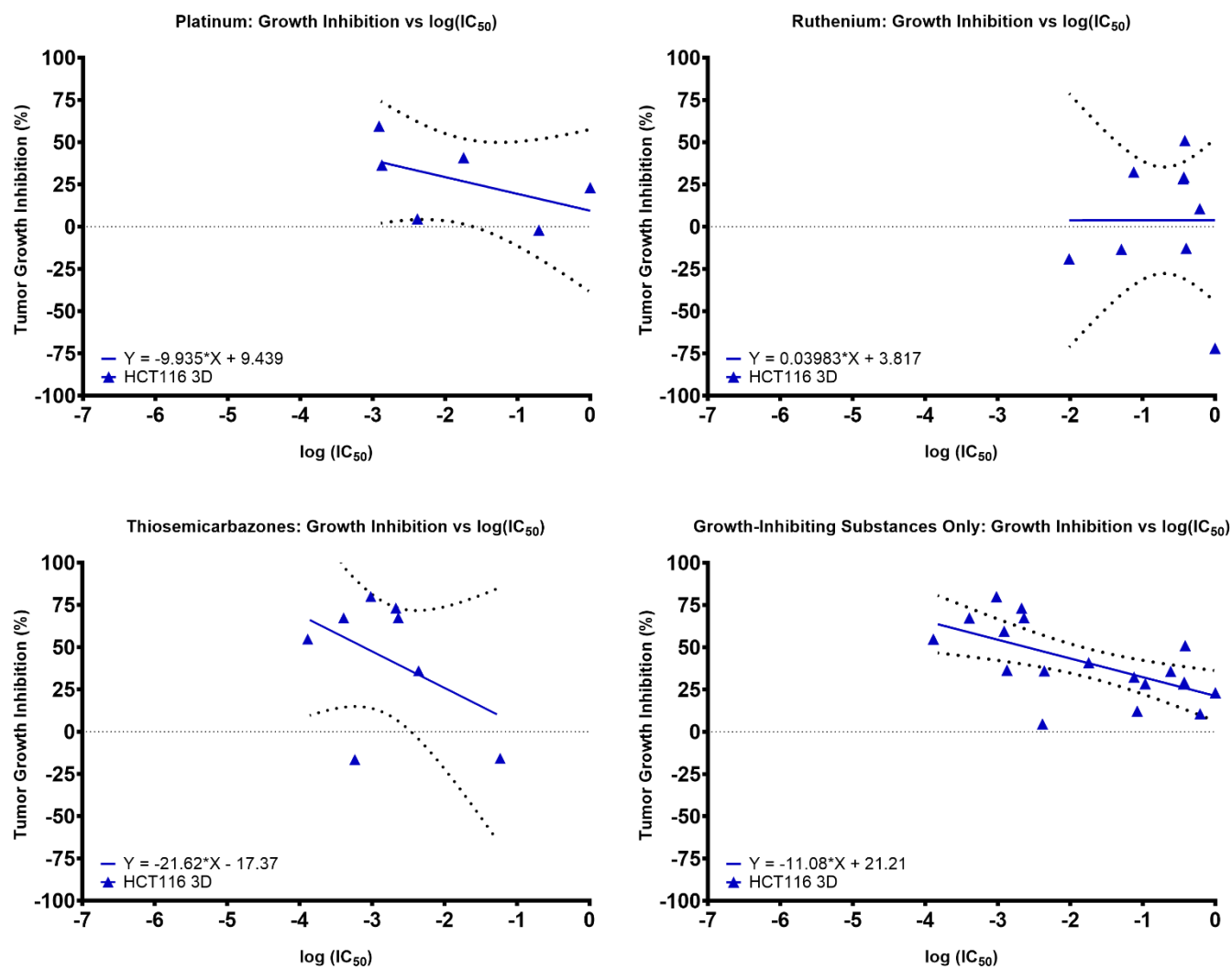
Analyzed subgroup	Correlation analysis		Linear Regression	
	Correlation coefficient $r$	$p$ -value	$Y =$	Statistical information
Pt(II) & Pt(IV) / tumor growth inhibition	-0.60	n.s.	$-9.94x + 9.44$	( $R^2 = 0.26$ $F(1, 4) = 1.43$ , $p = \text{n.s.}$ )
Pt(II) & Pt(IV) / tumor volume difference	-0.09	n.s.	$-14.09x + 71.21$	( $R^2 = 0.03$ $F(1, 4) = 0.14$ , $p = \text{n.s.}$ )
Ru(II) & Ru(III) / tumor growth inhibition	-0.05	n.s.	$0.04x + 3.82$	( $R^2 = 0.0000005$ $F(1, 7) = 0.000003$ , $p = \text{n.s.}$ )
Ru(II) & Ru(III) / tumor volume difference	-0.02	n.s.	$24.80x + 30.10$	( $R^2 = 0.01$ $F(1, 7) = 0.10$ , $p = \text{n.s.}$ )
TSC / tumor growth inhibition	-0.01	n.s.	$-21.62x - 17.37$	( $R^2 = 0.20$ $F(1, 6) = 1.47$ , $p = \text{n.s.}$ )
TSC / tumor volume difference	-0.26	n.s.	$-79.14x - 40.96$	( $R^2 = 0.13$ $F(1, 6) = 0.87$ , $p = \text{n.s.}$ )
Positive values only / tumor growth inhibition	-0.68	<0.01	$-11.08x + 21.21$	( $R^2 = 0.39$ $F(1, 17) = 10.96$ , $p < 0.01$ )
Positive values only / tumor volume difference	-0.34	n.s.	$-37.60x + 81.20$	( $R^2 = 0.16$ $F(1, 17) = 3.12$ , $p = \text{n.s.}$ )



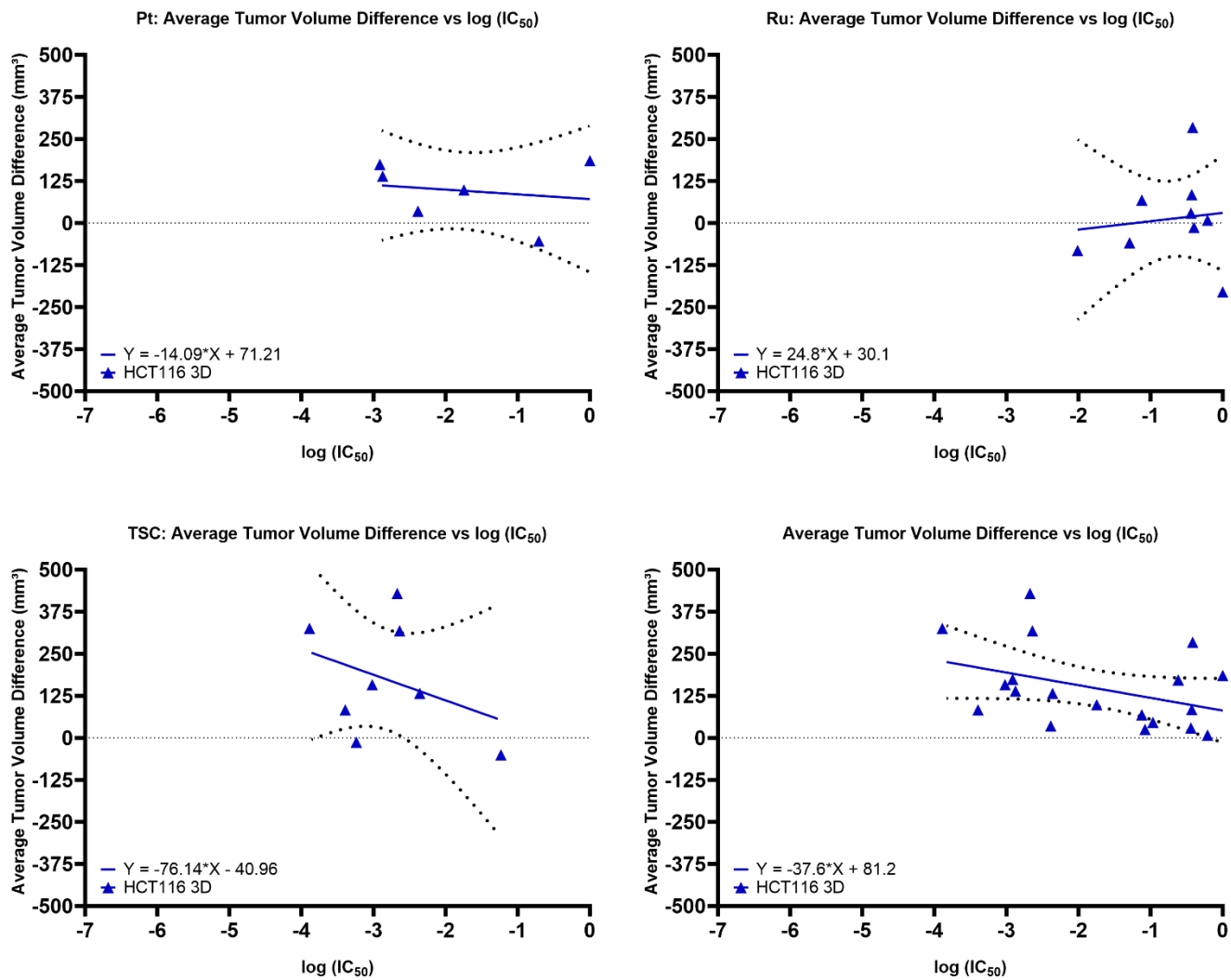
**Figure 50** Correlation analysis of tumor growth inhibition in CT26 *in vivo* and HCT116 spheroid *in vitro* data and linear regression.



**Figure 51** Correlation analysis of average tumor volume difference in CT26 *in vivo* and HCT11 spheroid *in vitro* data and linear regression.



**Figure 52** Linear regression for subgroup analysis of tumor growth inhibition in CT26 *in vivo* and HCT116 spheroid *in vitro* data.



**Figure 53** Linear regression for subgroup analysis of average tumor volume difference in CT26 *in vivo* and HCT116 spheroid *in vitro* data.

### 4.5.5 Analysis of CT26 *in vivo* vs CT26 Spheroid *in vitro* Data

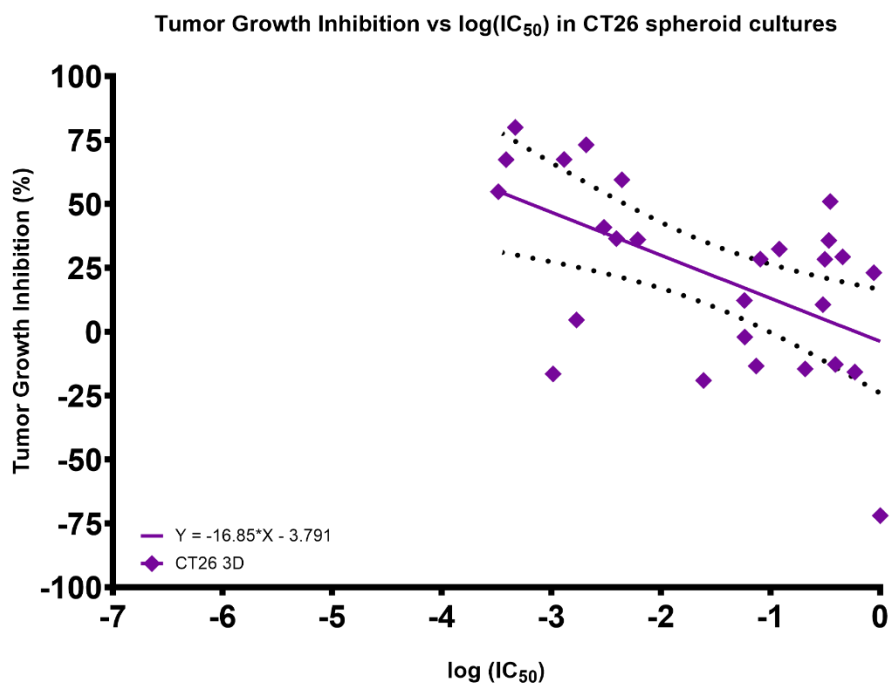
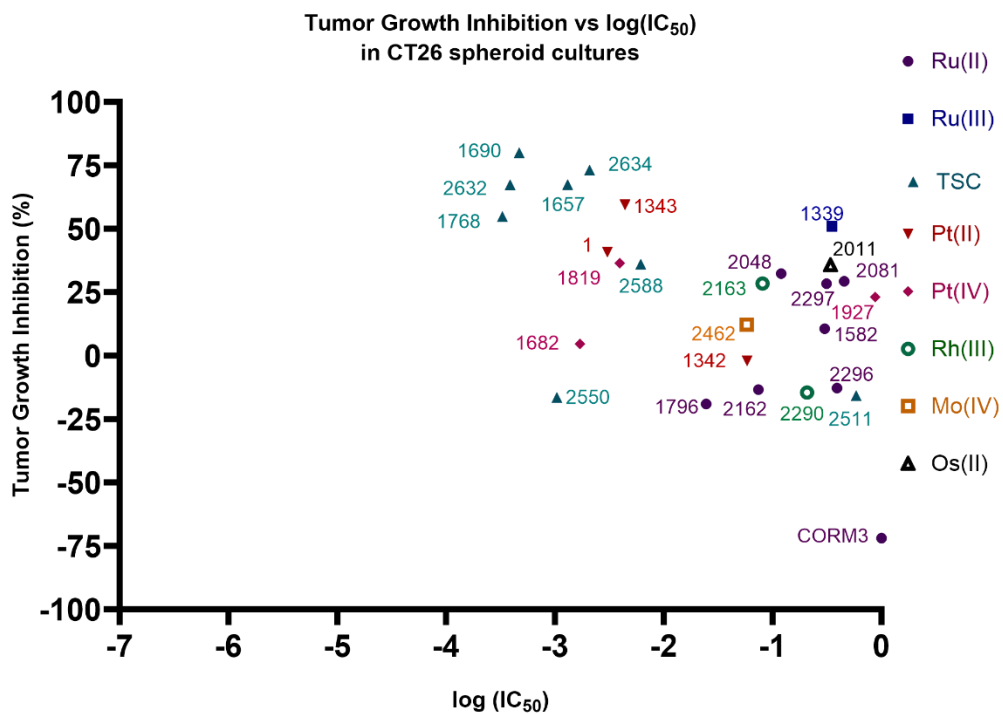
Figure 54 shows a scatter plot of IC<sub>50</sub> values in CT26 spheroid cultures vs inhibition CT26 tumor growth for all tested substances (27 data pairs). Linear regression with was plotted with the formula  $y = -16.85x - 3.79$  ( $R^2 = 0.30$   $F(1, 25) = 10.85$ ,  $p < 0.01$ ). Correlation was highly significant ( $r = -0.50$ ,  $p < 0.01$ ). In addition, the scatter plot of IC<sub>50</sub> values in CT26 spheroids vs average tumor volume difference is shown in Figure 55, as well as a plot of the corresponding linear regression with the formula  $y = -53.70x + 2.16$  ( $R^2 = 0.20$ ;  $F(1, 25) = 6.05$ ,  $p < 0.05$ ). Correlation was not significant ( $r = -0.34$ ,  $p = \text{n.s.}$ ).

Evaluation by subgroup was also carried out. Plots of the linear regression for all Ru(II) and Ru(III) compounds (9 data pairs), all thiosemicarbazone compounds (8 data pairs) and for all Pt(II) and Pt(IV) compounds (6 data pairs) tested are shown in Figures 56 and 57. In addition, linear regression plots are shown, taking into account only positive values for tumor growth inhibition and average tumor volume difference respectively (19 data pairs for each evaluation method); hence, only taking into account substances that had a tumor-inhibiting effect *in vivo* and thus were active in the CT26 tumor model were considered here. Only one analysis carried out within these subgroups showed a significant correlation – When tumor-promoting substances were excluded, CT26 tumor growth inhibition vs IC<sub>50</sub> values in CT26 spheroid cultures showed a correlation coefficient of  $r = -0.68$ . The linear regression was checked with the F-test (Table 24), yielding a high statistical significance for this model.

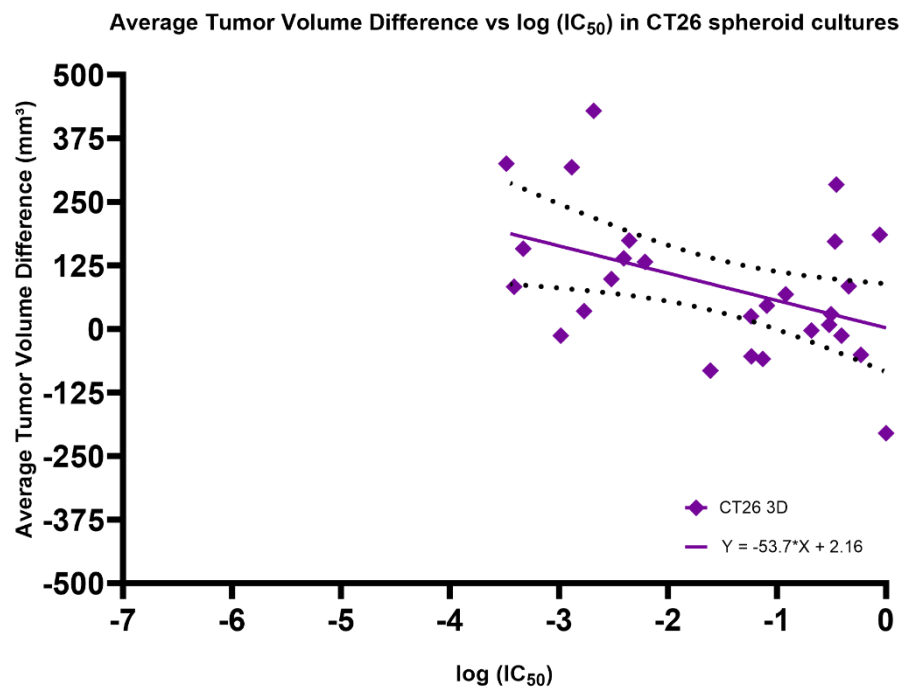
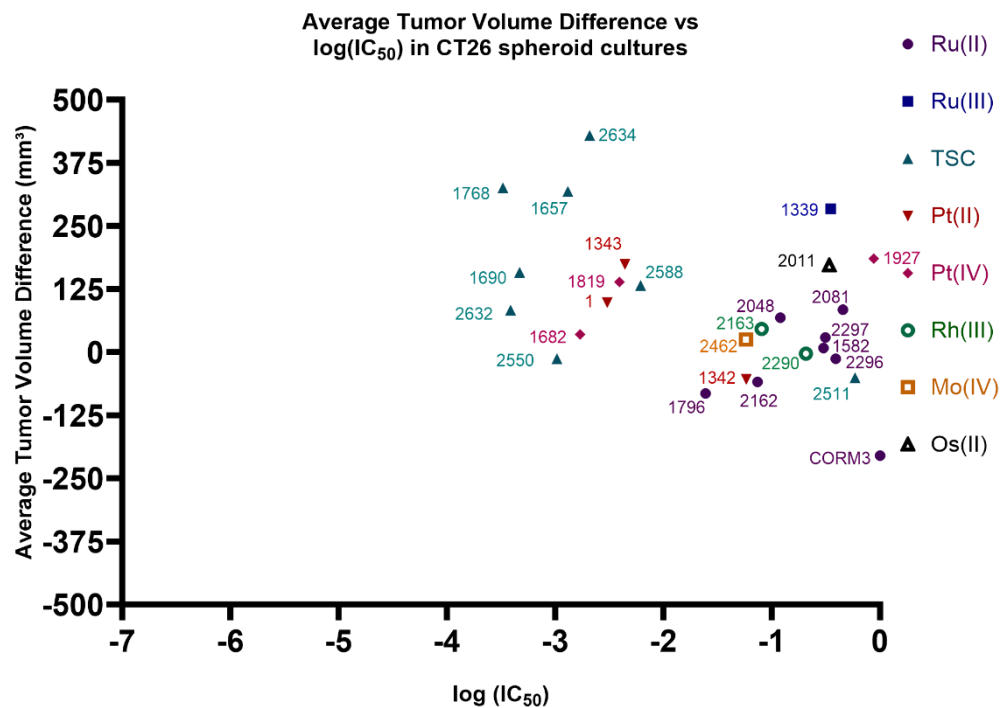
**Table 24:** Subgroup analysis of CT26 *in vivo* vs CT26 spheroid *in vitro* data.

Analyzed subgroup	Correlation analysis		Linear Regression	
	Correlation coefficient $r$	$p$ -value	$Y=$	Statistical information
Pt(II) & Pt(IV) / tumor growth inhibition	-0.14	n.s.	$-6.46x + 14.82$	( $R^2=0.08$ $F(1, 4)=0.37$ , $p=\text{n.s.}$ )
Pt(II) & Pt(IV) / tumor volume difference	0.43	n.s.	$10.78x + 116.50$	( $R^2=0.02$ $F(1, 4)=0.06$ , $p=\text{n.s.}$ )
Ru(II) & Ru(III) / tumor growth inhibition	-0.07	n.s.	$-4.97x + .54$	( $R^2=0.004$ $F(1, 7)=0.03$ , $p=\text{n.s.}$ )
Ru(II) & Ru(III) / tumor volume difference	-0.15	n.s.	$20.80x + 26.30$	( $R^2=0.01$ $F(1, 7)=0.04$ , $p=\text{n.s.}$ )
TSC/s tumor growth inhibition	-0.26	n.s.	$-23.35x - 18.65$	( $R^2=0.41$ $F(1, 6)=4.12$ , $p=\text{n.s.}$ )
TSC / tumor volume difference	-0.29	n.s.	$-74.01x - 23.60$	( $R^2=0.21$ $F(1, 6)=1.62$ , $p=\text{n.s.}$ )

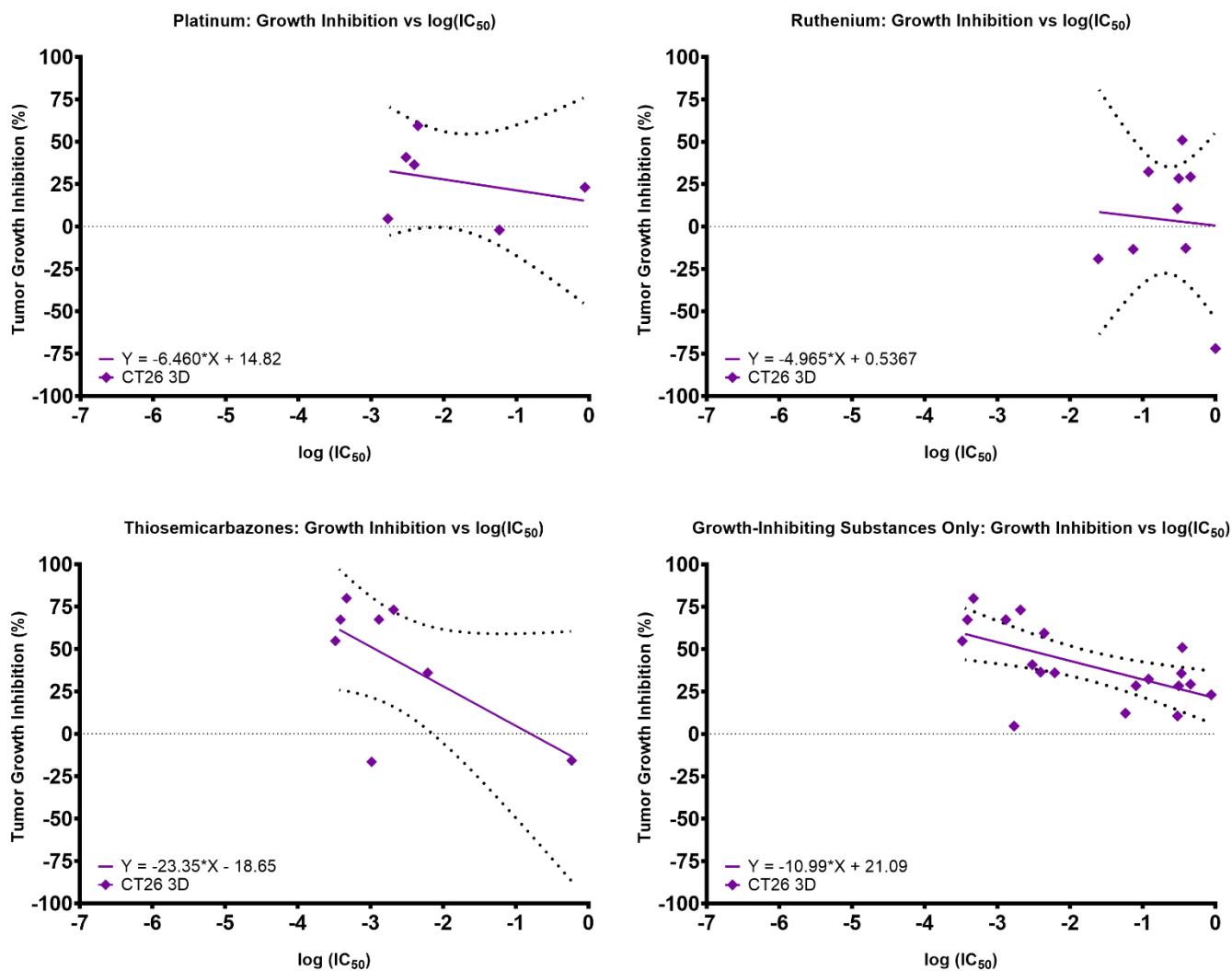
Positive values only / tumor growth inhibition	-0.58	<0.01	$-10.99x + 21.09$	$(R^2=0.36 \text{ } F(1, 17)=9.62, p<0.01)$
Positive values only / tumor volume difference	-0.21	n.s.	$-33.40x + 87.80$	$(R^2=0.11 \text{ } F(1, 17)=2.19, p=\text{n.s.})$



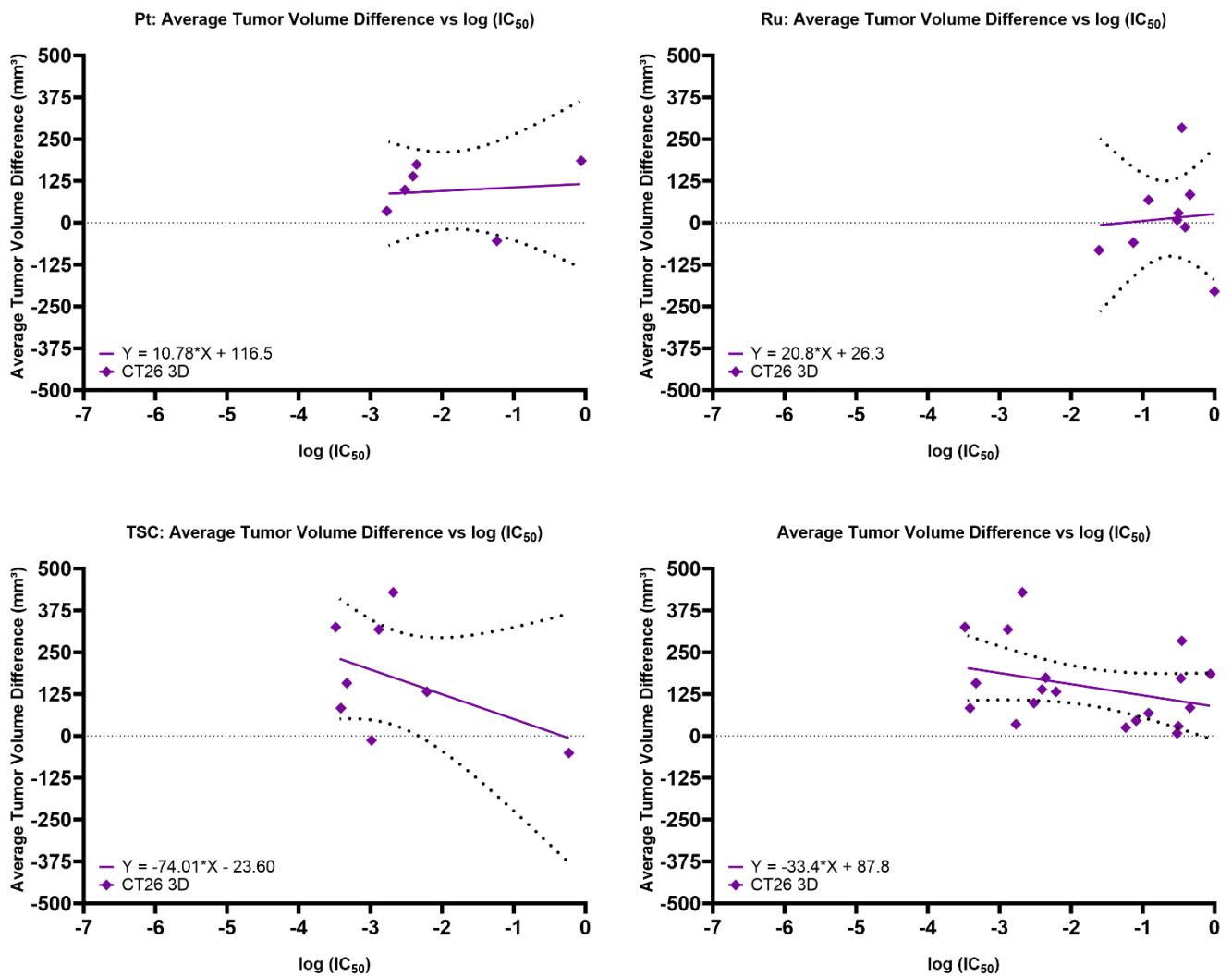
**Figure 54** Correlation analysis of tumor growth inhibition in CT26 *in vivo* and CT26 spheroid *in vitro* data and linear regression.



**Figure 55** Correlation analysis of average tumor volume difference in CT26 *in vivo* and CT26 spheroid *in vitro* data and linear regression.



**Figure 56** Linear regression for subgroup analysis of tumor growth inhibition in CT26 *in vivo* and CT26 spheroid *in vitro* data.



**Figure 57** Linear regression for subgroup analysis of average tumor volume difference in CT26 *in vivo* and CT26 spheroid *in vitro* data.

#### 4.5.6 Analysis of CT26 *in vivo* vs HCT116 *in vitro* IC<sub>50</sub> Quotients

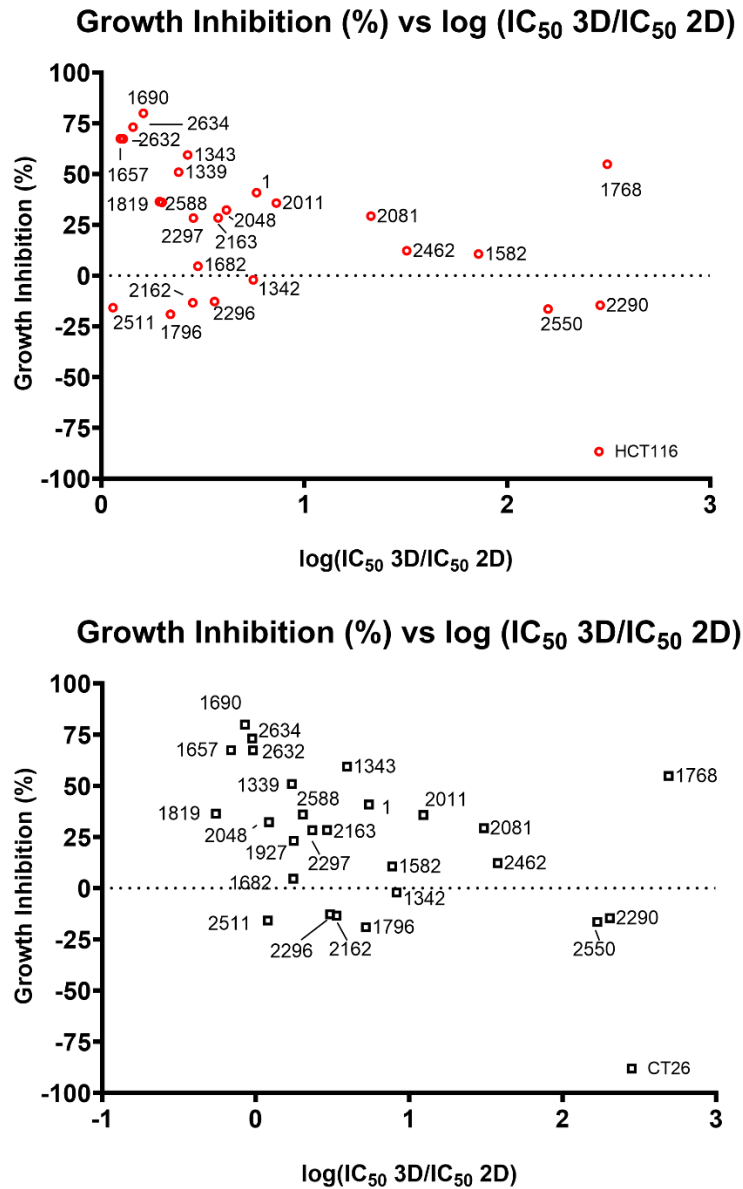
Figure 58 shows a scatter plot of IC<sub>50</sub> (3D/2D) quotients in the cell line HCT116 vs CT26 tumor growth inhibition for all tested substances (27 data pairs). Linear regression was plotted in Figure 60 with the formula  $y = 8.36x + 8.97$  ( $R^2 = 0.10$ ;  $F(1, 23) = 2.48$ ,  $p = \text{n.s.}$ ). Correlation was not significant ( $r = -0.36$ ,  $p = \text{n.s.}$ ). In Figure 59, the scatter plot of IC<sub>50</sub> values in HCT116 spheroids vs average tumor volume difference is shown, as well as a plot of the corresponding linear regression in Figure 60 with the formula  $y = -21.32x + 110.10$  ( $R^2 = 0.01$ ;  $F(1, 23) = 0.33$ ,  $p = \text{n.s.}$ ). Correlation was not significant ( $r = -0.21$ ,  $p = \text{n.s.}$ ). In Figure 61, a linear regression plot is shown, taking into account only positive values for tumor growth inhibition and average tumor volume difference (19 data pairs for each evaluation method); hence, only substances that had a tumor-inhibiting effect *in vivo* and thus were active in the CT26 tumor model were considered here. Linear regression of tumor growth inhibition (positive values only) vs IC<sub>50</sub> (3D/2D) quotients was plotted with the formula  $y = -13.42x + 51.13$  ( $R^2 = 0.16$ ;  $F(1, 16) = 3.15$ ,  $p = \text{n.s.}$ ). Correlation for this model was highly significant with  **$r = -0.64$  ( $p < 0.01$ )**. Linear regression of average tumor volume difference (positive values only) vs IC<sub>50</sub> (3D/2D) quotients was plotted with the formula  $y = -22.77x + 161.10$  ( $R^2 = 0.02$ ;  $F(1, 16) = 0.26$ ,  $p = \text{n.s.}$ ). Correlation for this model was not significant with  $r = -0.40$  ( $p = \text{n.s.}$ ). There was no significant correlation for any other subgroup.

#### 4.5.7 Analysis of CT26 *in vivo* vs CT26 *in vitro* IC<sub>50</sub> Quotients

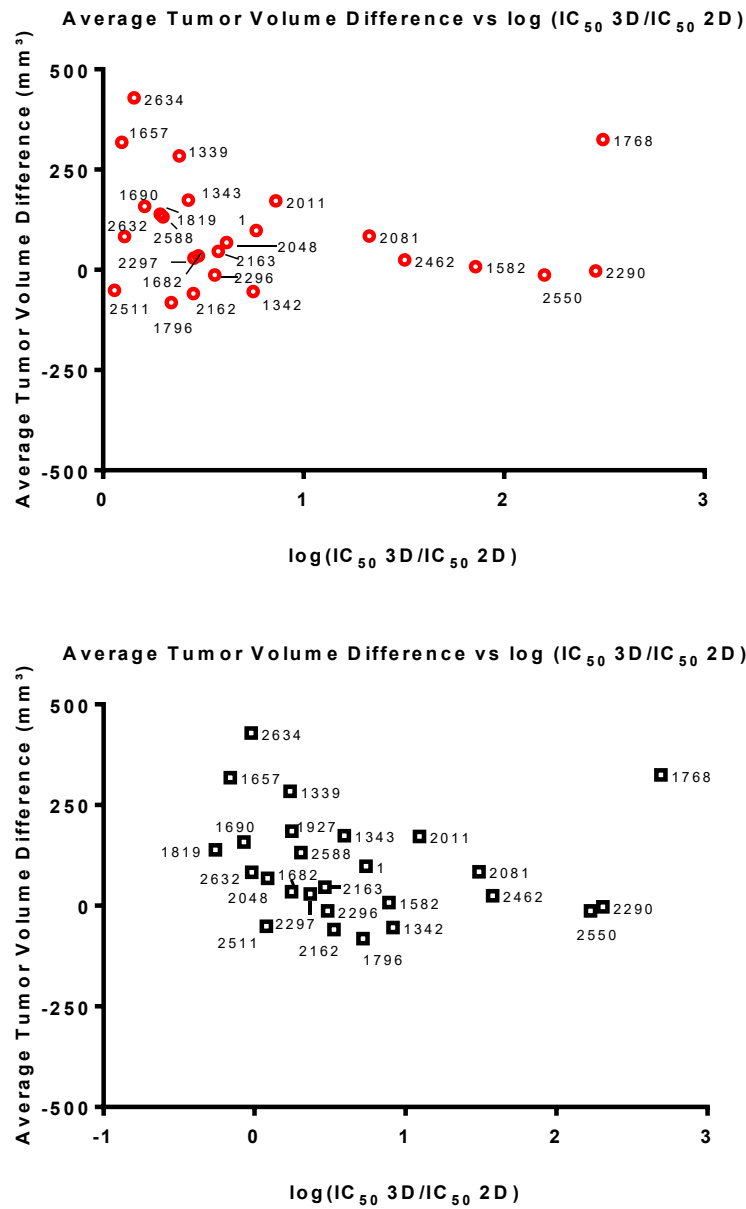
Figure 58 shows a scatter plot of IC<sub>50</sub> (3D/2D) quotients in the cell line CT26 vs CT26 tumor growth inhibition for all tested substances (27 data pairs). Linear regression was plotted in Figure 60 with the formula  $y = 7.46x + 7.70$  ( $R^2 = 0.12$ ;  $F(1, 24) = 3.28$ ,  $p = \text{n.s.}$ ). Correlation was significant ( **$r = -0.46$ ,  $p < 0.05$** ). In Figure 59, the scatter plot of IC<sub>50</sub> values in HCT116 spheroids vs average tumor volume difference is plotted, as well as a plot of the corresponding linear regression in Figure 60 with the formula  $y = -25.94x + 114.50$  ( $R^2 = 0.02$ ;  $F(1, 24) = 0.60$ ,  $p = \text{n.s.}$ ). Correlation was not significant ( $r = -0.33$ ,  $p = \text{n.s.}$ ). In Figure 61, a linear regression plot is shown for tumor inhibiting substances only, for tumor growth inhibition and average tumor volume difference (19 data pairs for each evaluation method). Linear regression for tumor growth inhibition (positive values only)

vs  $IC_{50}$  (3D/2D) quotients was plotted with the formula  $y = -7.57x + 44.74$  ( $R^2 = 0.07$ ;  $F(1, 17) = 1.19, p = \text{n.s.}$ ). Correlation for this model was significant with  $r = -0.46$  ( $p < 0.05$ ). Linear regression of average tumor volume difference (positive values only) vs  $IC_{50}$  (3D/2D) quotients was plotted with the formula  $y = -4.33x + 149.30$  ( $R^2 = 0.0007$ ;  $F(1, 17) = 0.01, p = \text{n.s.}$ ). Correlation for this model was not significant with  $r = -0.27$  ( $p = \text{n.s.}$ ).

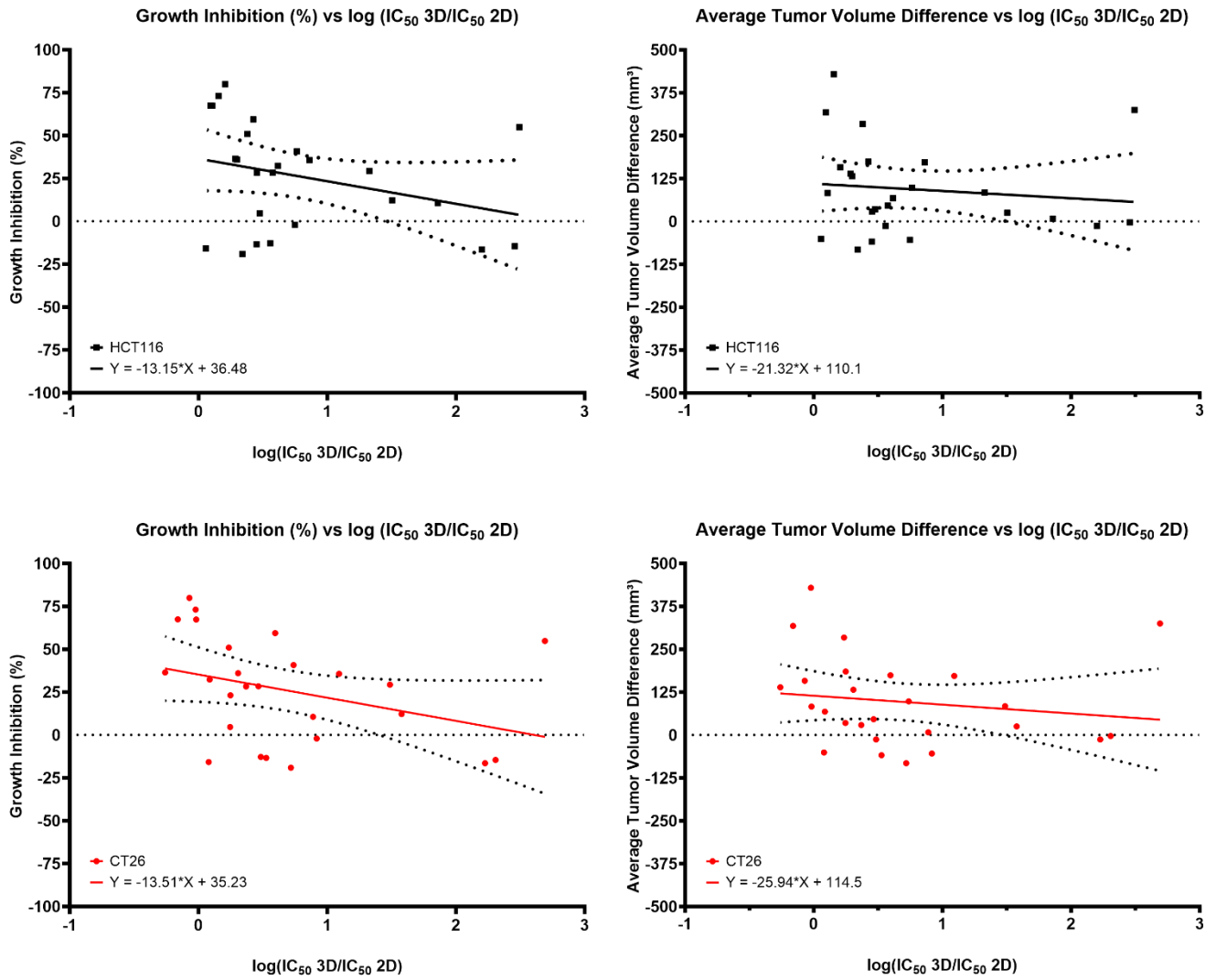
There was a significant correlation for  $IC_{50}$  (3D/2D) quotients in CT26 of thiosemicarbazones and tumor growth inhibition with  $r = -0.76$  ( $p < 0.05$ ). A linear regression plot is shown in Figure 62 for the formula  $y = -12.71x + 51.27$  ( $R^2 = 0.14$ ;  $F(1, 6) = 0.97; p = \text{n.s.}$ ). There was no correlation for the  $IC_{50}$  (3D/2D) quotients of platinum or ruthenium complex subgroups.



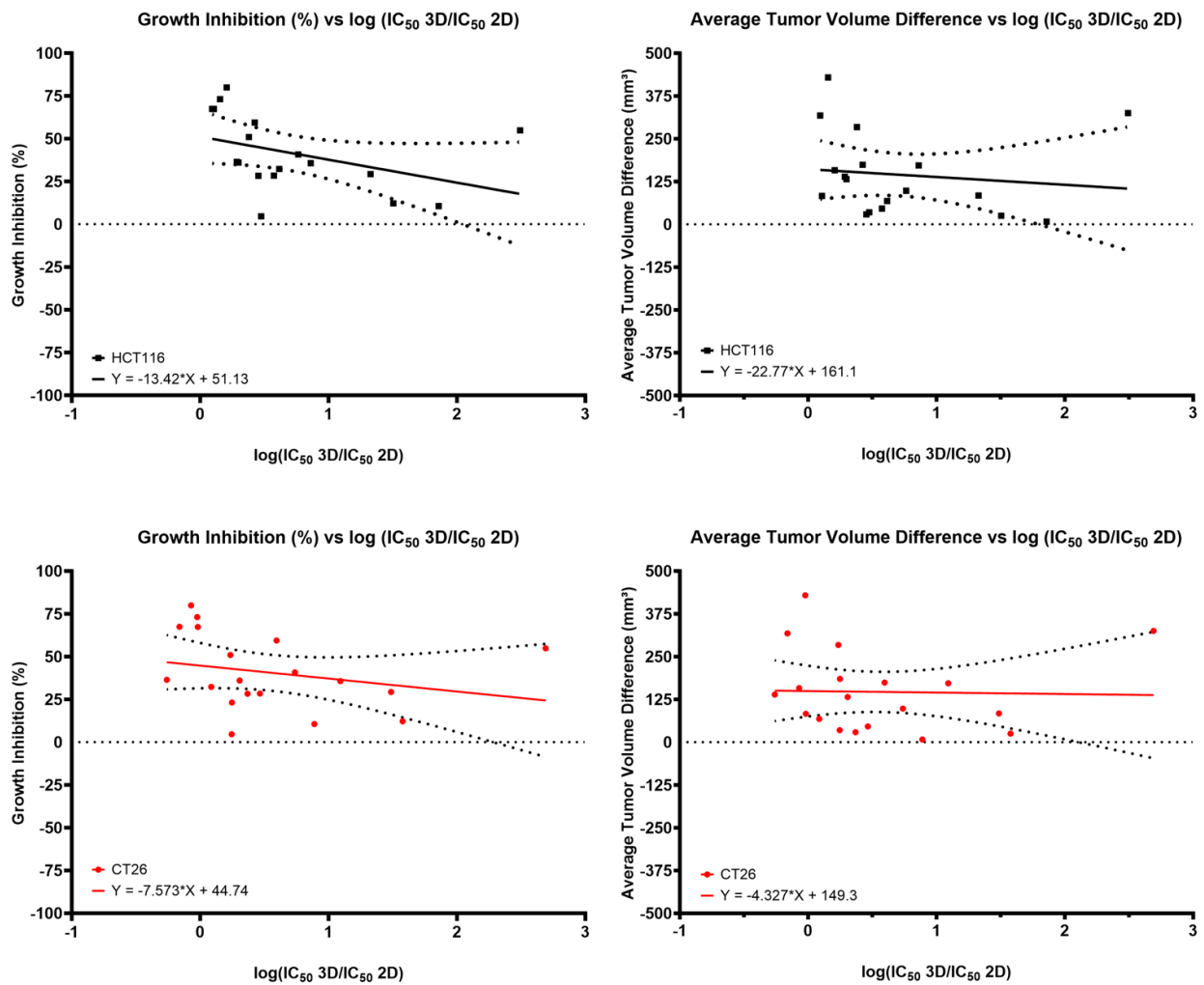
**Figure 58:** Scatterplots of CT26 tumor growth inhibition *in vivo* vs log (IC<sub>50</sub> 3D/IC<sub>50</sub> 2D) *in vitro* in the cell lines HCT116 (red, top) and CT26 (black, bottom).



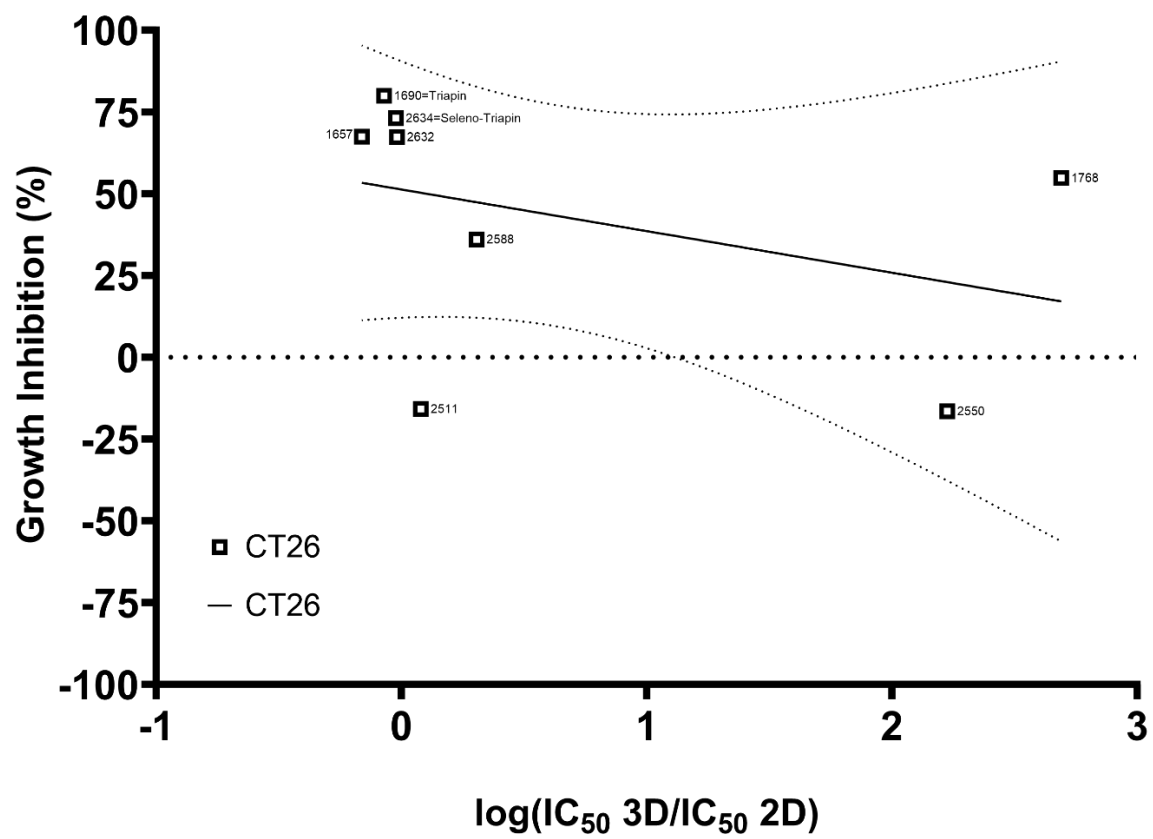
**Figure 59:** Scatterplots of average CT26 average tumor volume difference *in vivo* vs log (IC<sub>50</sub> 3D/IC<sub>50</sub> 2D) *in vitro* in the cell lines HCT116 (red, top) and CT26 (black, bottom).



**Figure 60:** Linear regression plotted for CT26 tumor growth inhibition (left) or average tumor volume difference (right) vs log (IC<sub>50</sub> 3D / IC<sub>50</sub> 2D) in the cell lines HCT116 (top) and CT26 (bottom).



**Figure 61:** Linear regression plotted for different evaluation methods in HCT116 and CT26 for log (IC<sub>50</sub> 3D / IC<sub>50</sub> 2D), taking into account only tumor inhibiting substances.



**Figure 62** Scatter plot and linear regression line for IC<sub>50</sub> values (3D/2D) of thiosemicarbazones in CT26 vs tumor growth inhibition (%) *in vivo*.

## 4.6 Discussion of *in vitro* Model Predictivity

The limited capacity to predict the *in vivo* efficacy of anticancer drugs by testing cytotoxicity in monolayer culture was confirmed in this study. Significant correlation between the entire sets of IC<sub>50</sub> values and growth inhibition (%) on day 15 (14) was observed only in one out of three monolayer models (HCT116). While there is significant correlation of cytotoxicity with growth inhibition in *in vivo* experiments, the linear regression is statistically not significant. This can be attributed to various factors, including a non-linear relationship between the two variables or the impact of a small sample size. We cannot see such a relationship between HCT116 monolayer culture and tumor volume reduction averaged over time *in vivo*.

The results and their statistical analysis are in agreement with the postulated superiority of predicting *in vivo* efficacy of drugs in high-throughput screenings in spheroid culture over monolayer culture. Significant correlation between tumor growth inhibition (%) and IC<sub>50</sub> values was found in both tested spheroid models (HCT116 and CT26). The slope of the linear regression was significantly non-zero for those spheroid models as well. In contrast to that, average tumor volume difference (mm<sup>3</sup>) did not correlate with any of the data sets.

Among all conducted subgroup analyses for classes of compounds, only one showed significant correlations. *In vivo* data, when all tumor-promoting substances are excluded, correlate with the IC<sub>50</sub> value data sets for all tested models except for SW480 monolayer culture. A relationship exists between tumor growth inhibition (%) and log IC<sub>50</sub> values in both tested spheroid models. In all models that showed significant correlation for the overall data set (including tumor-promoting substances), correlation for the subgroup was higher. This means that, if ways of identifying tumor-promoting substances beforehand could be found, predictivity for the degree of in-vivo activity would be markedly increased for the remaining compounds.

All other subgroup analyses were comprised of relatively small data sets (6 to 9) compounds. It is possible that low correlation for these small data sets stems from this very fact. Higher correlations

of *in vitro* with *in vivo* data would be plausible for substances with similar mechanisms of action. The evaluated subgroups included platinum compounds, ruthenium compounds, and thiosemicarbazones. Both platinum and ruthenium subgroups encompassed compounds with different oxidation states of the central metal: The platinum subgroup comprises Pt(II) and Pt(IV) compounds. Ruthenium compounds comprised Ru(III) as well as Ru(II) compounds. Ru(II) substances tested included Ru(II)–CO complexes, Ru(II)–arene complexes with various ligands such as maltol and flavonoid derivatives. Higher conformity within the subgroups regarding their metal center and mechanism of action as well as larger data sets for these subgroups might lead to an improved correlation. Future analysis with extended data sets is recommended.

Taking 3D/2D quotients for correlation analyses does not prove to be an advantage for overall analysis since correlation is not higher for the CT26 3D/2D quotient than for the 3D IC<sub>50</sub> value. In addition, there is no significant linear relationship between the *in vivo* data and the 3D/2D quotients in contrast to using log IC<sub>50</sub> values from spheroid culture. It might seem reasonable to infer that a highly decreased activity from 2D to 3D indicates decreased activity *in vivo* as well. Three substances had IC<sub>50</sub> values for 2D and 3D cell culture that differed by two orders of magnitude: KP1768 (3D/2D quotient for HCT116 = 310; CT26 = 490) inhibited tumor growth by 55% on day 14 of the *in vivo* experiment. KP2290 (3D/2D quotient for HCT116 = 290; CT26 = 200) promoted tumor growth by 15% on day 14. KP2550 (3D/2D quotient for HCT116 = 160; CT26 = 170) promoted tumor growth by 17% on day 14. This does not establish a conclusive trend, and it is worth noting that three data sets alone cannot provide a basis for a justified assumption. To draw meaningful conclusions from high 3D/2D quotients more data is necessary. However, within the subgroup of thiosemicarbazones the IC<sub>50</sub> (3D/2D) quotient had a significant correlation with tumor growth inhibition (%) on day 15(14). This was the only statistical analysis within this study for a limited substance class that showed significant correlation. Out of the eight tested thiosemicarbazones, two exhibited a noteworthy increase in IC<sub>50</sub> value from monolayer to spheroid culture (KP1768, KP2550 – see above). This may indicate an importance of 3D models for this substance class.

As already discussed in section 4.4.2, substances like KP1339 depend on their activity on protein carriers as well as effects that can only be observed within the tissue such as the EPR effect. These conditions are not mimicked in spheroid culture and therefore it can be concluded that the low effectiveness of KP1339 in spheroid culture is expected. Other substances might be influenced more by their ability to penetrate the tumor tissue and the reductive environment within the tumor. In these cases, decreased activity in spheroids could be an indicator of disadvantageous behavior *in vivo*.

Chemists optimize substances for their lipophilicity, *pK* value, presence of hydrogen donors and acceptors, solubility, and likelihood of protein and transporter interaction through a careful choice of ligands and central metal ions. High-throughput tests for cytotoxic or cytostatic properties are first indicators for their effectiveness and narrow down the compounds which will undergo further *in vitro* and *in vivo* testing. Generation of ROS, mutagenicity, subcellular localization, protein binding and other aspects can be tested *in vitro*.<sup>88</sup> Absorption, distribution, metabolism and excretion (ADME) and toxicity are typically evaluated *in vivo*, as standard high throughput models are insufficient to model these features. Combination of these properties with activity in xenografts (in mice) has demonstrated a higher predictivity for clinical efficacy compared to growth inhibition in animal models alone.<sup>89</sup> Attempts for incorporating the effects of protein binding in the blood stream and the characteristics of the organ environment have led to the emergence of methods for creating "organs-on-a-chip". Microfluidic devices aim to recreate mechanical and soluble clues, integrating biomaterials and co-cultured cells. A variety of such systems had been created, for mimicking angiogenesis, bone marrow, heart, kidney, intestine, liver, lung and muscle. It has been proposed that the improvement of these systems will lead to more efficient and cost-effective drug screenings. Connecting multiple systems in a "body-on-a-chip" might facilitate *in vitro* studies of drug toxicity.<sup>90,91</sup>

Although for HCT116 monolayer cultures a correlation between  $IC_{50}$  values and growth inhibition (%) on day 15 (14) in CT-26 tumors *in vivo* can be seen, it was lower than for the corresponding spheroid model. A linear relationship is evident for the log  $IC_{50}$  values in spheroid model in contrast to the monolayer model.  $IC_{50}$  values for CT26 spheroids also correlated with growth inhibition (%)

on day 15 (14). This suggests that the presumption was indeed correct: assuming higher predictivity for *in vivo* results from multicellular spheroids than from monolayer culture. It is crucial to note, however, that this can only be stated for certain for this limited data set, generated within this work. Although correlation between the two methods used for interpreting the *in vivo* data was very high, for predicting *in vivo* activity from *in vitro* data, growth inhibition (%) on day 15(14) in the CT26 tumor model in mice is favorable over tumor volume difference ( $\text{mm}^3$ ) averaged over time. Theoretically, the latter approach is favorable when dynamic information and delayed effects of the treatment are relevant. Different data evaluation methods may be adequate depending on the tumor growth rate and depending on whether cytostatic rather than cytotoxic substances are investigated. *In vivo* data were gathered in separate experiments using the same mouse strain and tumor model but partially differ in route of administration. However, numerous methods of *in vivo* data interpretation have been proposed to increase their ability to predict clinical efficacy.<sup>89,92</sup> CT26 spheroid data correlate with growth inhibition (%) in CT26 tumors *in vivo* slightly better than HCT116 spheroid data. Therefore, this model provides the highest predictivity. Although using CT26 spheroids for testing *in vitro* activity would accordingly provide the highest predictivity for *in vivo* results in CT26 solid tumor models in mice, the usage of this model should be considered carefully. HCT116 spheroid *in vitro* values provide an almost equally high correlation with the *in vivo* data, but are based on human cancer cells. This may not only provide insight into a possible performance in the *in vivo* model but may be more relevant for the actual target system, which is the human body.

## 5 Conclusion

Test conditions for experiments using monolayer cultures as well as multicellular spheroids were optimized for the murine colon cancer cell line CT26 and the human colon cancer cell line HCT116. Parallel testing of HCT116 monolayer, CT26 monolayer, HCT116 spheroids and CT26 spheroids was established by using the CellTiter-Glo® assay. Spheroids have a higher resemblance to tumor tissue than monolayer culture regarding cell morphology and metabolism. Immunostaining showed that a proliferating rim had formed in both spheroid models. Pimonidazole was used to detect hypoxia, and on day 8 both spheroid models had developed a hypoxic core. This environment provides proper test conditions also for drugs that are highly affected by a reductive environment and their (potentially limited) ability to penetrate tumor tissue.

The  $IC_{50}$  values gained from the cytotoxicity experiments and data provided from SW480 monolayer experiments were compared with the *in vivo* data for a set of 27 metal-based and metal-chelating compounds, and correlation and regression analyses were carried out. Various data combinations (using  $IC_{50}$  values of 5 different *in vitro* systems, quotients of  $IC_{50}$  values in corresponding 3D and 2D models, two different variables describing *in vivo* activity) were used.

Monolayer systems exhibited poor predictivity, as shown before, whilst  $IC_{50}$  values in both spheroid models correlate significantly with the tumor growth inhibition (%) on day 15 (14) in the *in vivo* experiment.

Within the subset of all tested thiosemicarbazones a correlation between decreased performance in 3D cell culture and tumor growth inhibition (%) on day 15 (14) is shown. Testing new compounds of this substance class in monolayer and spheroid culture in parallel might prove useful for choosing substances for further preclinical evaluation.

Using HCT116 spheroids as a preselection tool for further drug development could be a reasonable option for future compound testing. They do provide an only slightly lower correlation with the *in vivo* data than the use of CT26 spheroids, but consist of cells from the human body, the intended target for the tested compounds. Further improvement of this statistical analysis and constant expansion of the data set could lead to a tool that may decrease the number of required animal experiments, costs in drug development and might also provide further insights into mechanisms of action.

## References

- (1) Hackl, M.; Ihle, P. *Krebserkrankungen in Österreich*; Wien, 2018.
- (2) Global Cancer Observatory. *World Fact Sheets*; Lyon, 2019.
- (3) Alberts, B.; Johnson, A. *Molecular biology of the cell*, Sixth edition; The cell; Garland Science: New York, NY, 2015.
- (4) Hanahan, D.; Weinberg, R. A. Hallmarks of cancer: the next generation. *Cell* **2011**, *144*, 646–674.
- (5) Hawthorn, J.; Redmond, K. *A Guide to Cancer Drug Development and Regulation*; Macclesfield, 2006.
- (6) Jakupec, M. A.; Galanski, M.; Arion, V. B.; Hartinger, C. G.; Keppler, B. K. Antitumour metal compounds: more than theme and variations. *Dalton transactions (Cambridge, England : 2003)* **2008**, 183–194.
- (7) Junod, S. FDA and Clinical Drug Trials: A Short History. *FDLI Update* **2008**, *2008*, 55.
- (8) Blagosklonny, M. V. Teratogens as Anticancer Drugs. *Cell cycle* **2005**, *4*, 1518–1521.
- (9) Moehler, T. M.; Hillengass, J.; Glasmacher, A.; Goldschmidt, H. Thalidomide in multiple myeloma. *Current pharmaceutical biotechnology* **2006**, *7*.
- (10) European Medicines Agency. *The European regulatory system for medicines: A consistent approach to medicines regulation across the European Union*; London, 2016.
- (11) Teicher, B. A. *Anticancer Drug Development Guide: Preclinical Screening, Clinical Trials, and Approval*; Cancer Drug Discovery and Development; Humana Press: Totowa, NJ, 2013.
- (12) Han, C.; Wang, B. Factors That Impact the Developability of Drug Candidates: An Overview. In *Drug delivery: Principles and applications*; Wang, B., Siahaan, T., Soltero, R., Eds.; Wiley-Interscience: Hoboken, N.J., 2005; pp 1–14.
- (13) Johnson, J. I.; Decker, S.; Zaharevitz, D.; Rubinstein, L. V.; Venditti, J. M.; Schepartz, S.; Kalyandrug, S.; Christian, M.; Arbuck, S.; Hollingshead, M.; *et al.* Relationships between drug activity in NCI preclinical in vitro and in vivo models and early clinical trials. *British journal of cancer* **2001**, *84*, 1424–1431.

- (14) NIH National Cancer Institute. COMPARE Analysis: Introduction.  
[https://dtp.cancer.gov/databases\\_tools/compare.htm](https://dtp.cancer.gov/databases_tools/compare.htm) (accessed November 11, 2019).
- (15) The American Cancer Society medical and editorial content team. What Are the Phases of Clinical Trials? <https://www.cancer.org/treatment/treatments-and-side-effects/clinical-trials/what-you-need-to-know/phases-of-clinical-trials.html> (accessed December 18, 2019).
- (16) v Freshney, R. I. *Culture of Animal Cells*; John Wiley & Sons, Inc: Hoboken, NJ, USA, 2010.
- (17) Breslin, S.; O'Driscoll, L. Three-dimensional cell culture: the missing link in drug discovery. *Drug Discovery Today* **2013**, *18*, 240–249.
- (18) Baker, B. M.; Chen, C. S. Deconstructing the third dimension: how 3D culture microenvironments alter cellular cues. *Journal of cell science* **2012**, *125*, 3015–3024.
- (19) Thurber, G. M.; Wittrup, K. D. Quantitative spatiotemporal analysis of antibody fragment diffusion and endocytic consumption in tumor spheroids. *Cancer research* **2008**, *68*, 3334–3341.
- (20) Wilson, W. R.; Hay, M. P. Targeting hypoxia in cancer therapy. *Nature reviews. Cancer* **2011**, *11*, 393–410.
- (21) Santini, M. T.; Rainaldi, G. Three-dimensional spheroid model in tumor biology. *Pathobiology : journal of immunopathology, molecular and cellular biology* **1999**, *67*, 148–157.
- (22) Selby, M.; Delosh, R.; Laudeman, J.; Ogle, C.; Reinhart, R.; Silvers, T.; Lawrence, S.; Kinders, R.; Parchment, R.; Teicher, B. A.; *et al.* 3D Models of the NCI60 Cell Lines for Screening Oncology Compounds. *SLAS discovery : advancing life sciences R & D* **2017**, *22*, 473–483.
- (23) Vinci, M.; Gowan, S.; Boxall, F.; Patterson, L.; Zimmermann, M.; Court, W.; Lomas, C.; Mendiola, M.; Hardisson, D.; Eccles, S. A. Advances in establishment and analysis of three-dimensional tumor spheroid-based functional assays for target validation and drug evaluation. *BMC biology* **2012**, *10*, 29.
- (24) Lin, R.-Z.; Chou, L.-F.; Chien, C.-C. M.; Chang, H.-Y. Dynamic analysis of hepatoma spheroid formation: roles of E-cadherin and beta1-integrin. *Cell and tissue research* **2006**, *324*, 411–422.
- (25) Oloumi, A.; Lam, W.; Banáth, J. P.; Olive, P. L. Identification of genes differentially expressed in V79 cells grown as multicell spheroids. *International journal of radiation biology* **2002**, *78*, 483–492.

- (26) Steadman, K.; Stein, W. D.; Litman, T.; Yang, S. X.; Abu-Asab, M.; Dutcher, S. K.; Bates, S. PolyHEMA spheroids are an inadequate model for the drug resistance of the intractable solid tumors. *Cell cycle* **2008**, *7*, 818–829.
- (27) Kunz-Schughart, L. A.; Freyer, J. P.; Hofstaedter, F.; Ebner, R. The use of 3-D cultures for high-throughput screening: the multicellular spheroid model. *Journal of biomolecular screening* **2004**, *9*, 273–285.
- (28) Riffle, S.; Pandey, R. N.; Albert, M.; Hegde, R. S. Linking hypoxia, DNA damage and proliferation in multicellular tumor spheroids. *BMC Cancer* **2017**, *17*, 338.
- (29) Schreiber-Brynzak, E.; Klapproth, E.; Unger, C.; Lichtscheidl-Schultz, I.; Göschl, S.; Schweighofer, S.; Trondl, R.; Dolznig, H.; Jakupec, M. A.; Keppler, B. K. Three-dimensional and co-culture models for preclinical evaluation of metal-based anticancer drugs. *Investigational new drugs* **2015**, *33*, 835–847.
- (30) Göschl, S.; Schreiber-Brynzak, E.; Pichler, V.; Cseh, K.; Heffeter, P.; Jungwirth, U.; Jakupec, M. A.; Berger, W.; Keppler, B. K. Comparative studies of oxaliplatin-based platinum(IV) complexes in different in vitro and in vivo tumor models. *Metallomics : integrated biometal science* **2017**, *9*, 309–322.
- (31) Valley, M. P.; Zimprich, C.; Cali, J. J.; Lazar, D. F. *A Bioluminescent Cell Viability Assay Optimized for 3D Microtissues*; Madison, 2013.
- (32) Rosenberg, B.; VanCamp, L.; Trosko, J. E.; Mansour, V. H. Platinum compounds: a new class of potent antitumour agents. *Nature* **1969**, *222*, 385–386.
- (33) Köpf-Maier, P.; Köpf, H. Cytostatische Platin-Komplexe: eine unerwartete Entdeckung mit weitreichenden Konsequenzen. *Die Naturwissenschaften* **1986**, *73*, 239–247.
- (34) Abramkin, S. A.; Jungwirth, U.; Valiahdi, S. M.; Dworak, C.; Habala, L.; Meelich, K.; Berger, W.; Jakupec, M. A.; Hartinger, C. G.; Nazarov, A. A.; *et al.* {(1R,2R,4R)-4-methyl-1,2-cyclohexanediamine}oxalatoplatinum(II): a novel enantiomerically pure oxaliplatin derivative showing improved anticancer activity in vivo. *Journal of medicinal chemistry* **2010**, *53*, 7356–7364.
- (35) Rosenberg, B. Platinum coordination complexes in cancer chemotherapy. *Die Naturwissenschaften* **1973**, *60*, 399–406.

- (36) Wang, D.; Lippard, S. J. Cellular processing of platinum anticancer drugs. *Nature reviews. Drug discovery* **2005**, *4*, 307–320.
- (37) Harper, B. W.; Krause-Heuer, A. M.; Grant, M. P.; Manohar, M.; Garbutcheon-Singh, K. B.; Aldrich-Wright, J. R. Advances in platinum chemotherapeutics. *Chemistry* **2010**, *16*, 7064–7077.
- (38) Theiner, S.; Varbanov, H. P.; Galanski, M.; Egger, A. E.; Berger, W.; Heffeter, P.; Keppler, B. K. Comparative in vitro and in vivo pharmacological investigation of platinum(IV) complexes as novel anticancer drug candidates for oral application. *Journal of biological inorganic chemistry : JBIC : a publication of the Society of Biological Inorganic Chemistry* **2015**, *20*, 89–99.
- (39) Varbanov, H.; Valiahdi, S. M.; Legin, A. A.; Jakupec, M. A.; Roller, A.; Galanski, M.; Keppler, B. K. Synthesis and characterization of novel bis(carboxylato)dichloridobis(ethylamine)platinum(IV) complexes with higher cytotoxicity than cisplatin. *European journal of medicinal chemistry* **2011**, *46*, 5456–5464.
- (40) Varbanov, H. P.; Valiahdi, S. M.; Kowol, C. R.; Jakupec, M. A.; Galanski, M.; Keppler, B. K. Novel tetracarboxylatoplatinum(IV) complexes as carboplatin prodrugs. *Dalton transactions* **2012**, *41*, 14404–14415.
- (41) Hartinger, C. G.; Zorbas-Seifried, S.; Jakupec, M. A.; Kynast, B.; Zorbas, H.; Keppler, B. K. From bench to bedside--preclinical and early clinical development of the anticancer agent indazolium trans-[tetrachlorobis(1H-indazole)ruthenate(III)] (KP1019 or FFC14A). *Journal of inorganic biochemistry* **2006**, *100*.
- (42) Flocke, L. S.; Trondl, R.; Jakupec, M. A.; Keppler, B. K. Molecular mode of action of NKP-1339 - a clinically investigated ruthenium-based drug - involves ER- and ROS-related effects in colon carcinoma cell lines. *Investigational new drugs* **2016**, *34*.
- (43) Burris, H. A.; Bakewell, S.; Bendell, J. C.; Infante, J.; Jones, S. F.; Spigel, D. R.; Weiss, G. J.; Ramanathan, R. K.; Ogden, A.; Hoff, D. von. Safety and activity of IT-139, a ruthenium-based compound, in patients with advanced solid tumours: a first-in-human, open-label, dose-escalation phase I study with expansion cohort. *ESMO open* **2016**, *1*, e000154.
- (44) Medici, S.; Peana, M.; Nurchi, V. M.; Lachowicz, J. I.; Crisponi, G.; Zoroddu, M. A. Noble metals in medicine: Latest advances. *Coordination Chemistry Reviews* **2015**, *284*, 329–350.
- (45) Kandioller, W.; Hartinger, C. G.; Nazarov, A. A.; Kuznetsov, M. L.; John, R. O.; Bartel, C.; Jakupec, M. A.; Arion, V. B.; Keppler, B. K. From Pyrone to Thiopyrone Ligands–Rendering Maltol-

Derived Ruthenium(II)–Arene Complexes That Are Anticancer Active in Vitro. *Organometallics* **2009**, *28*, 4249–4251.

(46) Kurzwernhart, A.; Kandioller, W.; Bartel, C.; Bächler, S.; Trondl, R.; Mühlgassner, G.; Jakupec, M. A.; Arion, V. B.; Marko, D.; Keppler, B. K.; *et al.* Targeting the DNA-topoisomerase complex in a double-strike approach with a topoisomerase inhibiting moiety and covalent DNA binder. *Chemical communications* **2012**, *48*, 4839–4841.

(47) Hackl, C. M.; Schoenhacker-Alte, B.; Klose, M. H. M.; Henke, H.; Legina, M. S.; Jakupec, M. A.; Berger, W.; Keppler, B. K.; Brüggemann, O.; Teasdale, I.; *et al.* Synthesis and in vivo anticancer evaluation of poly(organo)phosphazene-based metallodrug conjugates. *Dalton transactions* **2017**, *46*, 12114–12124.

(48) Meier, S. M.; Hanif, M.; Adhireksan, Z.; Pichler, V.; Novak, M.; Jirkovsky, E.; Jakupec, M. A.; Arion, V. B.; Davey, C. A.; Keppler, B. K.; *et al.* Novel metal(ii) arene 2-pyridinecarbothioamides: a rationale to orally active organometallic anticancer agents. *Chemical Science* **2013**, *4*, 1837.

(49) Meier, S. M.; Kreutz, D.; Winter, L.; Klose, M. H. M.; Cseh, K.; Weiss, T.; Bileck, A.; Alte, B.; Mader, J. C.; Jana, S.; *et al.* An Organoruthenium Anticancer Agent Shows Unexpected Target Selectivity For Plectin. *Angewandte Chemie International Edition* **2017**, *56*, 8267–8271.

(50) Kandioller, W.; Balsano, E.; Meier, S. M.; Jungwirth, U.; Göschl, S.; Roller, A.; Jakupec, M. A.; Berger, W.; Keppler, B. K.; Hartinger, C. G. Organometallic anticancer complexes of lapachol: metal centre-dependent formation of reactive oxygen species and correlation with cytotoxicity. *Chemical communications (Cambridge, England)* **2013**, *49*, 3348–3350.

(51) Motterlini, R.; Otterbein, L. E. The therapeutic potential of carbon monoxide. *Nature reviews. Drug discovery* **2010**, *9*, 728–743.

(52) Tamasi, G.; Merlino, A.; Scaletti, F.; Heffeter, P.; Legin, A. A.; Jakupec, M. A.; Berger, W.; Messori, L.; Keppler, B. K.; Cini, R. {Ru(CO)<sub>x</sub>}-Core complexes with benzimidazole ligands: synthesis, X-ray structure and evaluation of anticancer activity in vivo. *Dalton transactions* **2017**, *46*, 3025–3040.

(53) Finch, R. A.; Liu, M.-C.; Grill, S. P.; Rose, W. C.; Loomis, R.; Vasquez, K. M.; Cheng, Y.-C.; Sartorelli, A. C. Triapine (3-aminopyridine-2-carboxaldehyde- thiosemicarbazone): A potent inhibitor of ribonucleotide reductase activity with broad spectrum antitumor activity. *Biochemical Pharmacology* **2000**, *59*, 983–991.

- (54) Kowol, C. R.; Trondl, R.; Heffeter, P.; Arion, V. B.; Jakupec, M. A.; Roller, A.; Galanski, M.; Berger, W.; Keppler, B. K. Impact of metal coordination on cytotoxicity of 3-aminopyridine-2-carboxaldehyde thiosemicarbazone (triapine) and novel insights into terminal dimethylation. *Journal of medicinal chemistry* **2009**, *52*, 5032–5043.
- (55) Schelman, W. R.; Morgan-Meadows, S.; Marnocha, R.; Lee, F.; Eickhoff, J.; Huang, W.; Pomplun, M.; Jiang, Z.; Alberti, D.; Kolesar, J. M.; *et al.* A phase I study of Triapine® in combination with doxorubicin in patients with advanced solid tumors. *Cancer Chemotherapy and Pharmacology* **2009**, *63*, 1147–1156.
- (56) Christian R. Kowol; Robert Trondl; Vladimir B. Arion; Michael A. Jakupec; Irene Lichtscheidl; Bernhard K. Keppler. Fluorescence properties and cellular distribution of the investigational anticancer drug Triapine (3-aminopyridine-2-carboxaldehyde thiosemicarbazone) and its zinc(II) complex. *Dalton Trans.* **2009**, *39*, 704–706.
- (57) Robert Trondl; Lea S. Flocke; Christian R. Kowol; Petra Heffeter; Ute Jungwirth; Georg E. Mair; Ralf Steinborn; Éva A. Enyedy; Michael A. Jakupec; Walter Berger; *et al.* Triapine and a More Potent Dimethyl Derivative Induce Endoplasmic Reticulum Stress in Cancer Cells. *Mol Pharmacol* **2014**, *85*, 451–459.
- (58) Kowol, C. R.; Miklos, W.; Pfaff, S.; Hager, S.; Kallus, S.; Pelivan, K.; Kubanik, M.; Enyedy, É. A.; Berger, W.; Heffeter, P.; *et al.* Impact of Stepwise NH<sub>2</sub>-Methylation of Triapine on the Physicochemical Properties, Anticancer Activity, and Resistance Circumvention. *Journal of medicinal chemistry* **2016**, *59*, 6739–6752.
- (59) Filipović, N. R.; Bjelogrić, S. K.; Pelliccia, S.; Jovanović, V. B.; Kojić, M.; Senćanski, M.; La Regina, G.; Silvestri, R.; Muller, C. D.; Todorović, T. R. Selenotriapine – An isostere of the most studied thiosemicarbazone with pronounced pro-apoptotic activity, low toxicity and ability to challenge phenotype reprogramming of 3-D mammary adenocarcinoma tumors. *Arabian Journal of Chemistry* **2020**, *13*, 1466–1489.
- (60) Kallus, S.; Uhlik, L.; van, S. S.; Pelivan, K.; Berger, W.; Enyedy, É. A.; Hofmann, T.; Heffeter, P.; Kowol, C. R.; Keppler, B. K. Synthesis and biological evaluation of biotin-conjugated anticancer thiosemicarbazones and their iron(III) and copper(II) complexes. *Journal of inorganic biochemistry* **2019**, *190*.

- (61) Kowol, C. R.; Berger, R.; Eichinger, R.; Roller, A.; Jakupec, M. A.; Schmidt, P. P.; Arion, V. B.; Keppler, B. K. Gallium(III) and iron(III) complexes of alpha-N-heterocyclic thiosemicarbazones: synthesis, characterization, cytotoxicity, and interaction with ribonucleotide reductase. *Journal of medicinal chemistry* **2007**, *50*, 1254–1265.
- (62) Hackl, C. M.; Legina, M. S.; Pichler, V.; Schmidlehner, M.; Roller, A.; Dömötör, O.; Enyedy, E. A.; Jakupec, M. A.; Kandioller, W.; Keppler, B. K. Thiomaltol-Based Organometallic Complexes with 1-Methylimidazole as Leaving Group: Synthesis, Stability, and Biological Behavior. *Chemistry* **2016**, *22*, 17269–17281.
- (63) Luo, X.-M.; Wei, H.-J.; Yang, S. P. Inhibitory Effects of Molybdenum on Esophageal and Forestomach Carcinogenesis in Rats<sup>23</sup>. *Journal of the National Cancer Institute* **1983**, *71*, 75–80.
- (64) Fujita, H.; Fujita, T.; Sakurai, T.; Yamase, T.; Seto, Y. Antitumor activity of new antitumor substance, polyoxomolybdate, against several human cancers in athymic nude mice. *The Tohoku journal of experimental medicine* **1992**, *168*, 421–426.
- (65) Kisker, C.; Schindelin, H.; Rees, D. C. Molybdenum-cofactor-containing enzymes: structure and mechanism. *Annual review of biochemistry* **1997**, *66*, 233–267.
- (66) Bandarra, D.; Lopes, M.; Lopes, T.; Almeida, J.; Saraiva, M. S.; Vasconcellos-Dias, M.; Nunes, C. D.; Félix, V.; Brandão, P.; Vaz, P. D.; *et al.* Mo(II) complexes: a new family of cytotoxic agents? *Journal of inorganic biochemistry* **2010**, *104*, 1171–1177.
- (67) Fricker, S. P. The therapeutic application of lanthanides. *Chemical Society reviews* **2006**, *35*, 524–533.
- (68) Biba, F.; Groessl, M.; Egger, A.; Roller, A.; Hartinger, C. G.; Keppler, B. K. New Insights into the Chemistry of the Antineoplastic Lanthanum Complex Tris(1,10-phenanthroline)tris(thiocyanato-κ N )lanthanum(III) (KP772) and Its Interaction with Biomolecules. *European Journal of Inorganic Chemistry* **2009**, *2009*, 4282–4287.
- (69) Heffeter, P.; Jakupec, M. A.; Körner, W.; Wild, S.; Keyserlingk, N. G. von; Elbling, L.; Zorbas, H.; Korynevskaya, A.; Knasmüller, S.; Sutterlüty, H.; *et al.* Anticancer activity of the lanthanum compound tris(1,10-phenanthroline)lanthanum(III)trithiocyanate (KP772; FFC24). *Biochemical Pharmacology* **2006**, *71*, 426–440.
- (70) Varbanov, H. P.; Göschl, S.; Heffeter, P.; Theiner, S.; Roller, A.; Jensen, F.; Jakupec, M. A.; Berger, W.; Galanski, M.; Keppler, B. K. A novel class of bis- and tris-chelate

diam(m)inebis(dicarboxylato)platinum(IV) complexes as potential anticancer prodrugs. *Journal of medicinal chemistry* **2014**, 57, 6751–6764.

(71) Kowol, C. R.; Trondl, R.; Arion, V. B.; Jakupec, M. A.; Lichtscheidl, I.; Keppler, B. K. Fluorescence properties and cellular distribution of the investigational anticancer drug triapine (3-aminopyridine-2-carboxaldehyde thiosemicarbazone) and its zinc(II) complex. *Dalton transactions* **2010**, 39, 704–706.

(72) Berasaluce, I.; Cseh, K.; Roller, A.; Hejl, M.; Heffeter, P.; Berger, W.; Jakupec, M. A.; Kandioller, W.; Malarek, M. S.; Keppler, B. K. The First Anticancer Tris(pyrazolyl)borate Molybdenum(IV) Complexes: Tested in Vitro and in Vivo-A Comparison of O,O-, S,O-, and N,N-Chelate Effects. *Chemistry – A European Journal* **2020**, 26, 2211–2221.

(73) Adachi, A.; Koenig, S.; Gendelman, H. E.; Daugherty, D.; Gattoni-Celli, S.; Fauci, A. S.; Martin, M. A. Productive, persistent infection of human colorectal cell lines with human immunodeficiency virus. *Journal of virology* **1987**, 61, 209–213.

(74) Brattain, M. G.; Fine, W. D.; Khaled, F. M.; Thompson, J.; Brattain, D. E. Heterogeneity of malignant cells from a human colonic carcinoma. *Cancer research* **1981**, 41, 1751–1756.

(75) Wang, M.; Bronte, V.; Chen, P. W.; Gritz, L.; Panicali, D.; Rosenberg, S. A.; Restifo, N. P. Active immunotherapy of cancer with a nonreplicating recombinant fowlpox virus encoding a model tumor-associated antigen. *Journal of immunology (Baltimore, Md. : 1950)* **1995**, 154, 4685–4692.

(76) Varshosaz, J.; Hassanzadeh, F.; Sadeghi-Aliabadi, H.; Firozian, F. Uptake of etoposide in CT-26 cells of colorectal cancer using folate targeted dextran stearate polymeric micelles. *BioMed research international* **2014**, 2014, 708593-11.

(77) Sun, P.; Zhao, J.-M.; Luo, Z.-C.; Zhang, P.; Chen, P.; Zhang, X.-L.; Luo, S.; Yang, D.-B.; Tan, J.; Zhou, Y.; *et al.* Diluted povidone-iodine inhibits tumor growth through apoptosis-induction and suppression of SOD activity. *Oncology reports* **2012**, 27, 383–388.

(78) Promega. CellTiter-Glo® 2.0 Assay: Instructions for Use of Products G9241, G9242 and G9243. [https://at.promega.com/products/cell-health-assays/cell-viability-and-cytotoxicity-assays/celltiter\\_glo-2\\_0-assay/?catNum=G9241&gclid=EAlaIQobChMIvdn3pPOw5wIVgYKyCh2D4wPuEAAYASAAEgLvD\\_BwE](https://at.promega.com/products/cell-health-assays/cell-viability-and-cytotoxicity-assays/celltiter_glo-2_0-assay/?catNum=G9241&gclid=EAlaIQobChMIvdn3pPOw5wIVgYKyCh2D4wPuEAAYASAAEgLvD_BwE) (accessed February 1, 2020).

(79) Promega. CellTiter-Glo® 3D Cell Viability Assay: Instructions for Use of Products G9681, G9682 and G9683. <https://at.promega.com/products/cell-health-assays/cell-viability-and->

cytotoxicity-assays/celltiter\_glo-3d-cell-viability-assay/?catNum=G9681 (accessed February 1, 2020).

(80) Ute Jungwirth; Dimitris N. Xanthos; Johannes Gojo; Anna K. Bytze; Wilfried Körner; Petra Heffeter; Sergey A. Abramkin; Michael A. Jakupiec; Christian G. Hartinger; Ursula Windberger; *et al.* Anticancer Activity of Methyl-Substituted Oxaliplatin Analogs. *Molecular pharmacology* **2012**, *81*, 719.

(81) Klose, M. H. M.; Theiner, S.; Kornauth, C.; Meier-Menches, S. M.; Heffeter, P.; Berger, W.; Koellensperger, G.; Keppler, B. K. Bioimaging of isosteric osmium and ruthenium anticancer agents by LA-ICP-MS. *Metallomics* **2018**, *10*, 388–396.

(82) Sobahi, T. R. A.; Ayyad, S.-E. N.; Abdel-Lateff, A.; Algandaby, M. M.; Alorfi, H. S.; Abdel-Naim, A. B. Cytotoxic Metabolites from *Callyspongia siphonella* Display Antiproliferative Activity by Inducing Apoptosis in HCT-116 Cells. *Pharmacognosy magazine* **2017**, *13*, S37-S40.

(83) Green, C. E.; Liu, T.; Montel, V.; Hsiao, G.; Lester, R. D.; Subramaniam, S.; Gonias, S. L.; Klemke, R. L. Chemoattractant signaling between tumor cells and macrophages regulates cancer cell migration, metastasis and neovascularization. *PloS one* **2009**, *4*, e6713.

(84) Wang, H.-X.; Zuo, Z.-Q.; Du, J.-Z.; Wang, Y.-C.; Sun, R.; Cao, Z.-T.; Ye, X.-D.; Wang, J.-L.; Leong, K. W.; Wang, J. Surface charge critically affects tumor penetration and therapeutic efficacy of cancer nanomedicines. *Nano Today* **2016**, *11*, 133–144.

(85) Escolà, A.; Crespo, M.; López, C.; Quirante, J.; Jayaraman, A.; Polat, I. H.; Badía, J.; Baldomà, L.; Cascante, M. On the stability and biological behavior of cyclometallated Pt(IV) complexes with halido and aryl ligands in the axial positions. *Bioorganic & medicinal chemistry* **2016**, *24*, 5804–5815.

(86) Christofferson, D. E.; Yuan, J. Cyclophilin A release as a biomarker of necrotic cell death. *Cell death and differentiation* **2010**, *17*, 1942–1943.

(87) Liu, Z.-G.; Jiao, D. Necroptosis, tumor necrosis and tumorigenesis. *Cell stress* **2019**, *4*, 1–8.

(88) Kerns, E. *Drug-like Properties: Concepts, Structure Design and Methods*; Elsevier Science: Burlington, 2010.

(89) Andy ZX Zhu. Quantitative translational modeling to facilitate preclinical to clinical efficacy & toxicity translation in oncology. *Future Science OA* **2018**, *4*, FSO306.

- (90) Jackson, E. L.; Lu, H. Three-dimensional models for studying development and disease: moving on from organisms to organs-on-a-chip and organoids. *Integrative biology : quantitative biosciences from nano to macro* **2016**, *8*, 672–683.
- (91) Leung, C. M.; Haan, P. de; Ronaldson-Bouchard, K.; Kim, G.-A.; Ko, J.; Rho, H. S.; Chen, Z.; Habibovic, P.; Jeon, N. L.; Takayama, S.; *et al.* A guide to the organ-on-a-chip. *Nat Rev Methods Primers* **2022**, *2*, 1–29.
- (92) Ubezio, P. Beyond The T/C Ratio: Old And New Anticancer Activity Scores In Vivo. *Cancer Management and Research* **2019**, *11*, 8529–8538.